

# POLITECNICO DI TORINO

Department of Mechanical and Aerospace Engineering (DIMEAS)

# Master's Degree in Biomedical Engineering

Master's Degree Thesis

# Range of Motion Enhancement in a Passive Upper-Limb Exoskeleton: Design Improvements to a Prototype Based on Pneumatic Artificial Muscles

#### **Supervisors:**

Dr. Carlo De Benedictis Dr. Maria Paterna Prof. Carlo Ferraresi <u>Candidate:</u> Miriam Filomena De Francesco

#### **Abstract**

# 1. Anatomy and biomechanics of the shoulder

- 1.1. Shoulder Anatomy
  - 1.1.1. Synovial Joints
  - 1.1.2. Physiological Joints
- 1.2. Shoulder Movement
  - 1.2.1. Shoulder Muscles
- 1.3. Shoulder Joint Center
  - 1.3.1. Estimation of SJC
  - 1.3.2. Shoulder Modeling

# 2. Industrial Upper-Limb Exoskeletons

- 2.1. Actuation systems
- 2.2. Mechanical design
  - 2.2.1. State of Art: Passive Upper-Limb Exoskeletons
  - 2.2.2. State of Art: Range of Motion Evaluation

# 3. Exoskeleton Prototype

- 3.1. Actuators: Pneumatic Artificial Muscles
  - 3.1.1. Mathematical Models
  - 3.1.2. Geometrical Model
  - 3.1.3. Empirical Model
  - 3.1.4. Phenomenological Model
- 3.2. Transmission System: The Shoulder Pad and The Bracelet
  - 3.2.1. Profile of Shoulder Pad
  - 3.2.2. Limited Range Of Motion: the torque profile
  - 3.2.3. Prototype kinematic chain
  - 3.3. Range Of Motion of the Prototype

#### 4. The New Bracelet

- 4.1. Design Goals
- 4.2. new Diameter
- 4.3 Release System
  - 4.3.1 Fixed Part
  - 4.3.2. Sliding Part and The Handle
  - 4.3.3. The Safety Catch
- 4.4. New Torque
- 4.5. New ROM
- 4.6. Finite Element Analysis
  - 4.6.1. Polylactic Acid
  - 4.6.2. Static Analysis

#### 4.6.3. Simulation Results

- 4.7. Static Test
- 4.8. Discussion

# **5. CAM-Based Transmission**

- 5.1. Redesign of the cam support structure
- 5.2. FEM Analysis
  - 5.2.1. FEM Results of the metal parts
- 5.2.2. FEM Results of the PLA parts 5.4. Displacements analysis
- 5.5. Parasitic Abduction Moments
- 5.6. Discussion

# 6. Conclusions and future developments

#### **Abstract**

shoulder joint provided by PAMs action.

Industrial passive exoskeletons are used to assist workers in performing repetitive and physically demanding tasks, in fields such as manufacturing and logistics. These devices aim to reduce biomechanical stress on specific joint or anatomical regions, with the ultimate goal of reducing the risk of work-related musculoskeletal disorders (WMSDs). Among the various joints subjected to overwork, the shoulder joint presents a unique challenge due to its high degrees of freedom (DOF) and wide range of motion (ROM), which make it difficult to design support mechanisms that do not interfere with physiological movements. This thesis focuses on the biomechanical analysis and functional enhancement of a passive upper-limb exoskeleton prototype which employs two Pneumatic Artificial Muscles (PAMs). In its initial configuration, the exoskeleton provides assistive torque during arm elevation, but the current transmission architecture imposes limitations on the functional ROM, effectively constraining the shoulder flexion between 90° and 135°. This causes discomfort while using the engaged exoskeleton for elevation angles below 90°, due to the excessive torque at the

The main objective of this work is to extend the ROM of the passive exoskeleton, ensuring continuous or manually disengaged assistance, without compromising mechanical simplicity or user comfort. To achieve this, two distinct mechanical solutions have been developed and/or analyzed.

The first solution involves the redesign of the bracelet, integrating a disengagement mechanism that allows the user to lower the arm with a simple gesture. This allows free movement of the arm down to a minimum angle of 26° with respect to the vertical axis. This adjustment does not alter the existing transmission architecture and preserves the advantages of the original prototype in terms of assistive torque.

The second solution, based on a cam transmission system developed in the earlier stages of the prototypes design project, was analysed in this thesis to evaluate its potential for torque modulation and integration into the exoskeleton because of its optimal ROM in terms of flexion. The cam profile has been designed to modulate the torque transfer from the PAMs as a function of the arm elevation angle. This solution has not been developed because of the complexity of the integration on the back structure and the poor supportive torque while holding an object. In order to evaluate the possibilities of the ROM expansion this solution has been optimized to be implemented in the current back-frame, evaluating the pros and cons of the solution.

Both design strategies have been modeled using CAD and evaluated through static simulation. Performance indicators such as achievable ROM, integration with existing components, and theoretical torque profiles were compared. The cam-based mechanism was subjected to analysis regarding manufacturability and integration into the existing structure. The results demonstrate that both approaches effectively expand the exoskeleton's functional ROM. The disengagement-based bracelet design allows the user to regain use of the lower workspace without adding complexity to the system and preserving the support torque while not disengaged, while the cam mechanism enables continuous support in the ROM but provides less support while having weight in the hands. A future work implementing passive adaptable springs in the current transmission design could be an aspect that preserves the pros of both solutions.

# Chapter 1

# Anatomy and biomechanics of the shoulder

In order to design an exoskeleton is mandatory to comprehend the anatomical part that the exoskeleton is going to support.

# 1.1. Shoulder Anatomy

The bones forming the shoulder complex are the clavicle, the humerus and the scapula. Their articulation is regulated by five joints which allow the shoulder complex to achieve the greatest range of movement among all human joints. This high degree of mobility, however, comes at the cost of reduced intrinsic stability and poses significant challenges in replicating its kinematics in assistive devices. The five joints include three synovial and two physiological articulations, whose coordinated movement is essential for full upper-limb mobility.[1]

The shoulder joints are in total five: Acromioclavicular, Sternoclavicular, Glenohumeral, Scapulothoracic and Subacromial as shown in Figure 1. These five can be divided into two groups, each group is mechanically coordinated. The first group is formed by the glenohumeral and the subacromial; the second group is formed by the scapulothoracic and the acromioclavicular and the sternoclavicular joints.

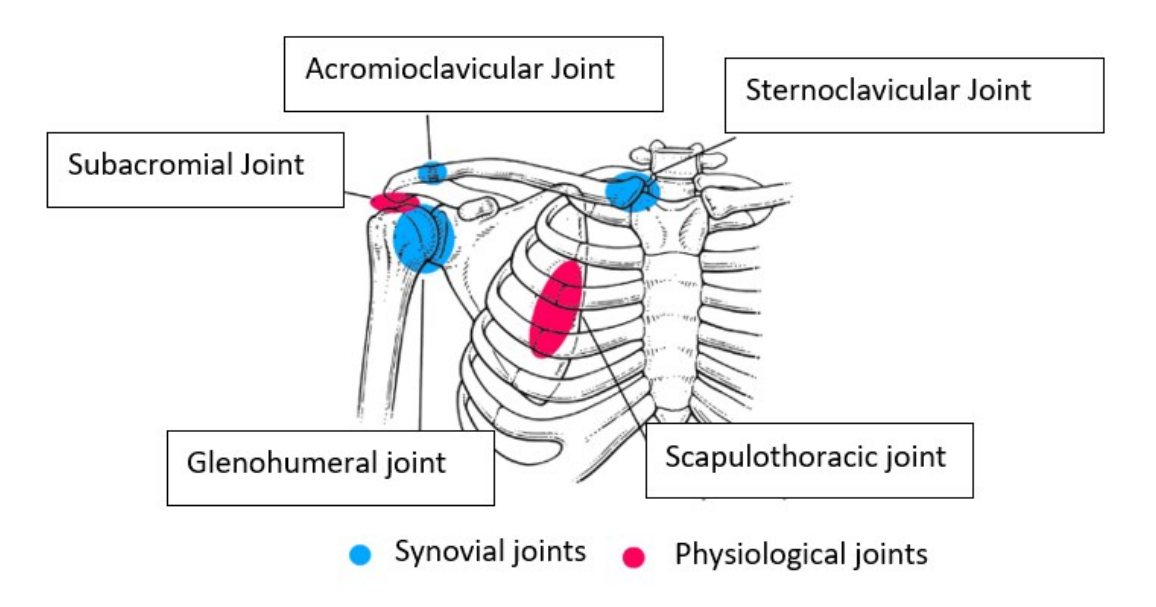


Figure 1: Position of joints on osseus anatomy [2]

# 1.1.1. Synovial joints

Synovial joints are the most common type of joint in the human body, characterized by a joint cavity filled with synovial fluid. This allows smooth contact between the articulating bone surfaces, facilitated also by the presence of the articular cartilage. Synovial joints are classified by the type of movement that they allow: hinge, saddle, gliding, pivot, condyloid, and ball-and-socket. [2]

In the shoulder there are three different types of synovial joints: acromioclavicular, sternoclavicular and glenohumeral. The acromioclavicular joint (ACJ) is a planar gliding joint that links the acromion and the distal portion of the clavicle. It rotates and translates into superior-inferior and anterior-posterior planes. It is stabilized by the acromioclavicular ligament and the coracoclavicular ligaments, shown in Figure 2,respectively for the horizontal and vertical stability.

The sternoclavicular joint (SCJ) is a saddle joint that links the proximal clavicle and the sternum. It is stabilized by the coracoclavicular and acromioclavicular ligaments.

The glenohumeral joint (GHJ) is a ball-and-socket joint that links the head of the humerus head and the glenoid fossa of the scapula. It provides the greatest ROM among all joints but in order to achieve that it is intrinsically unstable: it must rely on muscular e ligaments support to avoid injury through the movements.

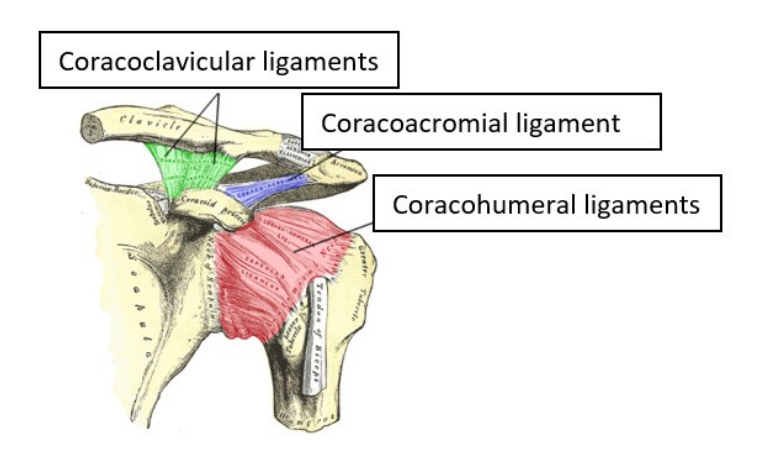


Figure 2: Shoulder ligaments. Adapted from[3]

#### 1.1.2. Physiological joints

Subacromial and scapulothoracic joints are not true anatomical joints, they are referred to as physiological or functional joints. They are indispensable to the kinematics and stability of the shoulder complex by adding additional degrees of freedom essential for upper limb mobility.

Scapulothoracic joint (STJ) is the sliding interface between the scapula and the rib cage.

The subacromial joint or subacromial space, aids via bursae the gliding between the acromion and the rotator cuff [4].

#### 1.2. Shoulder movements

As mentioned before, the shoulder has multiple degrees of motion that are achieved with the interactions of the joints as well as the muscles, the bony structures and the ligaments. It has three degrees of freedom which allow the orientation of the upper limb in the three planes of the body [Figure 3b]. It is possible to define three principal axes of the shoulder [Figure 3a], each one permits specific movement [5]. On the coronal plane there is the lateral axis which allows the movement of flexion and extension [Figure 4b] whose movements happen in the sagittal plane. On the sagittal plane there is the antero-posterior axis where, on the coronal plane, it allows the abduction and adduction movement [Figure 4a]. The last axis is the vertical one, orthogonal to the other two. This axis allows the movement of horizontal abduction and adduction [Figure 4c]. Also, the longitudinal plane of the humeral allows the internal and the external rotation of the arm [Figure 4d]. Table 1 shows the Range of Motion (ROM) of these movements.

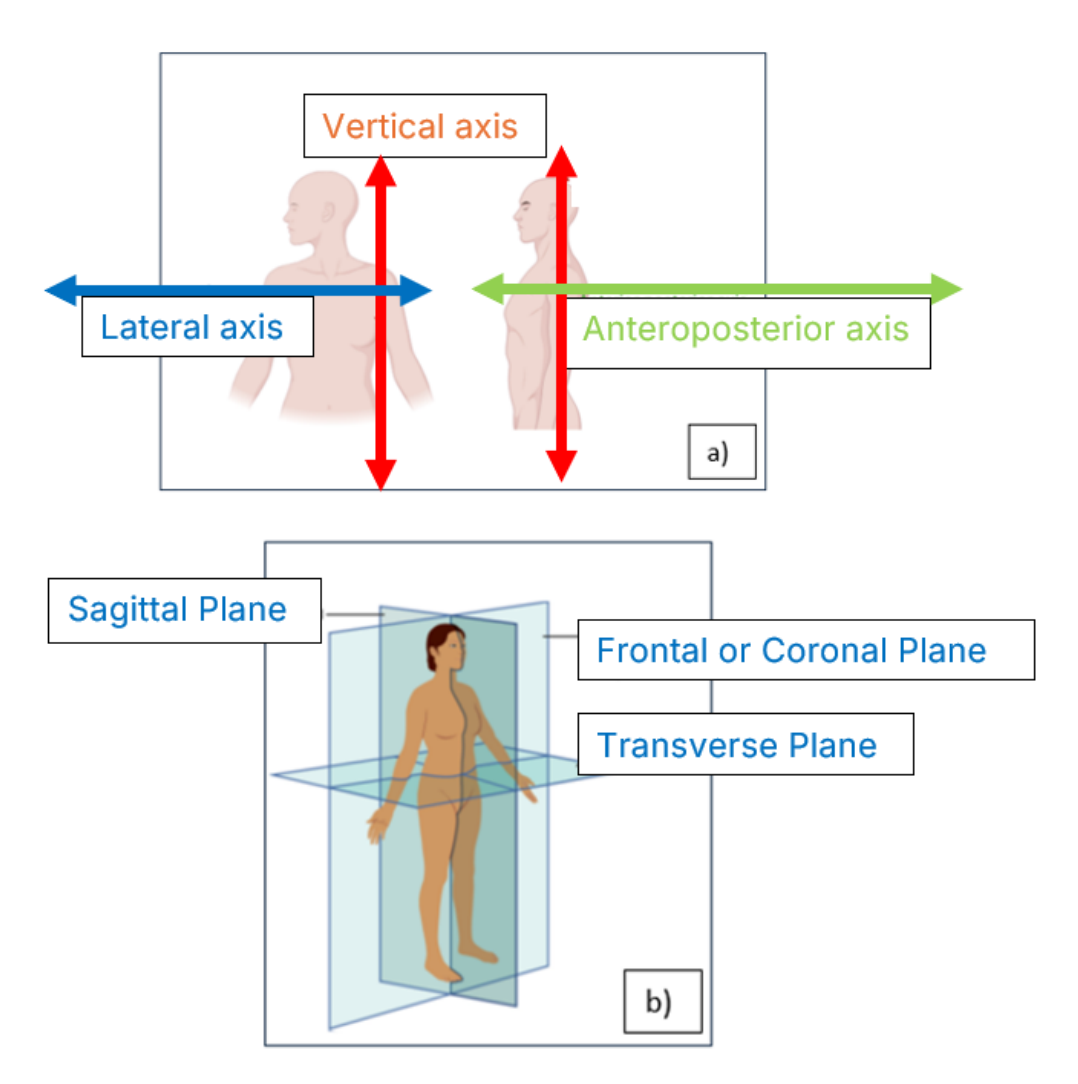


Figure 3 a) Shoulder principal axis: on the left coronal view, on the right sagittal view. Created in [13] b) Planes of the body.[14]

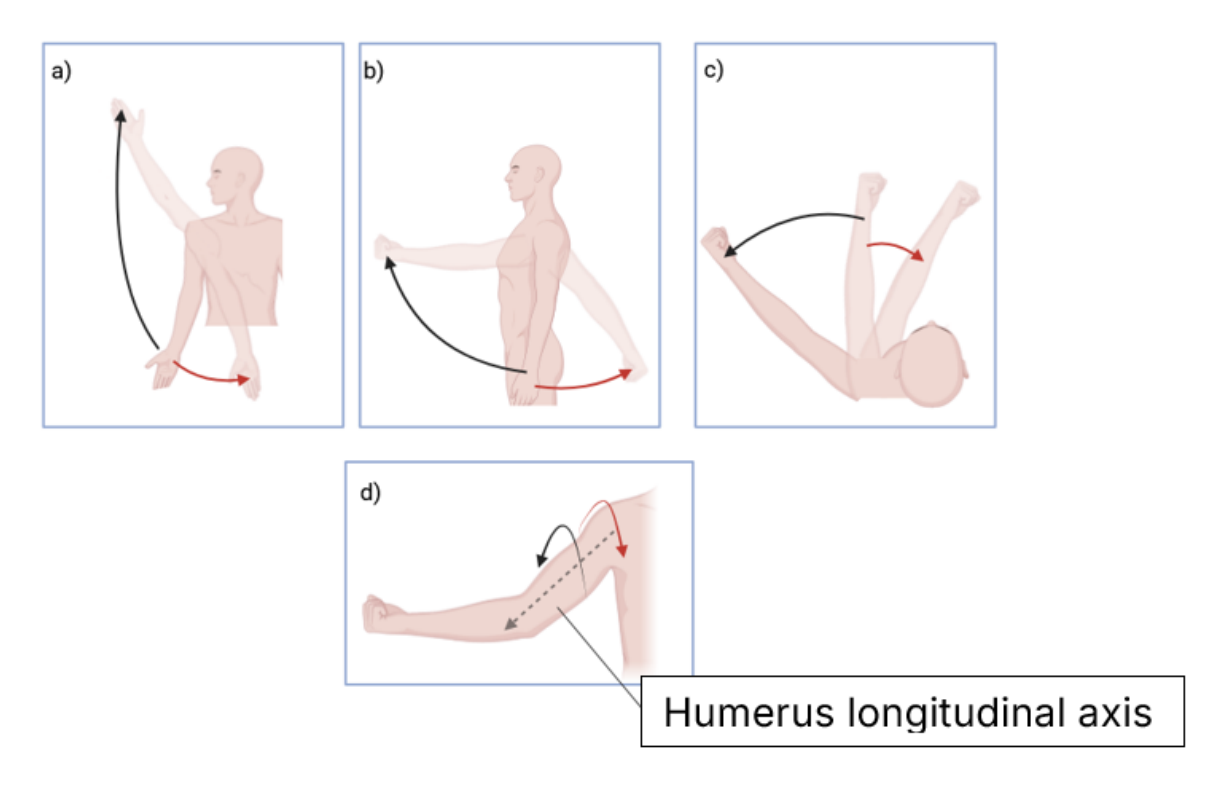


Figure 4: Shoulder movements. a) In black: Abduction; in red: Adduction b) In black: Flexion; in red: Extension c) in black: horizontal abduction; in red: horizontal Adduction d) In red: Internal rotation; in black: external rotation. Created in [6]

Movement	ROM
Abduction	0°-180°
Adduction	0°-50°
Flexion	0°-180°
Extension	0°-60°
Horizontal Abduction	0°-90°
Horizontal Adduction	0°-90°
Internal rotation	0°-90°
External rotation	0°-90°

Table 1: Shoulder range of motion

#### 1.2.1. Shoulder muscles

Muscles act as actuators, whose contraction or distension allows the movements of upper limbs; some muscles perform the movement while others stabilize it through resistance. This happens through the synergic action of the ligaments and the joints thanks to the conformation of the bony structure. A detailed illustration of the upper-limb muscles, whose role in the arm movements are described briefly below, is shown in [Figure 5].

The abduction of the shoulder [shown in Figure 4a, in black] raises the arm on the frontal plane. This movement can be divided into three phases: 0° to 90°, 90° to 150° and 150° to

180°; each phase involves different muscles. In the first phase, the primary abductor muscles are the deltoid and the supraspinatus, which act on the glenohumeral joint to elevate the arm until 90°. The abductor muscles of the second phase are the trapezius and the serratus anterior. In this phase the scapulothoracic joint is engaged until the arm reaches 150° on the coronal plane. Subsequent elevation is limited by passive tension in the pectoralis major and latissimus dorsi, which oppose the upward rotation of the scapula and full arm elevation. For this reason, to achieve the verticalization of the shoulder it is necessary to have a slight axial rotation of the trunk, while all the abductor muscles are engaged.[5]

The adduction of the shoulder [shown in Figure 4a, in red] brings the arm towards the midline of the body, with a maximum of 50°. The adductor muscles are teres major, rhomboid, latissimus dorsi and long head of the triceps.[5]

The flexion of the shoulder [shown in, in black] has a ROM of  $0^{\circ}$ - $180^{\circ}$ . Similar to abduction, also flexion can be divided into three phases.[5] The first one is between  $0^{\circ}$  and  $60^{\circ}$  degrees, where the anterior deltoid, the coracobrachialis and the pectoralis major are the flexors muscles of the glenohumeral joint; this flexion is limited by the tension of the coracohumeral ligament and the passive resistance of teres minor, teres major and subspinous muscles. The second phase is between  $60^{\circ}$  and  $120^{\circ}$ . The action of the trapezius and serratus major muscles allow the rotation of the scapula by  $60^{\circ}$  and the axial rotation of sternoclavicular and acromioclavicular joints by  $30^{\circ}$ . This flexion is limited by latissimus dorsi and the inferior pectoralis major. The last phase is where the rotation of the torso brings the upper limb in the vertical position.

The shoulder extension [shown in Figure 4b, in red] has a ROM of  $0^{\circ}$ - $50^{\circ}$ . In this movement there is the extension of the scapulothoracic and glenohumeral joints. The teres major, teres minor, posterior deltoid and latissimus dorsi muscles act on the scapulothoracic joint while the rhomboids, the trapezius and the latissimus dorsi are responsible for the movement of the glenohumeral joint.

To analyze the shoulder horizonal adduction and abduction [shown in Figure 4c, in red and in black respectively], it must be defined a reference position that is the arm abducted on the coronal plane to 90°. From this position the ROM is 90° for both horizontal abduction and horizontal adduction. The principal actor in these movements is the deltoid whose heads act sequentially during the full movement. The horizontal abductors are Middle Deltoid, Posterior Deltoid, Latissimus Dorsi, Infraspinatus, Teres Minor. The horizontal adductors are Anterior Deltoid, Pectoralis Major, Coracobrachialis.

For internal and external rotation [shown in Figure 4d, in red and black respectively], the rotator muscles rotate the glenohumeral joint by 90° each around the longitudinal axis of the humerus. Latissimus dorsi, teres major, subscapularis, pectoralis major are the internal rotators while the infraspinatus and the teres minor muscles allow external rotation. [5]

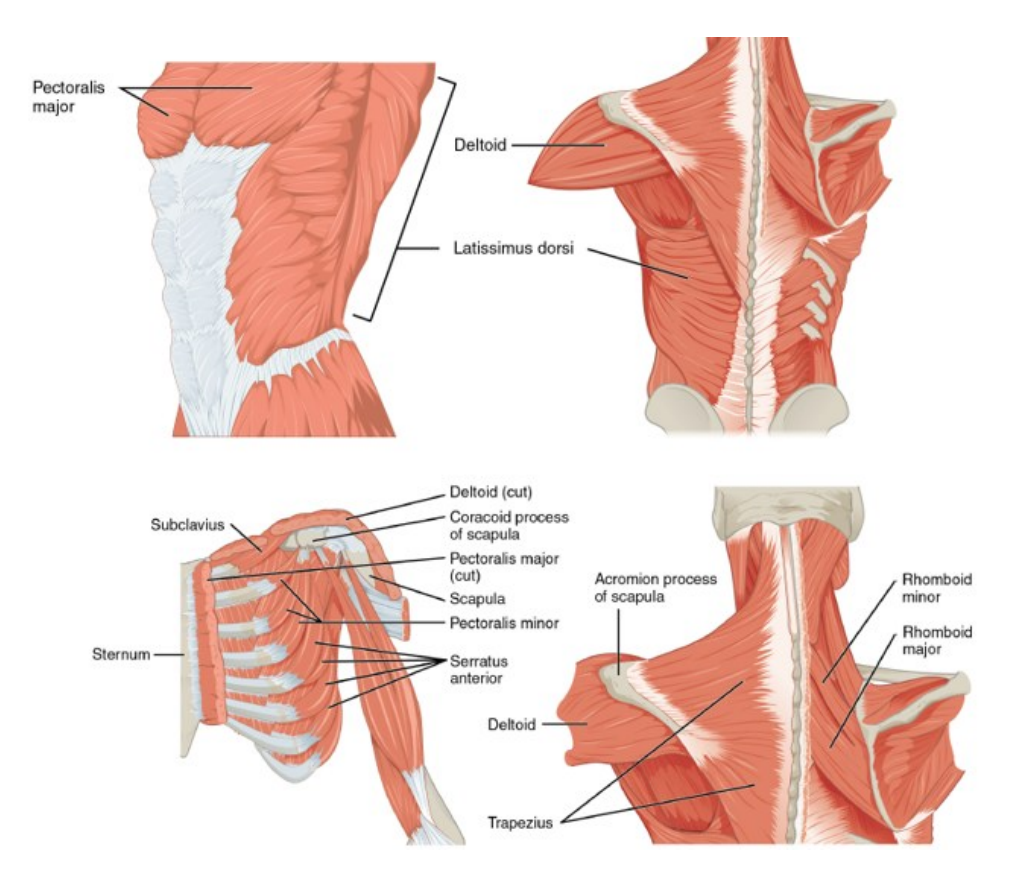


Figure 5: Shoulder Muscles. [7]

#### 1.3. Shoulder Joint Center

In developing exoskeletons that are going to support the shoulder, it is essential to estimate the Shoulder Joint Center (SJC).[8] Misalignment between the mechanical rotation axis of an exoskeleton and the anatomical SJC may lead to unwanted interaction forces, discomfort, or restricted range of motion. SJC describes the average rotation center of the shoulder, it varies between subjects, and it depends on the arm elevation angle.[8], [9]

#### 1.3.1. Estimation of the SJC

To estimate the position SJC, a model was developed by Nef and Riener[8]. This model is based on the synergic action of the scapula, humerus and clavicula while the arm raises, known as scapulohumeral rhythm. To estimate it, they made some simplification, as follows: individuals with similar body size have the same SJC articular movement pattern; training doesn't affect the movement of SJC; assume that the movement is spontaneously made, without conscious control.

The aim of the study is to estimate the position of SJC ( $x_{SJC}$ ;  $y_{SJC}$ ) as a function of the arm elevation  $\theta_1$  in the frontal plane, as shown in [Figure 6a]. The model proposed by Nef e Riener is to consider the Glenohumeral (GH), the Scapulothoracic (SC) and the Acromioclavicular(AC) joints as a ball-and-socket joints, shown in [Figure 6b].[8]

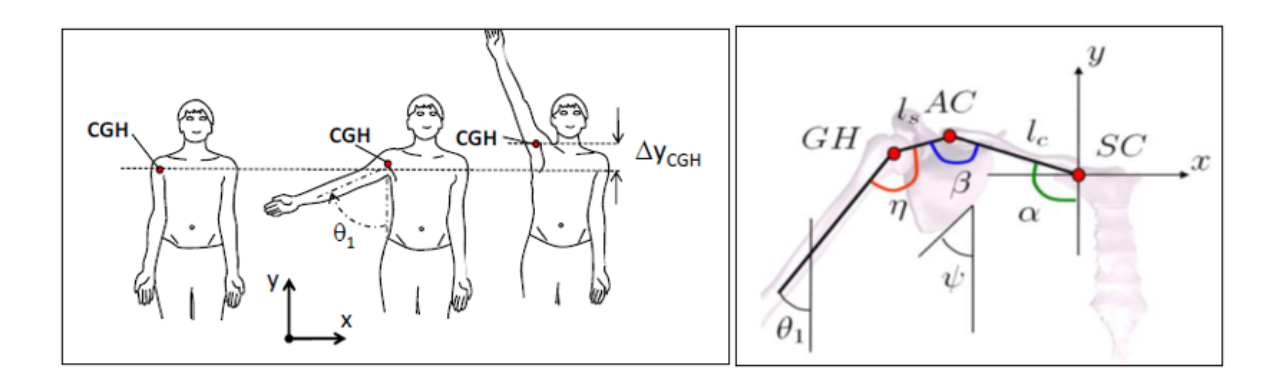


Figure 6: a) Visual representation of the movement of the SJC (referenced here as Center of Glenohumeral Joint CGH) when the arm elevates in the frontal plane.[8] b) Representation of the GH AC SC joints, with the three joint angles.[8]

Applying this model the estimation of the SJC position, assuming that SJC movement is independent of additional masses and the internal/external shoulder rotation, is presented in Eq.1 [8].

$${x_{SJC} \choose y_{SJC}} = {-l_c \cos(\alpha - 90) + l_s \sin(\alpha + \beta) \choose l_c \sin(\alpha - 90) + l_s \cos(\alpha + \beta)} \frac{h}{h_{ref}}$$
 (Eq. 1)

Where  $\alpha$  and  $\beta$  are respectively the joint angles of SC and AC and  $l_s$  and  $l_c$  are respectively the distance between AC and GH, and the distance between AC and SC. h and  $h_{ref}$  are the height of the subject and the reference height which is 180 cm in this case.

The results of the equation at different  $\theta_1$  is presented in and obtained by Ref and Riener using a Computed Tomography data from a man of 180 cm. [8]

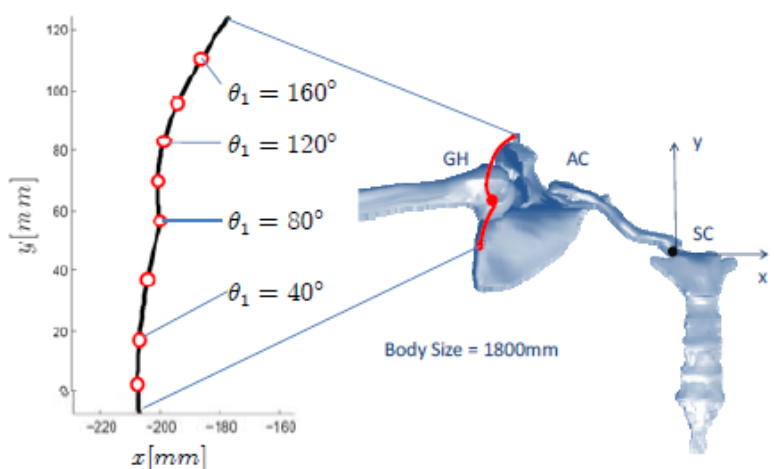


Figure 7: Position of SJC at different angles of elevation [8]

From this graph, it is evident that the displacement in the vertical plane is non negligible, while the displacement in the coronal plane is less significant. So, it is necessary to consider the mismatch of the SJC during the design process of an upper arm exoskeleton.

# 1.3.2. Shoulder Modeling in exoskeleton design

The many degree of freedom (DOF) of the shoulder are the reason why the upper-limb has been modeled in various way. The main challenge is that the position of the shoulder joint centre (SJC) can only be estimated, and the kinematics of the shoulder are intrinsically complex. Different approaches have been proposed in the literature: simplified models that treat the shoulder as a single ball-and-socket joint, intermediate models that add translational components, and more advanced representations that explicitly the scapulohumeral rhythm. While complex models better capture physiological kinematics, they are rarely practical for exoskeleton design, since high accuracy often comes at the cost of increased mechanical complexity and bulkier structures. A balance must be achieved between biomechanical fidelity and design simplicity to ensure ergonomics, safety, and usability.[10]

# **Chapter 2**

# **Industrial Upper-Limb Exoskeletons**

Exoskeletons are mechanical devices designed for the enhancement, support and assistance of the human body.[11] They can be classified according to the anatomical region they support: upper-limb, lower-limb, full-body. Wearable exoskeletons are used and developed for industrial, medical or military sectors.[11], [12] Industrial exoskeletons, on which this thesis is focused, are developed for enhance efficiency and to reduce the work-related musculoskeletal disorders (WMSDs) that manual labour, mostly labour that includes repetitive work, can cause. Among WMSDs, shoulder pain is one of the most prevalent among workers [13]. Besides being categorized by the sector in which they are used, exoskeletons can also be classified as active or passive. Active exoskeletons use powered actuators to assist movement, while passive ones rely on mechanical elements such as springs or dampers to store and release energy. Passive exoskeletons result in the best choice for industrial applications, thanks to their affordability, simplicity of use, lightweight and reliability[11]. In this chapter the state of art of upper-limbs exoskeletons has been analysed.

# 2.1. Passive and Active Torque Generators

During daily activities, human body uses muscles to generate forces that, when exchanged with the external environment, allow interaction with it. To support the body, exoskeletons must generate an assisting force that reduces the workload of the muscles. This force is generated through an actuator within the actuation system for the active exoskeletons. While passive

exoskeletons use passive elements that do not require external energy. Figure 8 shows the most common[14] used actuators and passive elements in passive and active exoskeletons.

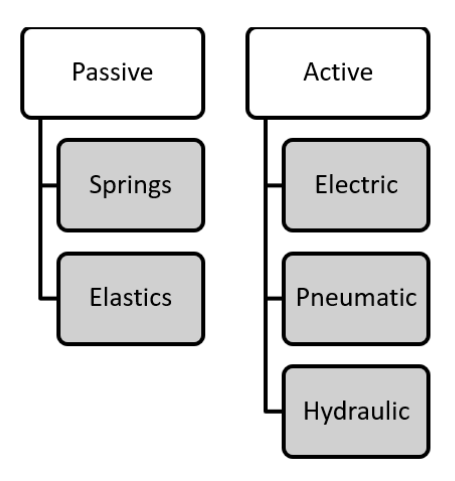


Figure 8: Most common types of passive elements and actuators in exoskeletons

The choice between the actuator and the passive element should consider four main categories [15]:

- Functional activities: health benefits, safety, wearability, comfort.
- Technological characteristics: Torque to weight ratio, DoF, portability, battery, efficiency.
- Financial benefits: purchase cost, repair and maintenance costs.
- Phycological benefits: acceptance and appearance.

This choice strongly affects the overall design of an exoskeleton. While active solutions provide adaptability and higher control, passive systems are lighter, simpler and more suitable for industrial use. However, regardless of the exoskeleton type, the mechanical design must ensure that physiological movements are respected. For this reason, the range of motion (ROM) becomes a key parameter to guarantee ergonomics, safety and effectiveness, as described in the following section.

#### 2.2 Mechanical design

To follow the physiological movements of the shoulder, the design of rigid exoskeletons includes a series of joints that mimic the complex movements of the shoulder.

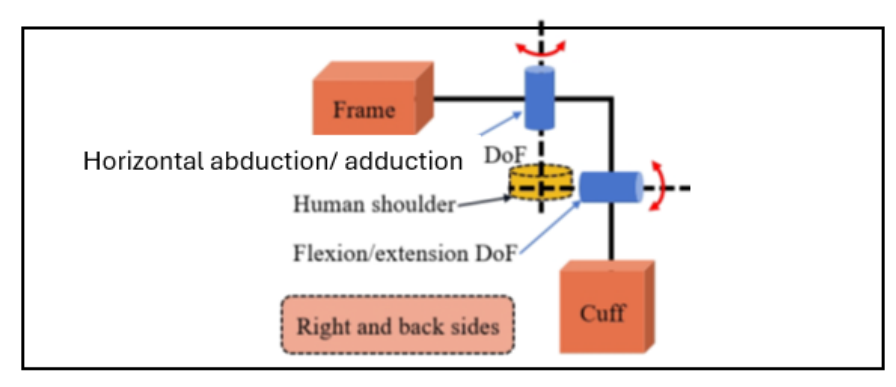
According to Tian et al., industrial upper limb exoskeletons can be classified into two categories based on the arrangement of these joints. They differ in the presence or absence of a joint above the shoulder. [16]

Usually, exoskeletons with the presence of the joint have two degrees of freedom, which allow horizontal abduction/adduction of the shoulder and flexion/extension. These types of exoskeletons are versatile but, regarding ROM, a typical limitation is that it can restrict shoulder movement at higher elevation angles because of inevitable contact between the device and the user.[16]

When the joint is not placed above the shoulder, one solution is to shift it on the back, shown in Figure 9b, or simplify the exoskeleton structure with an arm bar and a back bar connected by

a hinge joint as shown in Figure 9c. These types of solutions result usually in a larger exoskeleton, which may prevent their use in narrow spaces.[16]

#### With a joint above the shoulder



#### Without a joint above the shoulder

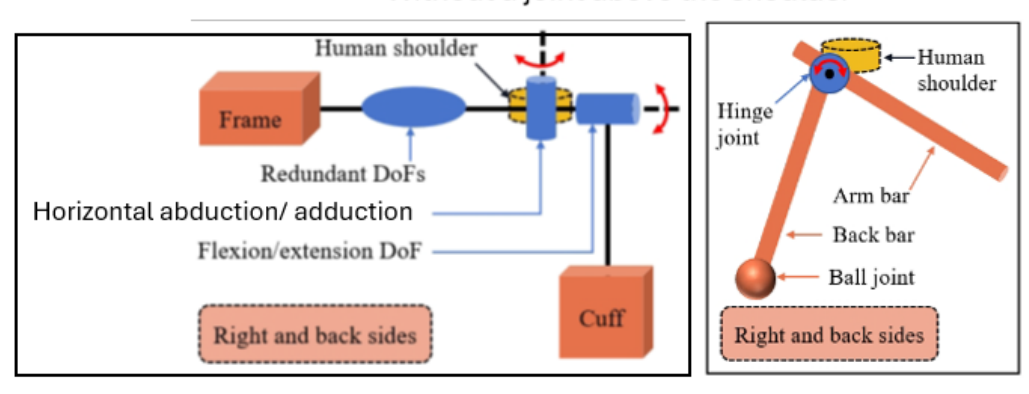


Figure 9: Diagrams of DoF of industrial exoskeletons[16]

The design of the exoskeleton, in addition to providing the right assistance during movement, must also provide maximum mobility and therefore range of motion during use [17]. This is necessary because limited ROM can lead to unnatural positions, which would imply a greater risk of WMSDs as well as a decrease in productivity [18].

If ROM is too limited, the exoskeleton becomes intrusive and may obstacle task execution. On the contrary, if ROM is too permissive without synchronized support profiles, the assistance provided may be insufficient.

Therefore, understanding the influence of ROM in passive exoskeletons is critical both for ergonomic compatibility and support optimization.

#### 2.2.1 State of Art: Passive Upper-Limb Industrial Exoskeletons

To provide a practical perspective on the concepts discussed so far, some examples of industrial upper-limb exoskeletons are presented.

MATE is a portable passive upper-limb exoskeleton commercialized by COMAU[19] which weighs 3.5 kg and uses a set of parallel springs to produce the support torque. As the arm is

lifted, the support provided by the elastic mechanism changes naturally with the movement. The exoskeleton, shown in Figure 10, offers the most assistance when the arm reaches a horizontal position and gradually decreases as the arm lowers back to a relaxed position. The torque is modulable with four different levels. In a study conducted by Pacifico et al. [20] is noticeable that MATE can reduce significantly the level of muscular load, in a range that vary from -2% to -40%. In terms of ROM, it is noticed that in the static trial shoulder abduction-adduction vary from the trial with the exoskeleton and the trial without. Interestingly, this phenomenon has been described by the authors not as a result of uncontrolled forces from the exoskeleton, but rather as an alternative motion strategy adapted by the user in consequence of the fatigue reduction.

Torque Generator

pDOF
pHMI

Figure 10: Photo of proto-MATE[20]

PAEXO is a passive exoskeleton that only weighs 1.8 kg manufactured by Ottobock [21]. It is also based on a spring actuator positioned on the back.

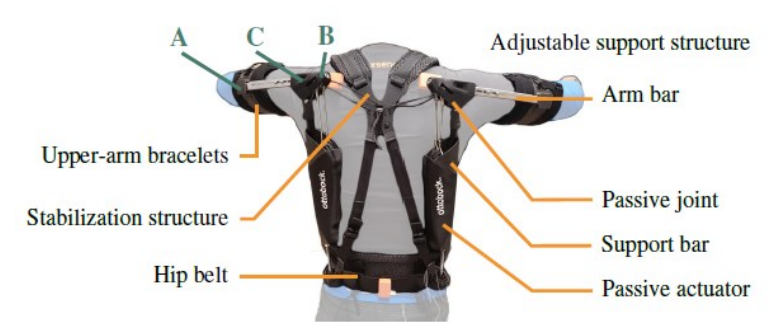


Figure 11: Illustration of passive exoskeleton PAEXO [22]

As shown in Figure 11, the actuator transfers an adjustable arm weight to the hip belt. The actuator is connected with the upper arm through upper-arm bracelets that are connected to the back structure through an arm bar. In a study conducted by Maurice et al. [22] it is proven that PAEXO effectively reduce the deltoid workload by 55%. Interestingly, subjects of this study did not perceive a restrain in ROM and the position with the exoskeleton resulted, like MATE, in a more abducted position.

# 2.2.2 State of Art: Range Of Motion Evaluation

Tiejun Ma, Erik Jonathan and Shuping Xiong [18] noticed that the effects of exoskeletons on ROM has not been extensively studied. They highlighted that an inadequate ROM due to the exoskeleton could lead to work-related musculoskeletal disorders. However, their study suggests also that thanks to the performance enhancement that exoskeletons provide, exoskeleton can also improve the subject ROM, especially when subjected to external load.

So, they conducted a preliminary study in order to investigate the ROM's mechanism changes determined by the use of the exoskeleton.

The study involved 9 healthy young subjects and a passive shoulder exoskeleton, the CDYS developed by Crimson Dynamics.

According to the manufacturer[23], the CDYS exoskeleton has a total weight of 2.6 kg and provides seven adjustable support levels. It is suitable for users with a height ranging from 165 cm to 195 cm.



Figure 12: CDYS Passive exoskeleton by Crimson Dynamics[18], [23]

It was designed to assist with repetitive arm-raising tasks and, to achieve this, it incorporates passive springs systems into the waist strap.

To investigate on ROM changes, the authors defined three user-exoskeleton configurations:

- ExoForce: Tasks done with the engaged exoskeleton
- ExoNoForce: Tasks done with the disengaged exoskeleton
- NoExo: Tasks done without the exoskeleton

To further investigate the external load impact on ROM with or without the exoskeleton, each configuration was test under three load condition: no load, 3 kg load and 6 kg load.

Each subject conducted three shoulder ROMs tasks summarized in Table 2 and visualized in Figure 13.

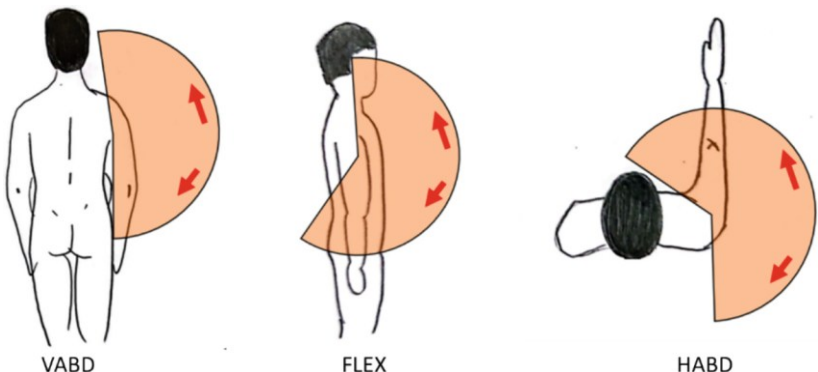


Figure 13: Visualization of the three shoulder ROMs tass[18]

Table 2: Summary of the three ROM exercises. R=Repetitions

Task	Starting position	Movement	R
Vertical Abduction/Adduction VABD	Standing upright, dominant arm straight at shoulder height, parallel to coronal plane.	Arm abducted upwards along coronal plane to maximum limit, then adducted back as close to the plane as possible, returning to initial position.	5
Flexion/Extension FLEX	Standing upright, dominant arm along the trunk, thumb pointing forward.	Arm flexed upwards along sagittal plane to maximum limit, then extended backwards, returning to initial position.	5
Horizontal Abduction/Adduction HABD	Standing upright, dominant arm straight at shoulder height, parallel to coronal plane.	Arm moved horizontally towards the non-dominant side (adduction), then extended backwards (abduction), returning to initial position.	5

In order to measure the motions of the subjects, the subjects were equipped with the wearable Xsens MVN system, an inertial motion capture technology based on wearable inertial sensors (accelerometers, gyroscopes, magnetometers) that track body movements in 3D.

The main findings of the pilot study are summarized below:

- 1. VABD (Vertical Abduction/Adduction)
  - a. ROM was significantly reduced in the ExoWithForce condition compared to NoExo.
  - b. A similar, though non-significant, reduction was observed in FLEX.
  - c. These results align with previous studies reporting decreased shoulder extension and adduction with passive exoskeletons [24]
- 2. ExoNoForce condition
  - a. The presence of the exoskeleton acted as an additional load, slightly reducing ROM.
  - b. Mechanical design features may introduce friction or resistance during movement.
  - c. Users appeared to adopt a more conservative ROM, likely influenced by the presence of the exoskeleton.
- 3. Supportive force effects
  - a. For VABD and FLEX, the supportive force had minimal impact, indicating that physical design is the primary factor limiting ROM.

b. For HABD, ROM in ExoWithForce was higher than in ExoNoForce, suggesting that supportive forces can partially counteract gravity, enhancing mobility in this plane.

This case study demonstrates that both the mechanical design and supportive forces of passive exoskeletons significantly influence shoulder ROM, with implications for ergonomics, safety, and performance in industrial applications.

# **Chapter 3**

# **Exoskeleton Prototype**

In this thesis, the study focused on the exoskeleton prototype designed by Paterna et al. [25]. The device is an upper-limb exoskeleton designed for industrial applications, intended to support the workers during overhead tasks. A distinctive feature of this prototype is its actuation system, which relies on two Pneumatic Artificial Muscles (PAMs). When pressurized, these muscles act through a transmission mechanism to assist the shoulder joint during arm elevation. A CAD overview of the prototype can be seen in Figure 14.

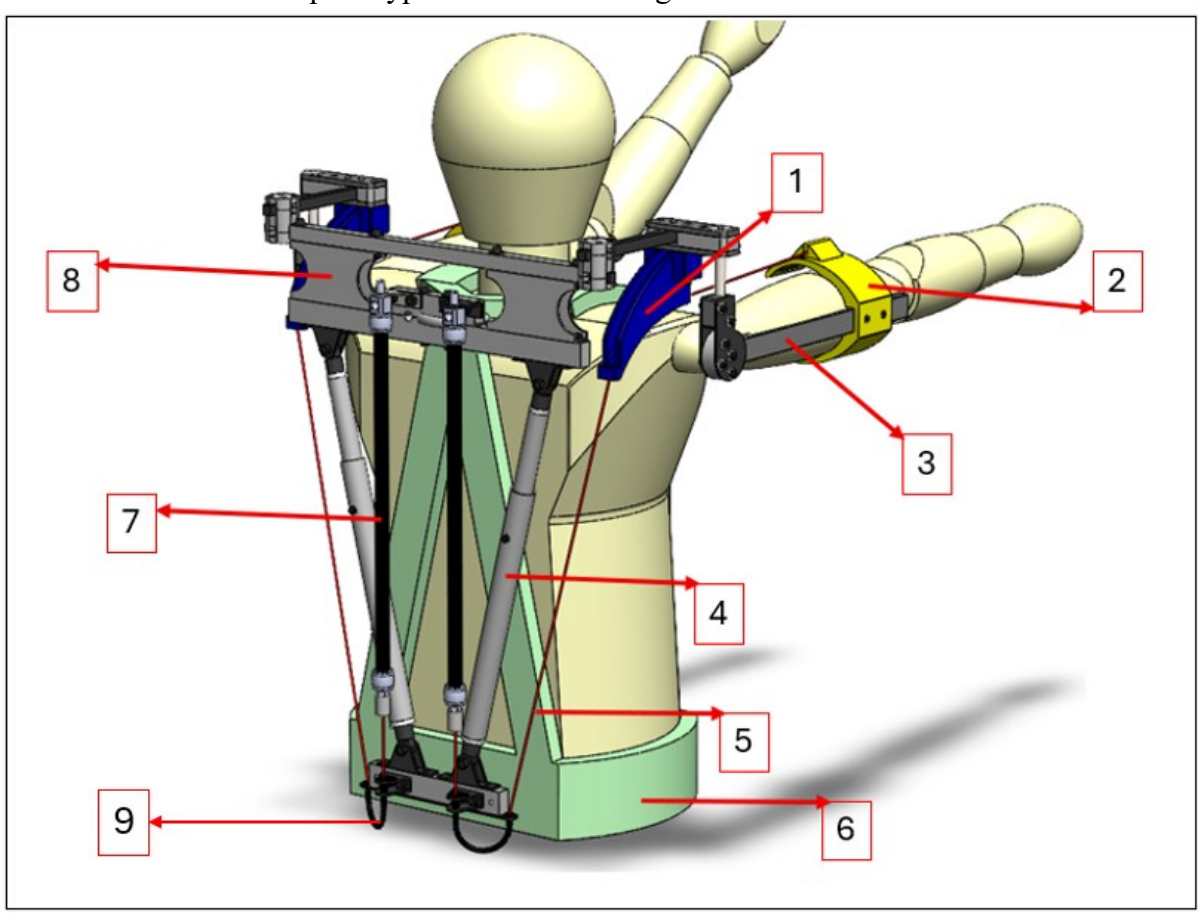


Figure 14: Prototype CAD with mannequin. 1.Shoulder Pad 2. Bracelet 3. Guide for the bracelet 4. Telescopic rod 5. Transmission wire 6. Harness 7. Pneumatic artificial muscle

The prototype developed by Paterna[25] is structured as follows:

The actuation system is based on two pneumatic artificial muscles (7). The PAMs are used as a passive torque generator: the PAMs are pressurized at a specific pressure, which depends on the load that the user will have in the hand. So, in this prototype they are used as a passive elastic element.

These PAM generate a tensile force that is transmitted through an inextensible cable (5) that is attached to the free end of the PAM. The other end of the PAMs is anchored to the back frame (8). The cable is guided by a sheath (9) through the shoulder pad (1). The shoulder pad regulates the support moment delivered to the user via the bracelet (2), which is sustained by a bracelet guide (3) that also allows the adjustment of the bracelet's distance.

The back frame is integrated with a wearable harness (6) to ensure proper fitting on the user. Additionally, the back frame (8) incorporates a telescopic rod that enables the adjustment of

the device's width across the shoulders, allowing adaptation to different body sizes. To ensure that the prototype have also two vertical telescopic rod that can adjust the height of the back frame structure.

The device can be worn by subjects with a height ranging from 160 to 175 cm. The shoulder width is adjustable between 370 and 410 mm.

The overall weight of the device is 5.5 kg, and it provides assistance to the upper limbs for loads not exceeding 2 kg.

#### 3.1 Pneumatic Artificial Muscles

The core of the prototype is its torque generator, the pneumatic artificial muscle. In this design, two PAMs are used, fixed in the back frame as shown in Figure 15. These muscles generate the support torque which is intended to assist the shoulder and reduce fatigue during overhead tasks.

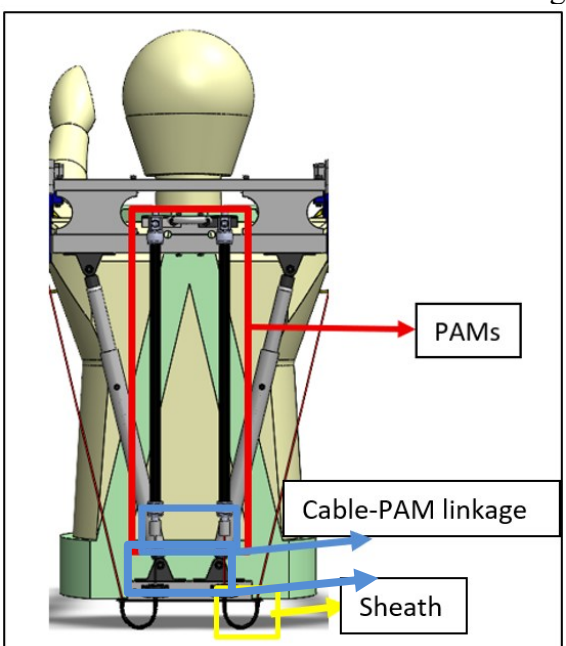


Figure 15: PAMs positioning in the prototype with transmission elements.

PAMs are essentially closed elastic membranes that can be pressurized. Their peculiarity is that the membrane is overlaid with a braided fibre mesh. The mesh and the geometry of the membrane varies depending on the type of pneumatic artificial muscle, some examples are shown in Figure 16.

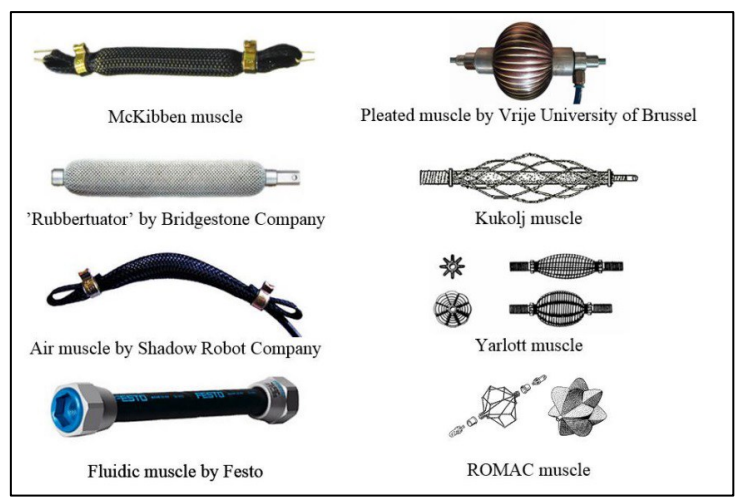


Figure 16: Different PAM types[26]

PAMs have several advantages, the most important is their high power-to-weight ratio [27]. So, PAMs are lightweighted and can generate powerful forces with easily controlled compliance. Thanks to their advantages they are used in various contexts, also in the medical field. [28]

McKibben muscle (MKMs), which functioning is shown in Figure 17, is the most used and improved braided PAM[29][30], thanks to their simple structure and their easy assembly[28]. Their design is based on an inner elastic tube that inflates when air pressure is applied, while a braided fibre mesh around it limits the radial expansion. The inner elastic tube and the braid are fixed to end fittings on both sides[28]. As a result, the actuator shortens along its length and generates a pulling force. This principle allows MKMs to behave in a way that is quite similar to natural muscles.

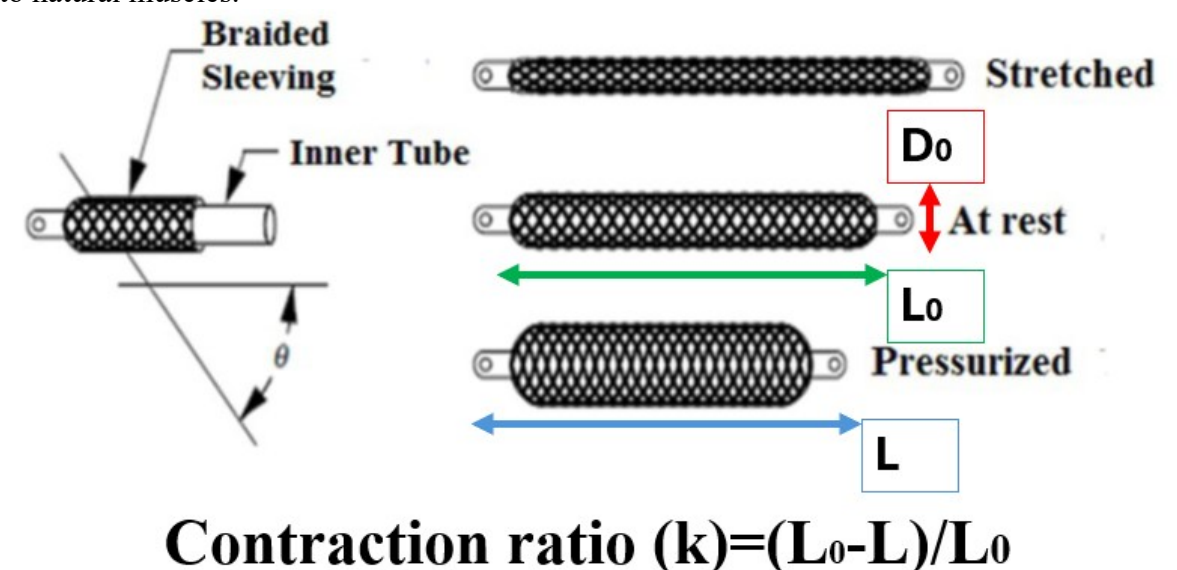


Figure 17: Braided PAM functioning[31]

The performance of MKMs depends on different factors, such as the angle of the fibers in the mesh  $(\theta)$ , the material of the elastic bladder, the diameter  $(D_0)$ , the nominal length  $L_0$ , the supply pressure (p), and the contraction ratio (k).

Briefly, these parameters, shown in Figure 17, influence the generated force in the following manner[32]:

> Pressure (p): The generated axial force increases with the internal pressure.

- ➤ Contraction ratio (k): As the muscle shortens and the contraction ratio increases, the axial force decreases. This occurs because the braid angle becomes larger during contraction, which reduces the component of force acting along the muscle's longitudinal axis.
- Angle of the fibers in the mesh  $(\theta)$ : A smaller initial angle produces higher forces but limits the achievable shortening, whereas a larger angle allows greater contraction but leads to a lower output force. Since the braid angle changes during actuation, the instantaneous force depends on its current value.
- ➤ Initial diameter (D₀): A larger initial diameter increases the effective cross-sectional area on which the pressure acts, thereby increasing the output force for the same internal pressure.
- ➤ Initial Length (L₀): Increasing the initial length generally leads to a slight reduction in the overall force for a given pressure, because the same pressure must deform a longer structure, distributing the load over a greater distance.

Because of this, MKMs can be designed to fit different applications. On the other hand, their mechanical response is nonlinear and shows hysteresis, which makes them more difficult to model and to control compared to traditional actuators.

The hysteresis mainly due to the friction of the mesh but also the viscoelastic proprieties of the PAM membrane and the compressibility of the air.[33]

Even with these limitations, MKMs are very interesting for robotics and biomedical applications. They are light, flexible, and safe to use with humans, because of their controllable compliance. At the same time, they have a very high power-to-weight ratio, being able to generate forces up to 6000 N while weighing less than one kilogram. This makes them suitable for wearable systems, exoskeletons, or rehabilitation devices, where both force and portability are important.[27]

Thanks to these characteristics, MKMs represent a practical solution for developing an actuation system that is at the same time powerful, lightweight, and suitable for assistive technology.

In this prototype, McKibben Muscles produced by FESTO S.p.A., shown in Figure 18, (model DMSP-10-350N-RM-CM) were used. These actuators have a nominal length of 350 mm and were chosen because they offer a good compromise between size and performance. They are also commercially available and well documented, which makes it easier to integrate and to test.



Figure 18: FESTO MKM[34]

As described previously, the prototype utilizes two MKMs, one for each limb. Each of these MKMs is capable of contracting up to 25% of its nominal length and can exert a maximum force of 650 N.

It should be noted that, as said before, the force output is not a linear function of the contraction ratio. This nonlinearity is illustrated in Figure 19, which shows the relationship between the force generated by the FESTO DMSP-10 PAM and its contraction ratio.

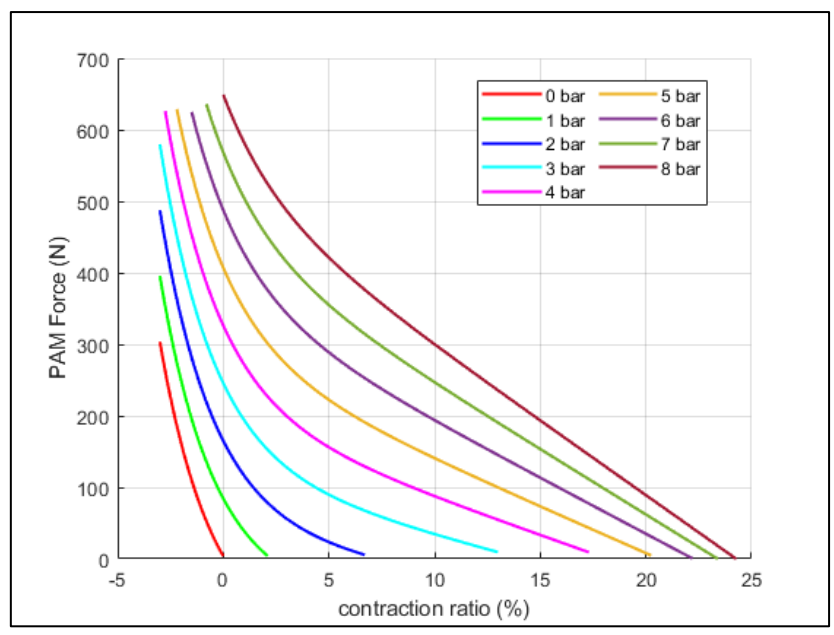


Figure 19: Static characteristics of MKM FESTO DMSP-10[25]

#### 3.1.1. Mathematical Models

The behaviour of McKibben Muscles and PAMs has been investigated through different mathematical models, because, as mentioned before, their response is strongly nonlinear and depends on several parameters.

According to Wafaa Al-Mayahi et al. [27] there are three different modelling types for PAMs: geometrical, phenomenological and empirical.

#### 3.1.2. Geometrical Model

The first approach that is usually considered in literature [27], [30] is the geometrical model. The Chou and Hannaford model [35] and the Tondu and Lopez model [36] are the most commonly used [28].

The Chou and Hannaford model is a static physical model of MKMs based on the assumptions[35]:

- 1. The PAM is modelled as a perfect cylinder with a negligible thickness.
- 2. The PAM volume depends only on its length.
- 3. The system is without leakage and without energy storage.

So, under these assumptions they were able to find the relationship between pressure, tension and length by applying the principle of the conservation of energy:

$$dW_{out} = dW_{in} (Eq. 2)$$

Where the input work ( $W_{in}$ ) is done by the gas pushing on the inner surface of the MKM and the output work ( $W_{out}$ ) is done by the shortening of the actuator:

$$dW_{in} = PdV (Eq.3)$$

$$dW_{out} = -FdL (Eq.4)$$

Combining (Eq. 2) with (Eq. 3) and (Eq. 4):

$$F = -P\frac{dV}{dL} \tag{Eq. 5}$$

Where P is the relative pressure, F is the tension and dL the displacement. Under the assumption 1. and the following geometry parameters illustrated in Figure 20.

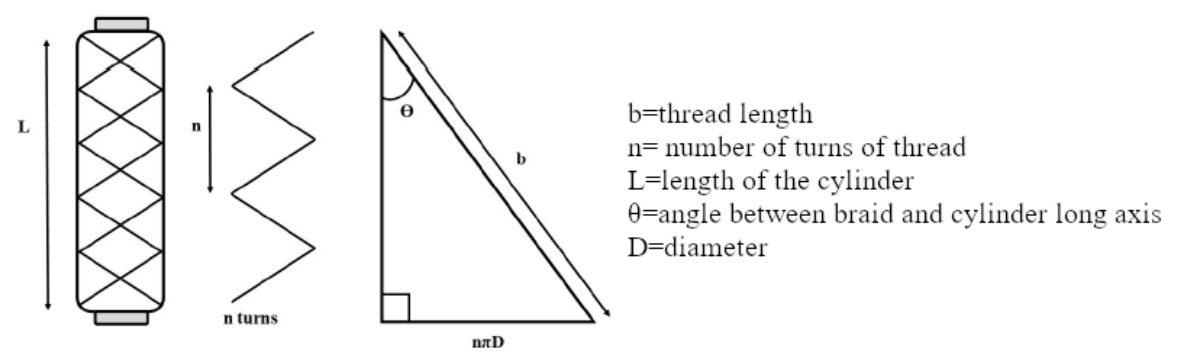


Figure 20: Simplified geometry of MKM. Adapted from [28]

Force F can be expressed as a function of  $D_{90^{\circ}}$ , the diameter of when theta equals  $90^{\circ}$ , P and theta as shown in equation (Eq.6).

$$F = \frac{\pi D_{90^{\circ}}^{2} P}{4} (3\cos^{2}\theta - 1)$$
 (Eq. 6)

So, based on this model, the maximal shortening will be at theta 54.7° while the force is linearly proportional to P.

Tondu and Lopez model is based on the principle of virtual works, and they express the contraction force as a function of the pressure and the contraction as shown in (Eq.7)

$$F(\varepsilon, P) = \pi r_{90^{\circ}}^{2} P[\alpha(1 - \varepsilon)^{2} - \beta]$$
 (Eq. 7)

Where  $\alpha = \frac{3}{\tan^2 \theta_0}$ ,  $b = \frac{1}{\sin^2 \theta_0}$ ,  $\varepsilon = \frac{l_0 - l}{l_0}$ ,  $0 \le \varepsilon \le \varepsilon_{max}$  with  $\theta_0$  the initial angle.

#### 3.1.3. Empirical model

PAMs mechanical behaviour is similar to a spring, while the compilance of the spring remains the same and depends on the material properties and the geometry, the PAM compliance is variable and depends also on the inside pressure.

Wickramatunge et al. [37] developed an experimental model where the force generated by PAM is similar to a force generated by a mechanical spring, where the stiffness of PAM, k, is described by a second order polynomial of the pressure (p) and the stretched length of the PAM (L<sub>s</sub>). Eq.8 describes the relation between generated force (F) and stiffness, Eq. 9 describes the relations between stiffness, stretched length and pressure. Applying the least square method, the coefficients q<sub>1</sub>, q<sub>2</sub>, q<sub>3</sub> and q<sub>4</sub> can be found through the experimental data.[37][28]

$$F = K(P, L_s)L_s (Eq.8)$$

$$F = K(P, L_s)L_s$$
 (Eq. 8)  

$$k = q_1 + q_2L_s^2 + q_3PL_s + q_4P^2$$
 (Eq. 9)

#### 3.1.4. Phenomenological Model

In order to describe better the dynamic performance of PAM, the phenomenological model has been introduced[27]. The dynamic model of PAM can be described with a dumper, a spring and a contractile element[38] as shown in Figure 21.

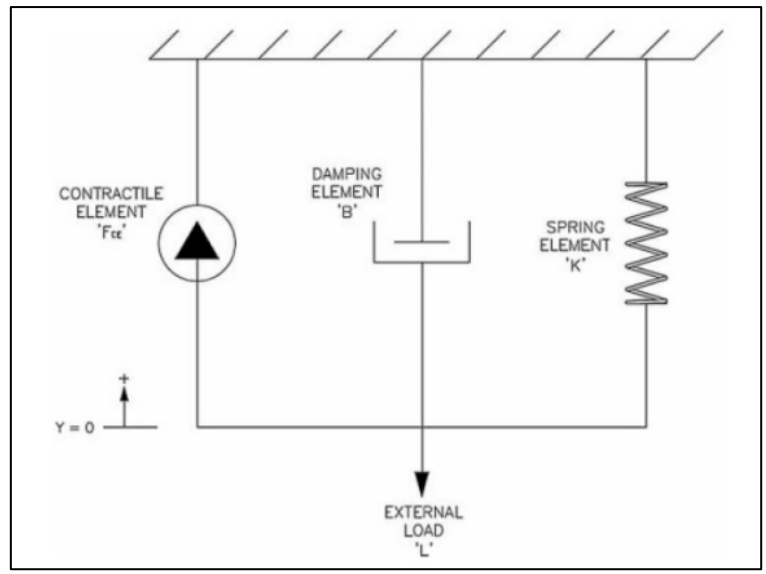


Figure 21: Phenomenological model[38]

This model can be mathematically described by (Eq. 10) where y is the displacement of the contractile element, L is the external load, M is the mass, B the damping coefficient, k the spring coefficient and F<sub>ce</sub> is the contractile force.

$$My + B\dot{y} + ky = F_{ce} - L \tag{Eq. 10}$$

Pitel et al. [39] used one of the oldest phenomenological model, the modified Hill's muscle model [40], to describe the PAM dynamic behaviour. This model consists in a variable dumper and a variable spring in parallel.

Pitel et al. approximated the dynamic response of the PAM using six unknown parameters as shown in Eq.11 [40]

$$F(k,p) = (a_1p + a_2)e^{a_3k} + a_4kp + a_5p + a_6 (Eq. 11)$$

Where k is the contraction ratio, p the pressure and the coefficients  $a_i$  (i=1,2,3,4,5,6) can be found interpolation of the experimentally obtained characteristic curves.

#### 3.2 Transmission system: The Shoulder Pad and the Bracelet

So, PAMs are the actuators responsible for generating the force required to support the user's arm. When the PAM is pressurized, it contracts and produces a pulling force, which is transmitted through a non-extensible cable attached to one end of the actuator, the PAM-cable

linkage shown in Figure 15. This cable is guided through a sheath, shown in Figure 15, and guided toward the shoulder pad.

The shoulder pad constitutes a fundamental component of the exoskeleton, as it modulates the assistive torque generated by the PAM and delivered to the upper arm through the bracelet. So, the cable, resting on the shoulder pad, is ultimately connected to arm bracelet that transfers the torque to the user's arm, enabling mechanical support during motion. An overview of the exoskeleton arm is shown in Figure 22.

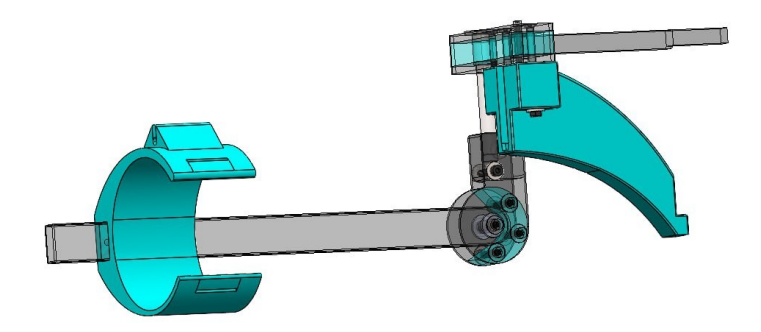


Figure 22:CAD visualization of bracelet and shoulder pad

#### 3.2.1. Profile of Shoulder Pad

Paterna[25] designed the shoulder pad to achieve an optimal balance between gravitational forces and the torque provided by the exoskeleton.

The design has been achieved through graphical method, keeping in mind that the profile need to compensate the PAM's decreasing pulling force when the angle of elevation increases. Although the gravitational torque also decreases with arm elevation, the reduction in the PAM traction force is not proportional and occurs more rapidly. Therefore, it is necessary to compensate for this effect by varying the moment arm. So, it is necessary to increase it as the elevation angle rises.

The first step is to define the initial shoulder pad radius, when  $\theta_1$ , shown in Figure 23, is equal to 90 degrees.

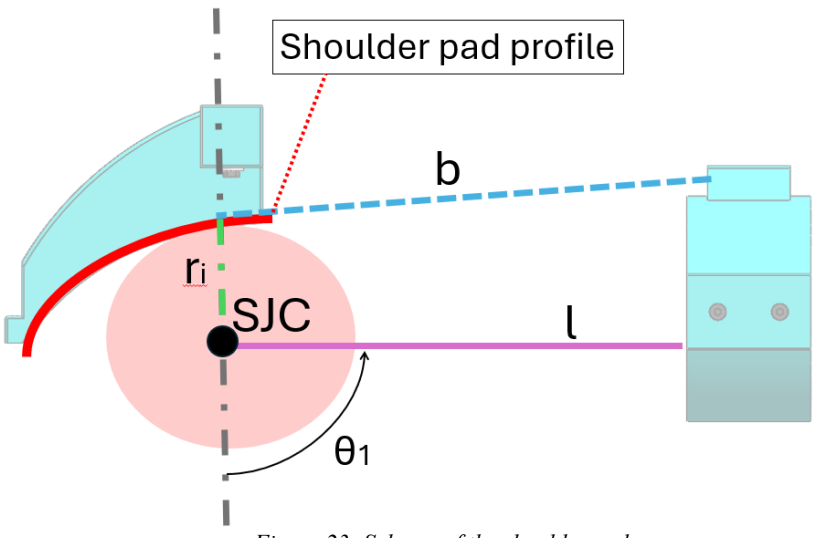


Figure 23: Scheme of the shoulder pad

It is essential that the shoulder pad does not come into contact with the shoulder and does not obstruct the user's field of view. For this reason, the initial radius  $(r_i)$  was set to  $r_i = 0.045$  m. The final radius $(r_f)$ , on the other hand, was selected to minimize the root mean square error (E), shown in Eq.12, between the gravitational torque  $(M_g)$  and the torque generated by the exoskeleton  $(M_{MKM})$  while ensuring that the shoulder pad would not become excessively large or invasive. This final radius resulted in  $r_f$ =0.07 m.

Once the initial and final radius were defined, the shoulder pad profile was achieved graphically through circular interpolation.

$$E = \sqrt[2]{\frac{1}{N} \sum_{i=1}^{N} (M_{MKM_{\theta_1}} - M_{g_{\theta_1}})^2}$$
 (Eq. 12)

#### 3.2.2. The Torque profiles

As previously mentioned, the support torque generated by the shoulder pad was designed to minimize the root mean square error between the assistive torque and the gravitational torque. This evaluation was performed under three conditions: with only the arm weight, with an additional 1 kg load, and with a 2 kg load held in the user's hand. The pad profile was specifically optimized for a range of  $\theta_1$  between 90° and 135°. In fact, in the prototype, arm flexion was limited to 70°, since below 90° angle the support torque increases, requiring the user to apply a considerable force to lower the arms comfortably.

Figure 24 illustrates the support torque of the shoulder pad compared to the gravitational torque within the operational range of the prototype. The pressures indicated in Figure 24 correspond to the pressures applied to the pneumatic muscle, selected in order to apply the most appropriate torque in order to minimize the mismatch between gravitational and support torque.

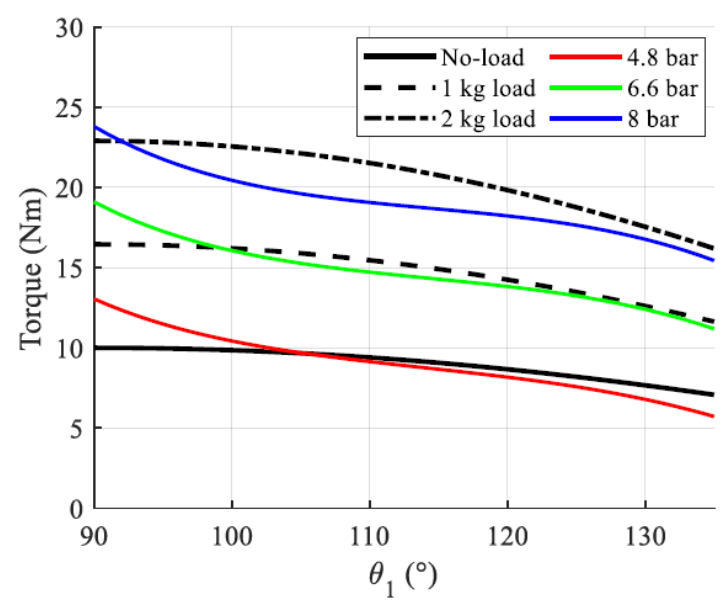


Figure 24:In black: Gravitational torque Colored: Support torque. Comparison between support and gravitational torque in three different configuration: without external load in the user's hand (red line e and solid black line), with 1kg external load (green line and dashed black line), with 2kg external load (blue line and dotted and dashed black line)[25]

The force of MKMs has been calculated using the model proposed by Pitel et al. with the equation shown in Eq. (11). The lever arm at four different angles has been measured in the CAD, and in order to obtain the values at the other angles, a fourth-degree polynomial fitting has been applied.

#### 3.2.3. Prototype kinematic chain

The exoskeleton relies on a kinematic chain with two degrees of freedom, enabling shoulder abduction and flexion—extension. This configuration offers advantages in terms of compactness and mechanical simplicity, but it does not eliminate the issue of joint misalignment. To minimize this problem, it is essential to align the SJC with the exoskeleton joint center (ExoJC). The challenge lies in the fact that the anatomical SJC shifts during arm elevation as previously discussed. As a result, when the user lifts the arm, the SJC moves upward while the ExoJC remains stationary. This relative displacement causes the bracelet to slide along the arm, generating shear forces between the interface and the user's skin. Furthermore, the exact location of the SJC cannot be determined with absolute precision, which adds another layer of complexity.

To evaluate the consequences of this misalignment, Paterna[25] conducted an analysis under the assumption that when the angle of elevation is 90 degrees, the SJC and ExoJC are perfectly aligned. Under that hypothesis the results of Paterna's study showed that, under most working conditions, the support torque provided by the device is adequate and the induced shear force in the arm remained within acceptable limits.

To obtain the two DoF in the prototype, two hinges have been proposed:

A vertical axis hinge joint that allows the abduction and a horizontal axis hinge joint that allows flexion. The two axes, in an ideal situation, must intersect in the SJC. Figure 25 shows the abduction/adduction and flexion/extension hinge joint adopted in the prototype of the exoskeleton with highlighted their axis and the intersection point that is ideally SJC.

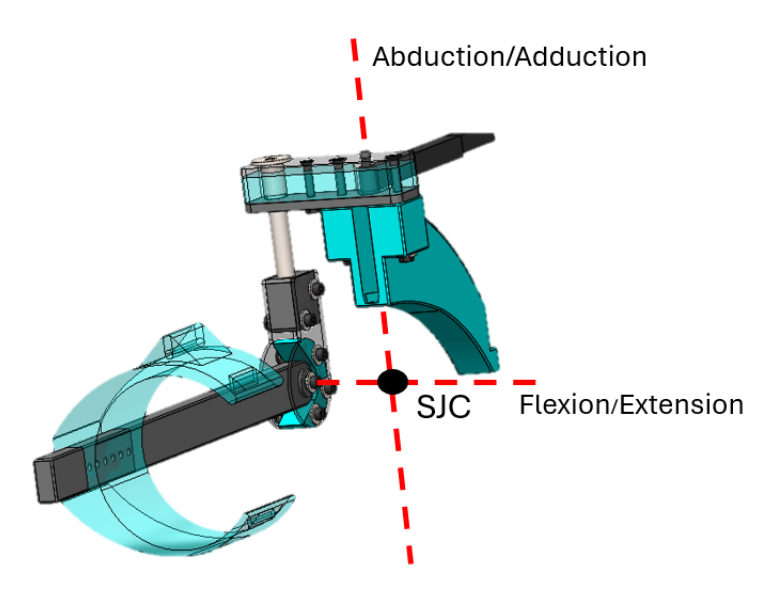


Figure 25: Prototype hinge joints

#### 3.3. Range Of Motion of the Prototype

The prototype allows shoulder flexion between  $70^{\circ}$  and  $135^{\circ}$ . However, moving the arms below  $90^{\circ}$  requires the user to exert a considerable effort. Although the exoskeleton is capable of providing at least 75% of the gravitational torque between  $90^{\circ}$  and  $135^{\circ}$ , the inability to comfortably lower the arms significantly compromises its usability with the current transmission system. To address this limitation, two potential design solutions will be presented.

# Chapter 4

#### The New Bracelet

The first proposed solution was specifically designed to avoid major alterations to the existing structure of the exoskeleton prototype.

After analyzing the available options, it was decided to intervene by modifying the final component of the transmission system: the bracelet. As mentioned earlier, the bracelet is the last element that connects the inextensible cable to the arm and is responsible for applying the support torque to the user's arm.

#### 4.1. Design goals

The redesign of the bracelet was structured with the following considerations in mind:

- The previous bracelet had a very small diameter, which prevented larger arms from fitting.
- The modifications made to the bracelet must not substantially alter the support torque.
- The bracelet must include a release mechanism that allows the arm to be lowered with ease while the artificial muscles are pressurized.
- The release mechanism has the mainly scope of enhance the Flexion ROM.
- The design has to take account of the assembly process.
- The bracelet will be 3D printed.
- This release mechanism should be:
  - o Intuitive and easy to use
  - Safe

#### 4.2. New Diameter

To select the new diameter, a literature review was carried out. Data were taken from the National Health Statistics Report 2003–2006 US [41]. This report provided the mean and standard deviation of the mid-arm circumference for women and men over the age of 20. The averages were further divided not only by sex but also by age groups.

Considering the industrial context of the exoskeleton in question, the mean and standard deviation of the mid-arm circumference for women and men aged between 20 and 59 years were selected. The means and standard deviations (std) are reported in Table 3 for women and in Table 4 for men.

Table 3: Mid-arm circumference in centimetres for females in working age.

Mid-arm circumference in cm for females

Age [Years]	Mean [cm]	Std [cm]
20-29	30.3	0.3
30-39	31.9	0.29
40-49	32.7	0.28
50-59	32.8	0.23

Table 4: Mid-arm circumference in centimetres for males in working age.

Mid-arm circumference in cm for males			
Age [Years]	Mean [cm]	Std [cm]	
20-29	33.7	0.23	
30-39	34.6	0.17	
40-49	35.1	0.2	
50-59	34.2	0.2	

The grand mean and the mean of the standard deviations were calculated for women and men, obtaining the results shown in Table 5.

Table 5: Grand mean and std mean for female and males in working age

[cm]	Females	Males
Grand Mean	31.9	34.4
Std mean	0.275	0.2

Based on the obtained values, a circumference of 34.5 cm was selected for the new bracelet. Meaning that the 75th percentile of women and the 50th percentile of men aged from 20-59 years [41]can fit their arm in the bracelet.

# 4.3. Release System

As mentioned before, the release system should be safe and intuitive.

The mechanism must be safe to prevent unintentional release or break. It should also be intuitive and easy to use, so as not to unnecessarily complicate the use of the exoskeleton.

To develop a release mechanism that allows the arm to be lowered, the bracelet was designed in five parts, as shown in Figure 26.

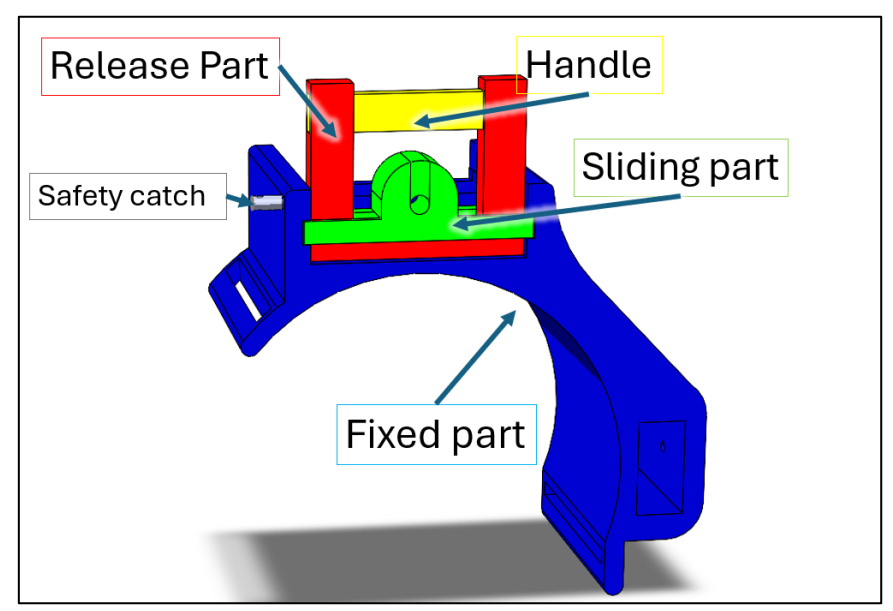


Figure 26: Cad overview of the new bracelet with the release system

The fixed part will be fixed with two bolts to the bracelet guide shown in Figure 26. The sliding part is connected with the transmission cable as shown in Figure 27.

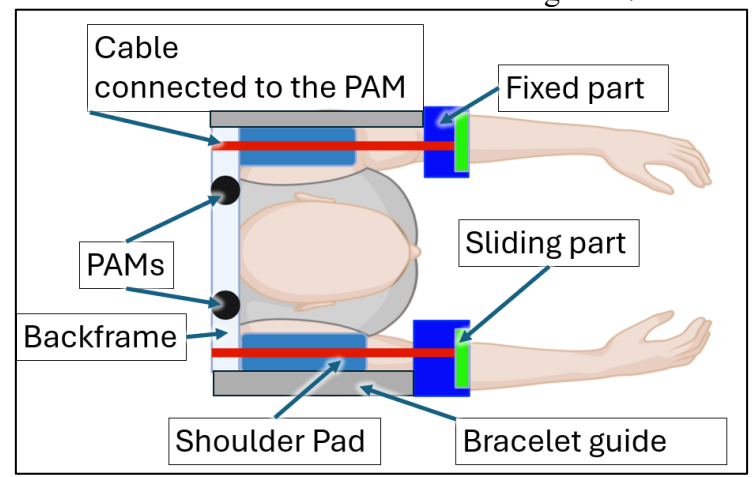


Figure 27: Simplified Schematization of the new bracelet in the exoskeleton prototype

The functioning of the release mechanism follows the following steps:

- Safety Catch removal, as shown in Figure 28a and 28b.
- Handle lifted till the release part is entirely in the sliding part. As shown in Figure 28c and 28d.

• Under the pulling force of the transmission cable, the now free sliding part will slide through the fixing part, as shown in Figure 28e and 28f, allowing the arm to be lowered thanks to the lack of tension.

For the future chapters the state shown in Figure 28d will be referred as the "Released state" and the initial state shown in Figure 28a as "Locked state".

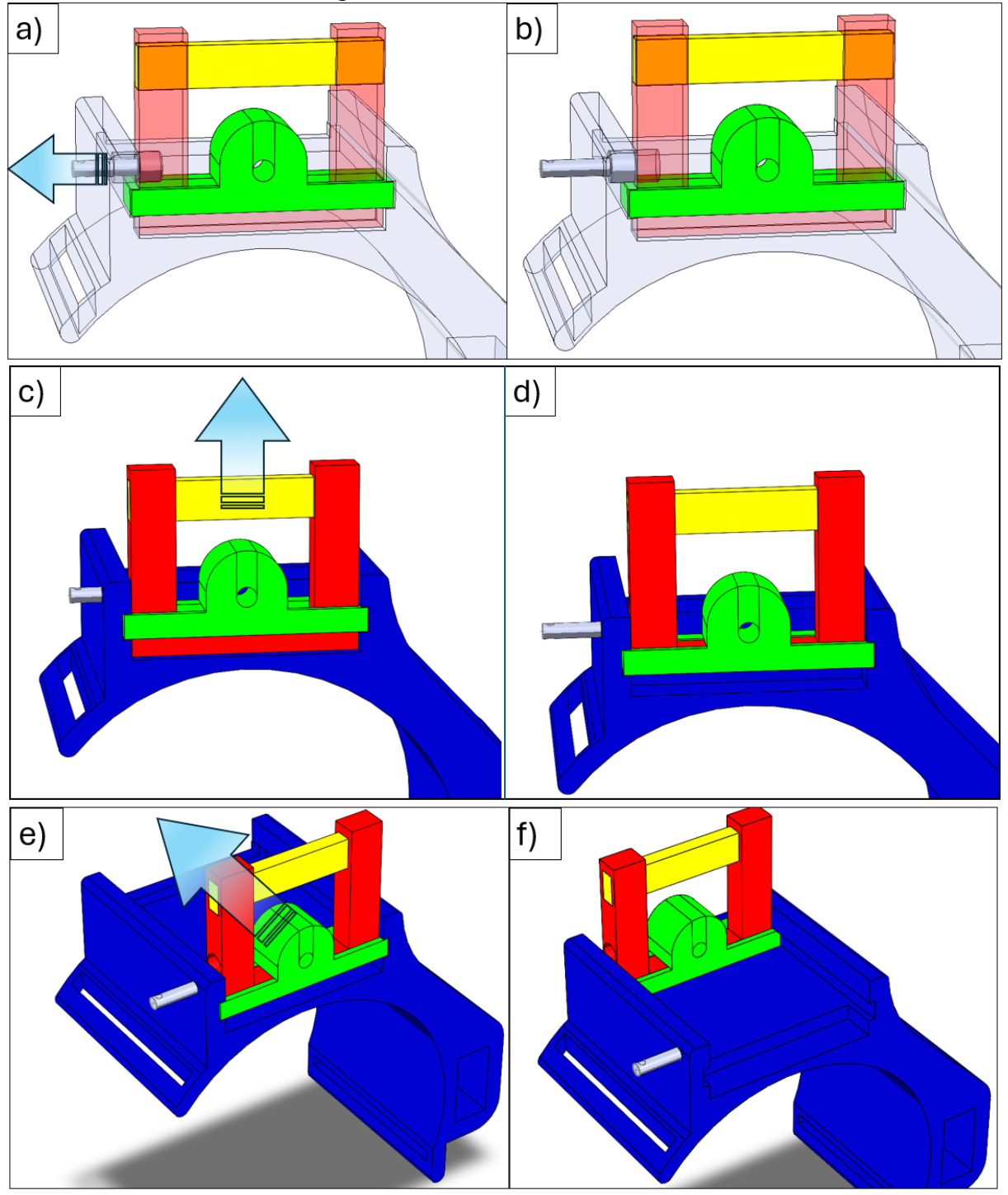


Figure 28: CAD assembly of the new bracelet in different state: a) locked state, locked safety catch. b) locked state, removed safety catch. c) Locked state, lifting of the release part. d) Release state, release part totally lifted. e) Release state, sliding of the Sliding Part. f) Release state, Release Part stopped by the stop block.

In the following sections, the components of the new bracelet will be described in detail.

#### 4.3.1. Fixed Part

Figure 29 shows in more detail the fixed part, highlighting some of its features:

- 1. Loops: Two loops allow a Velcro strip to be inserted and adjusted according to the user's arm size.
- 2. Step for locking: The lower part of the release part locks the sliding part here when the system is in locked state.
- 3. Opening for the safety catch: Provides a passage for the narrowed part of the safety catch, blocking the largest part.
- 4. Stop block for sliding part: Prevents the sliding part being dragged by the cable while in the released state.
- 5. Passage for bracelet guide: The bracelet guide passes through this hole and is secured with two screws.
- 6. Guide for sliding part: Allows the sliding part to move in the desired direction when in the released state.
- 7. Dimensions: Height: 70 mm, Width: 112 mm, Length: 124 mm. The 70 mm choice is a compromise between achievable ROM and the overall bulk of the bracelet.

So, the fixed part is attached to the exoskeleton arm through the bracelet guide which passes (5), which is fastened with two screws. The loops (1) provide adjustable points for securing a Velcro strap around the user's arm. The step (2) ensures that the release part is locked when the handle is not lifted, while the guide (6) allows controlled sliding when in the release state. Finally, the opening (3) accommodates the passage of the safety catch, completing the secure and functional design of the fixed part.

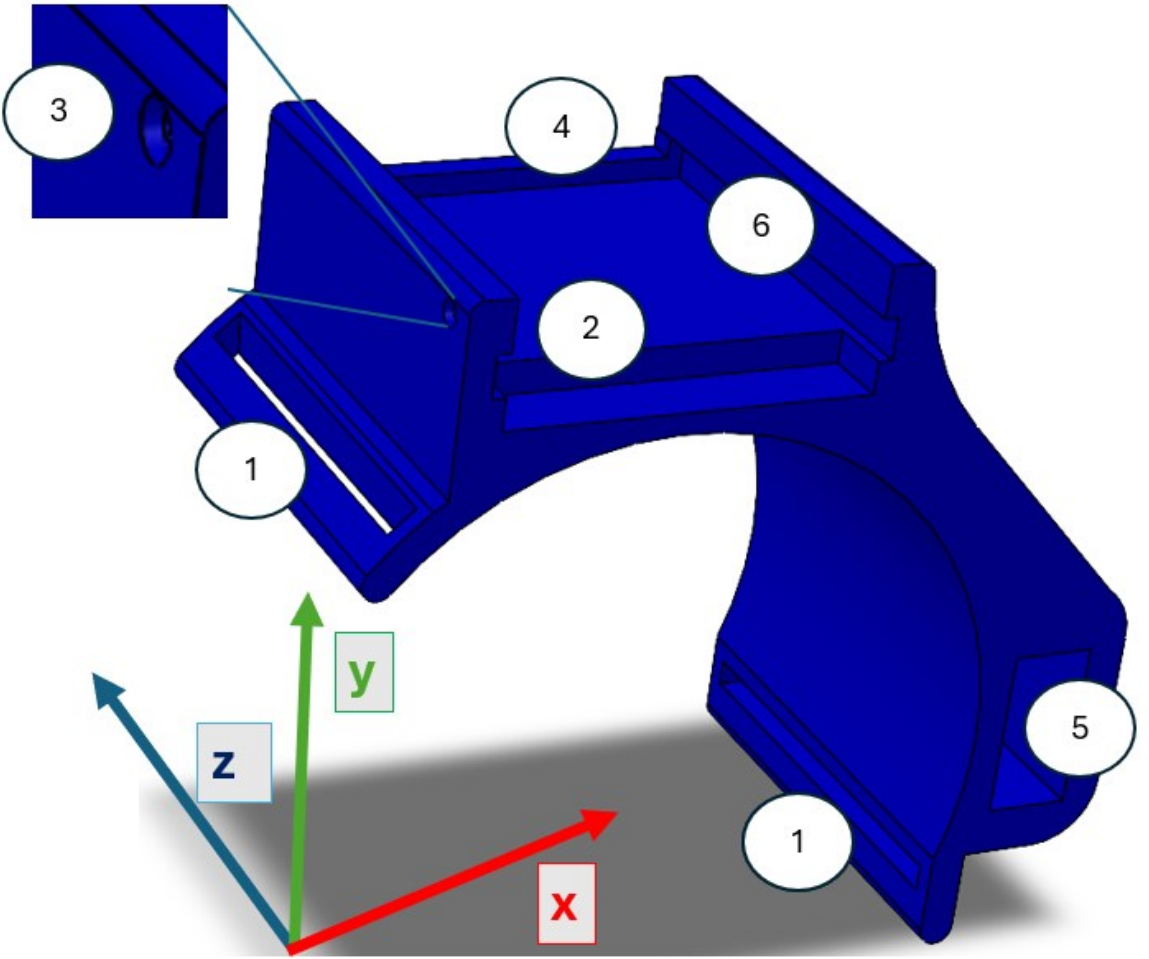


Figure 29: CAD of the Fixed Part with highlighted parts

## 4.3.2. Sliding Part and the Handle

Figure 30 and Figure 31 shows in more detail the sliding and the handle part, highlighting some of their features:

- 8. Passage for the cable
- 9. Handle
- 10. Release Part
- 11. Passage in the Release Part to insert the Handle
- 12. Safety Catch holding for the locked state.
- 13. Dimension of the Sliding Part: Length: 60, Width 21, Height 15.
- 14. Dimension of the Handle: Length: 4.8, Width 9.8, Height 56.

The sliding part features a passage (7) through which the inextensible cable connected to the PAM passes. Its position is maintained by the release part (9). When the release part is lowered, it engages with the step for locking (2) of the fixed part, preventing the sliding part from moving along the guide (6). The release part also includes a recess (11) that accommodates the safety

catch. A handle is integrated into the release part, allowing the latter to be easily lifted when needed.

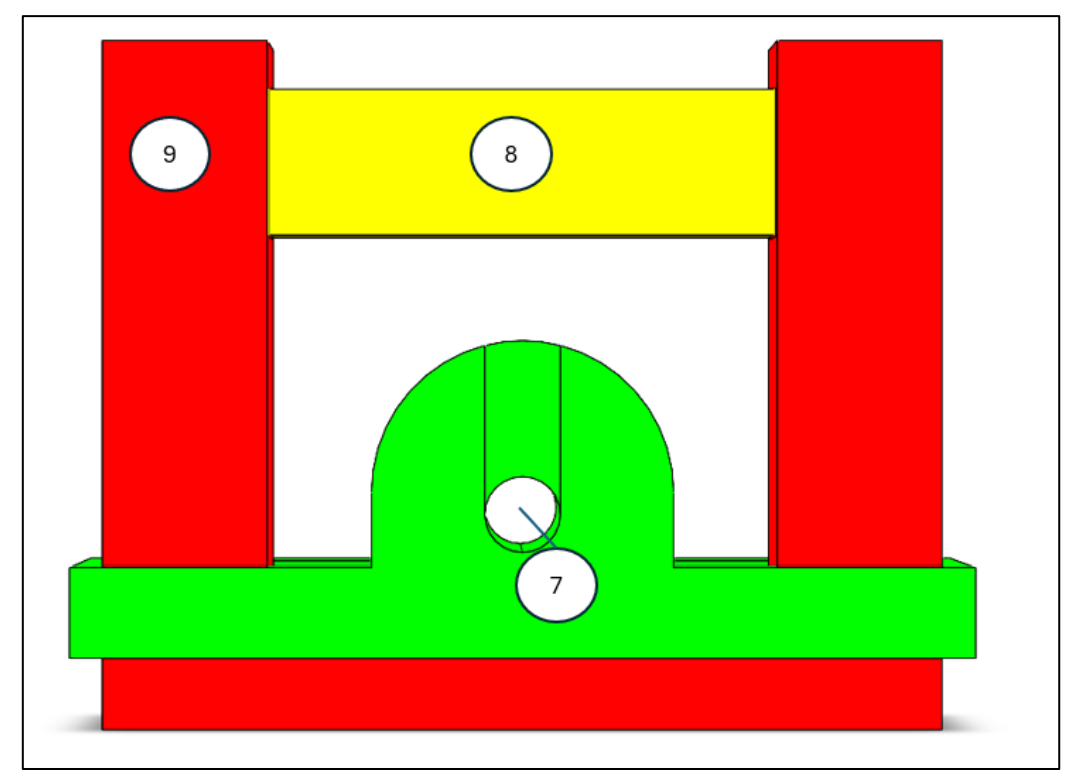


Figure 30: Cad of Sliding Part, Release Part and Handle in the locked state

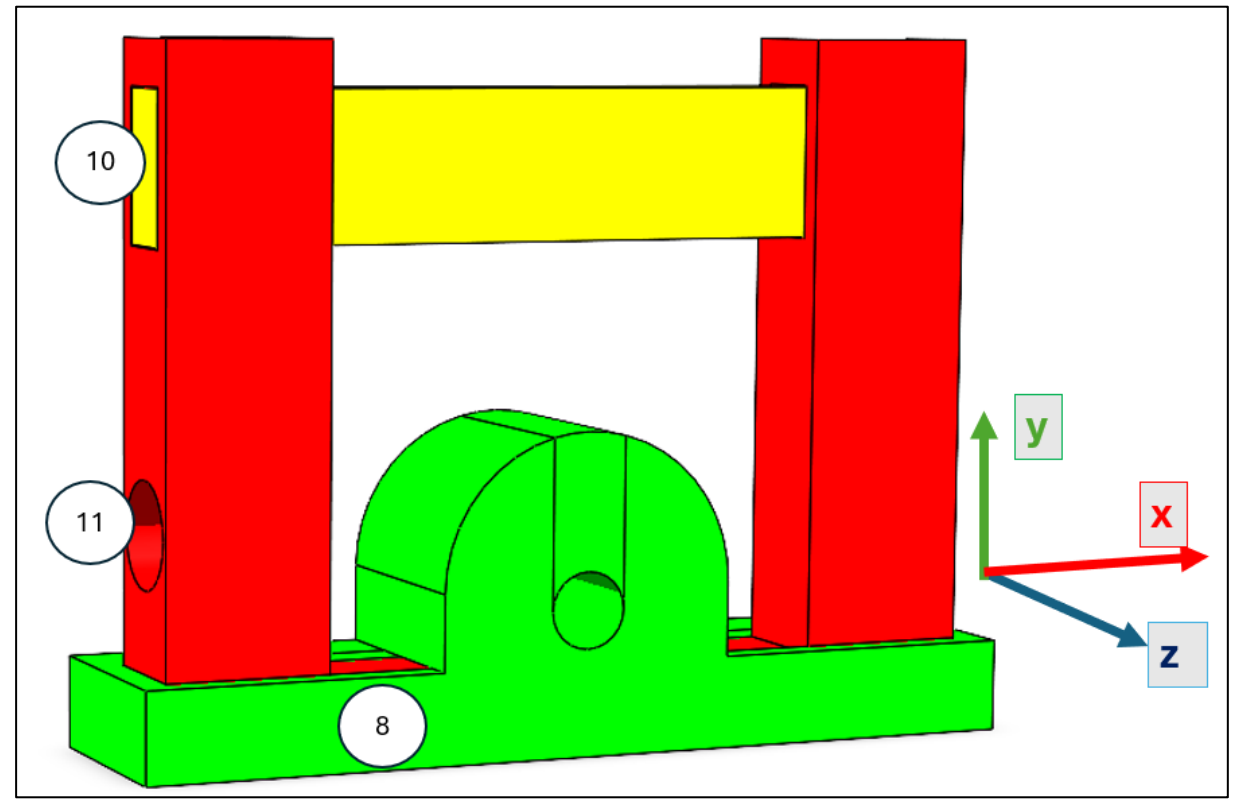


Figure 31: Cad of Sliding Part, Release Part and Handle in the released state

### 4.3.3. The Safety Catch

The safety catch has been integrated into the system to prevent any unintentional engagement of the mechanism.

Dimensions of the safety catch: Length: 6.7, Width 6.7, Height 20

The safety catch consists of a cylindrical element with two distinct sections, as shown in Figure 32. When the system is in the locked state, the larger section is positioned simultaneously within the release part (11) and the fixed part, thereby preventing the accidental lift of the handle. By pulling the protruding end of the safety catch outward from the fixed part (3), the safety element is released from the release part, enabling the handle to be lifted. The functioning system is shown in Figure 28a where the safety catch is inserted and in Figure 28b where the safety catch is only in fixed part where it remains in the release state.

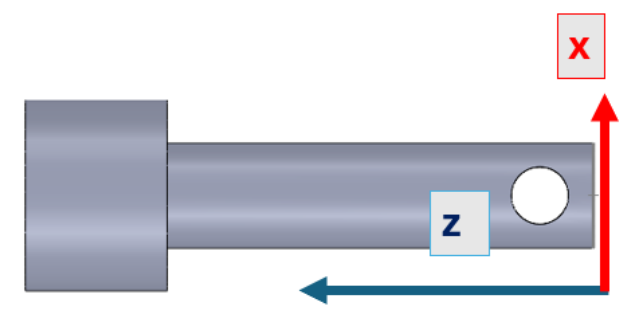


Figure 32: CAD of the safety catch

#### 4.4. New Torque

Since the attachment point of the wire has changed, the new support moment has been calculated together with the new operation pressure in three different load in the hand: 1 kg load, 2 kg load and no load. The support torque exerted by the new bracelet is shown in Figure 33.

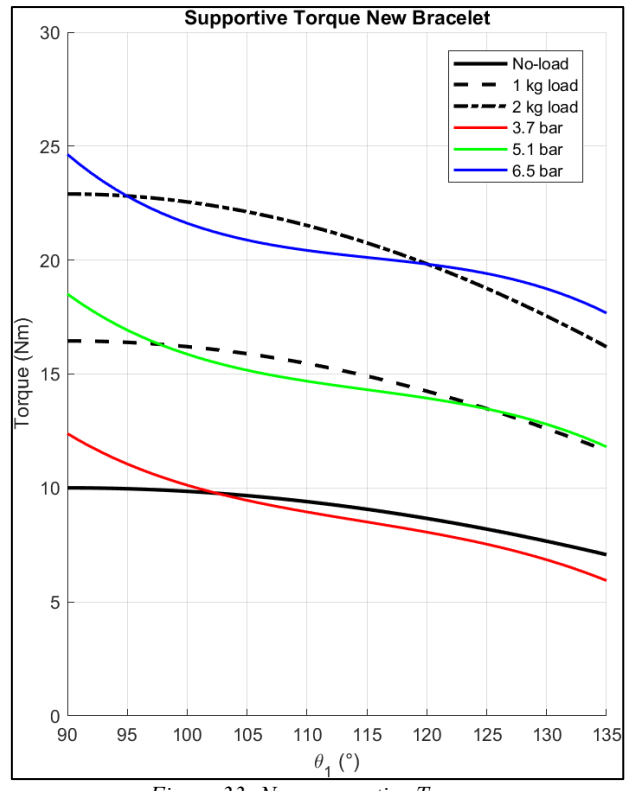


Figure 33: New supportive Torque

The force of MKMs has been calculated through Eq.11 and the lever arm has been measured in the CAD of the exoskeleton arm for four different angles. Then, to estimate the lever arm for intermediate angles, a forth order polynomial interpolation was used.

The pressure has been chosen in order to minimize the mismatch in the three different situations.

The comparison between the root mean square error (E) of the previous bracelet and the new one is presented in Table 6.

The increase in RMSE between the physiological and exoskeleton torques, ranging from about 23% to 44%, indicates a noticeable reduction in similarity with the gravitational torque. However, this worsening of the torque is compensated by augment of the reachable workspace, as detailed in the next section.

Table 6: Comparison of Root mean square error with the new bracelet (Enew) and with the previous one (Eprevious)

Load	Enew	EPrevious	
	[Nm]	[Nm]	
No load	1.236	0.859	
1 kg	0.056	0.041	
2 kg	0.059	0.048	

# 4.5. New Range Of Motion

It was evaluated how the new release system affected the arm's downward motion. For design and clearance reasons, the fixed component was designed with a height of 70 mm. This height directly influences the stroke length, which corresponds to the travel of the moving element within the fixed part during the arm-lowering phase. The resulting stroke length is illustrated in Figure 34.

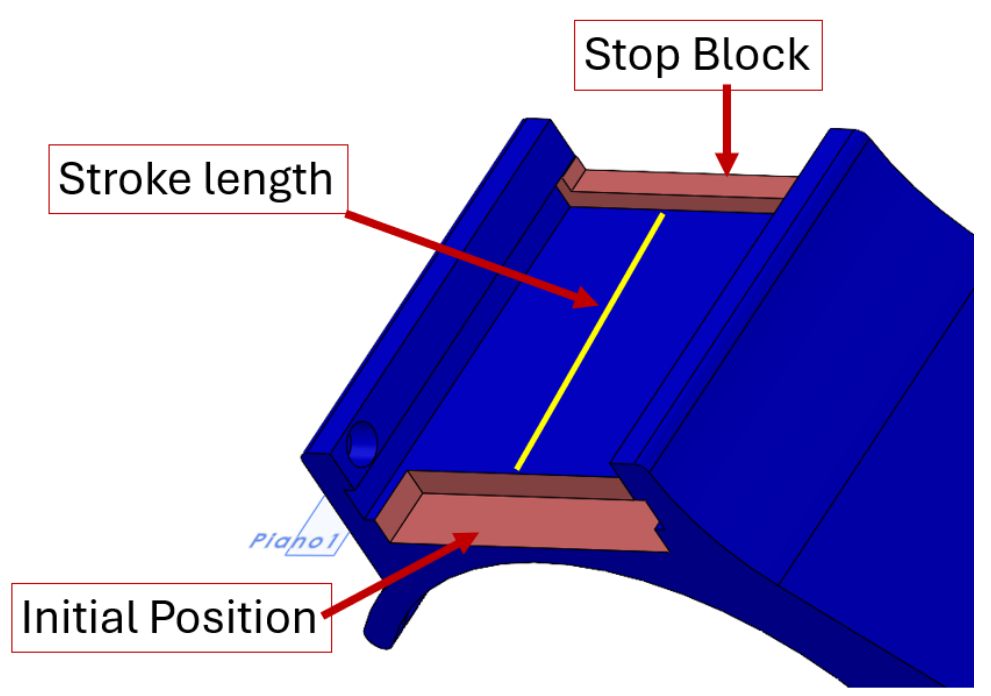


Figure 34: Stroke length seen in the CAD of the fixed part

This stroke length is equal to 55 mm.

When the system disengages, the mechanism is no longer under tension until the arm lowers by a specific angle.

Therefore, to determine the required arm lowering before the cable is in tension again, seven measurements were taken on the CAD model.

The calculation is based on determining the length of the cable between the shoulder pad and the bracelet attachment point.

Knowing that the cable is tensioned at 90°, the difference in length between the cable at 90° and at a lower angle represents the minimum sliding distance along the bracelet required to allow the arms to lower before the cable becomes tensioned again.

Therefore, the difference between the cable length at  $90^{\circ}$  and the cable lengths at  $75^{\circ}$ ,  $60^{\circ}$ ,  $45^{\circ}$ ,  $30^{\circ}$ ,  $15^{\circ}$ , and  $0^{\circ}$  was then computed. As illustrated in Figure 35, the distance between the shoulder pad and the bracelet attachment point is visually shown for both  $90^{\circ}$  and  $75^{\circ}$ .

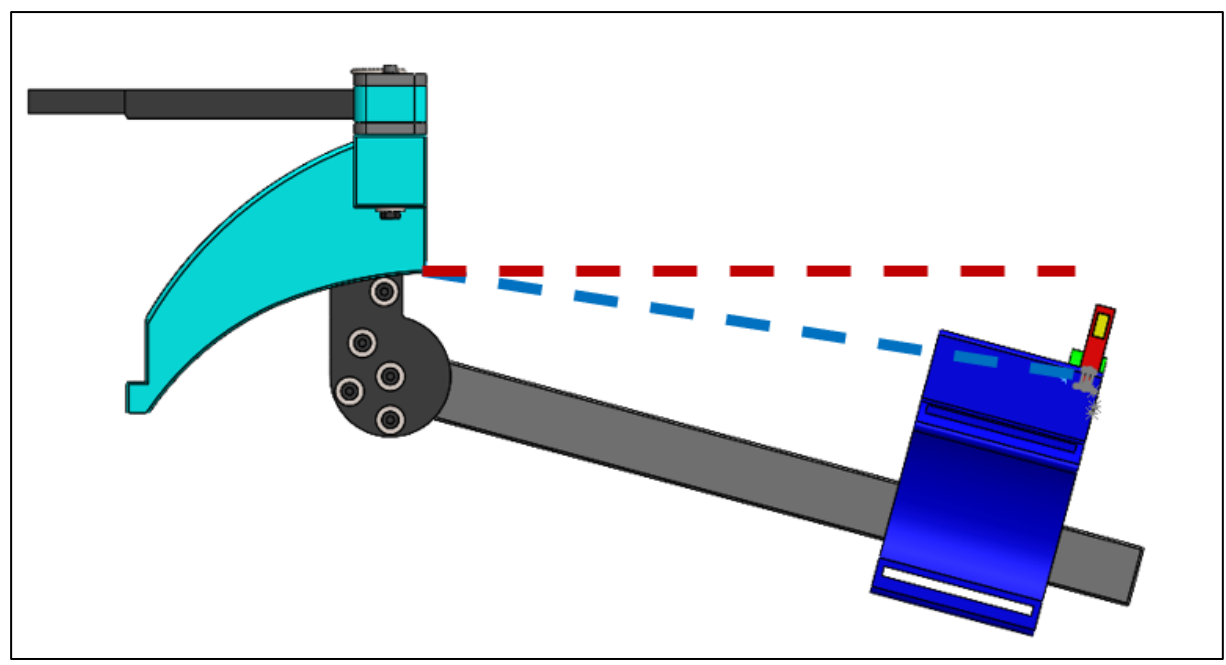


Figure 35: visualization of the distance between shoulder pad and attachment point of the bracelet for 90°(dashed line in red) and for 75° (dashed line in blu)

The measured differences at various angles are reported in Table 7.

Table 7: Distance and distance difference for seven angles.

Angle [°]	Distance [mm]	Difference [mm]
90	252,65	0,00
75	264,13	11,48
60	276,42	23,77
45	288,63	35,98
30	299,98	47,33
15	309,83	57,18
0	317,68	65,03

A fourth-degree polynomial interpolation was performed to estimate intermediate values between those obtained from the CAD model. This approach enabled the calculation of the maximum arm lowering allowed by the release system. As a result, the release mechanism permits the arm to be lowered up until 18°. The results of the interpolation and the sliding distance required for the elevation angle are presented in Figure 36.

This calculation also makes it possible to estimate the required stroke length to lower the arms down to  $0^{\circ}$ , which results to be 65 mm.

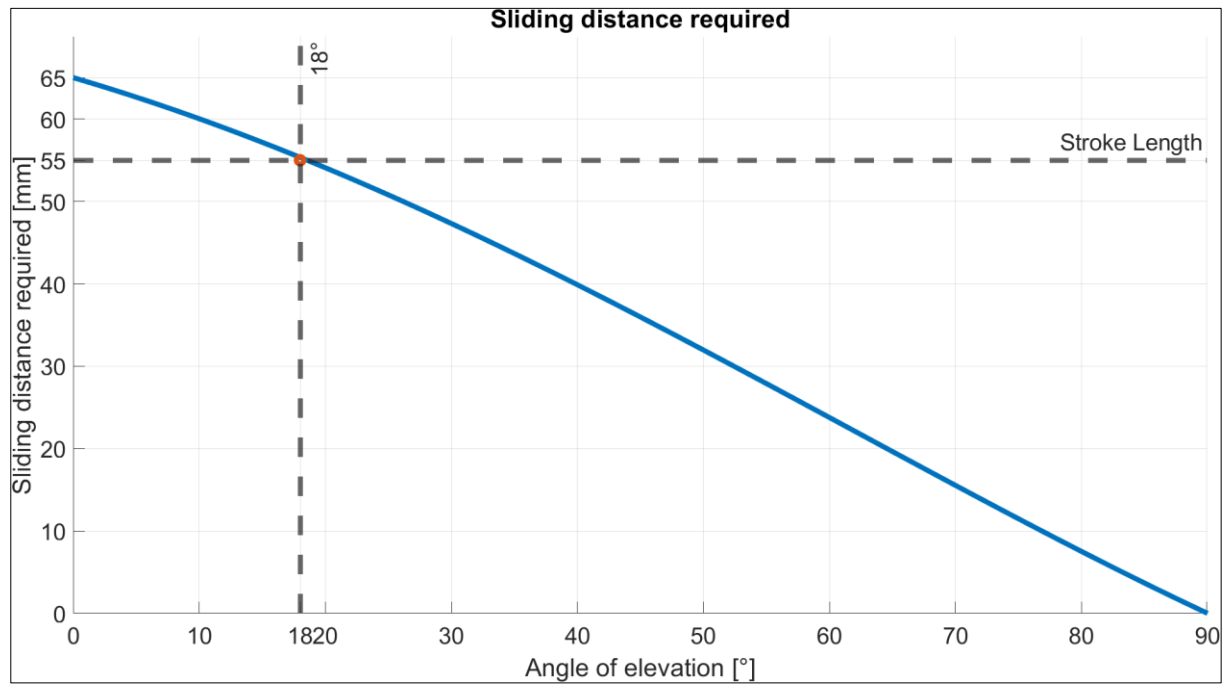


Figure 36: Sliding distance required in order to lower the arms by a certain angle

## 4.6. Finite Element Analysis

Before 3D printing the new bracelet, the parts designed in SolidWorks were tested using the SolidWorks Simulation tool in order to verify the strength of the components under the expected loads.

Therefore, a Finite Element Analysis (FEM) was carried out using SolidWorks. Knowing that the pieces of the new bracelet will be printed by a 3D printer, the material that has been imposed on the bracelet parts is Polylactic acid (PLA).

#### 4.6.1. Polylactic Acid

Polylactic Acid (PLA) is a thermoplastic polymer widely employed in fused filament fabrication 3D printing due to its ease of processing. It exhibits relatively high stiffness, with a Young's modulus of about 3.5 GPa and tensile strength between 50 and 70 MPa. However, 3D printed PLA is anisotropic because of its layer-by-layer deposition process, which causes mechanical strength to be higher along the printing direction than between layers.

So, the printing direction affects the results of the simulation. Figure 37 shows the printing direction of the components and how they were printed. Table 8 shows the mechanical characteristics of the PLA used for the simulation.[42]

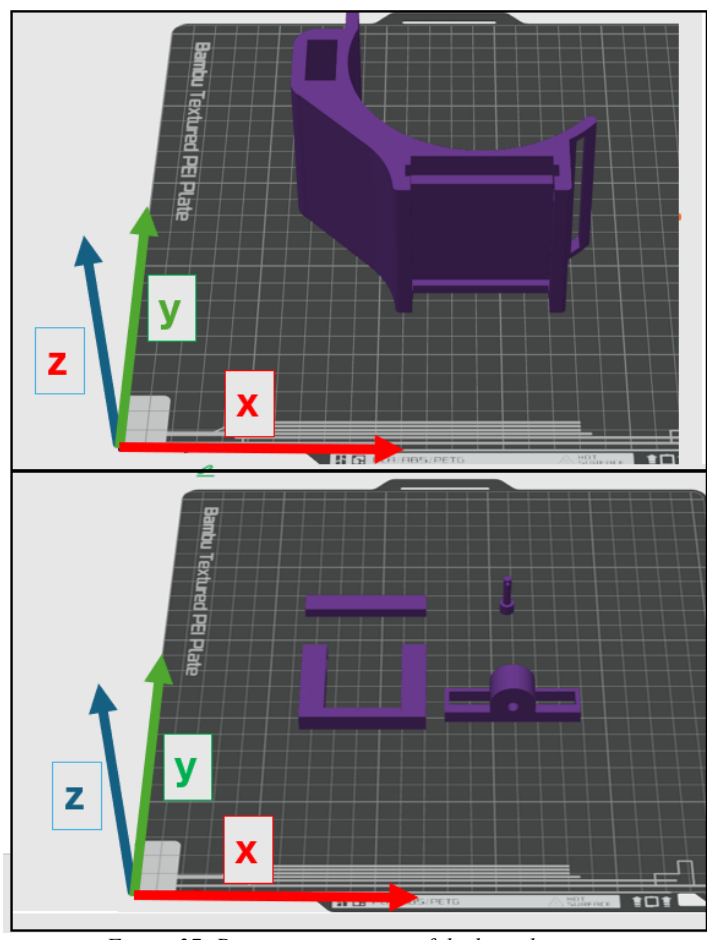


Figure 37: Printing orientation of the bracelet parts

Table 8: Mechanical Properties of PLA[42]

PLA	Young's Modulus [MPa]	Poisson	Shear Modulus [Mpa]	Tensile Strength [Mpa]
Printing direction Z	2790	0.35	955	36
Layers direction Y-X	2160	0.35	763	32

#### 4.6.2. Static analysis

Figure 38 represents the bracelet with mesh with highlighted the forces and the constraint in order to simulate the condition of the traction of the cable (1) and the weight of the arm (2).

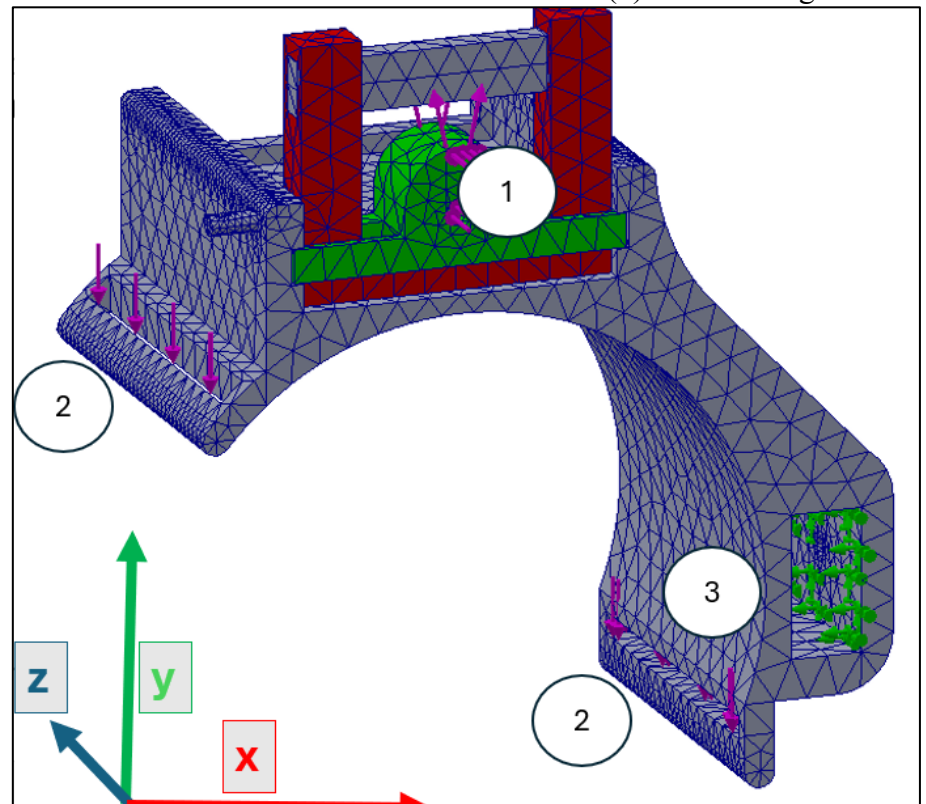


Figure 38: Bracelet with mesh and applied forces.

The traction force transmitted through the cable, indicated in (1), consists of two components. In the worst-case scenario at 90 degrees, with a 2 kg load held in the hand and the PAM pressurized at 6.5 bar, the resulting force reaches approximately 600 N along the z axis and 40 N along the z axis and 40 N along the arm load, it was assumed that the arm weighs about 7 kg with a load in the hand of 2 kg.

A curvature-based tetrahedral mesh with a maximum element size of 10.73 mm and a minimum element size of 0.70 mm has been applied.

#### 4.6.3. Simulation Results

Since PLA is a fragile polymer the maximum normal stress criterion has been used to evaluate its failure. According to this criterion, fracture occurs when the maximum principal stress exceeds the material's tensile strength.

Figure 39 illustrates the normal stresses in the three directions  $S_z$ ,  $S_x$  and  $S_y$ . By analyzing the maximum and minimum stress values and comparing them with the material's tensile strength, it can be concluded that the components should not fail. The maximum normal stress among the three direction, in magnitude, is in the y direction is 34.4 MPa.

Figure 40 shows the displacements along the three directions, highlighting how deformations are distributed throughout the structure. Overall, the displacements are below 1 mm. The sliding part exhibits a maximum displacement of 0.97 mm along the z direction. This behavior is consistent with expectations, as it aligns with the direction of the tensile force applied by the cable.

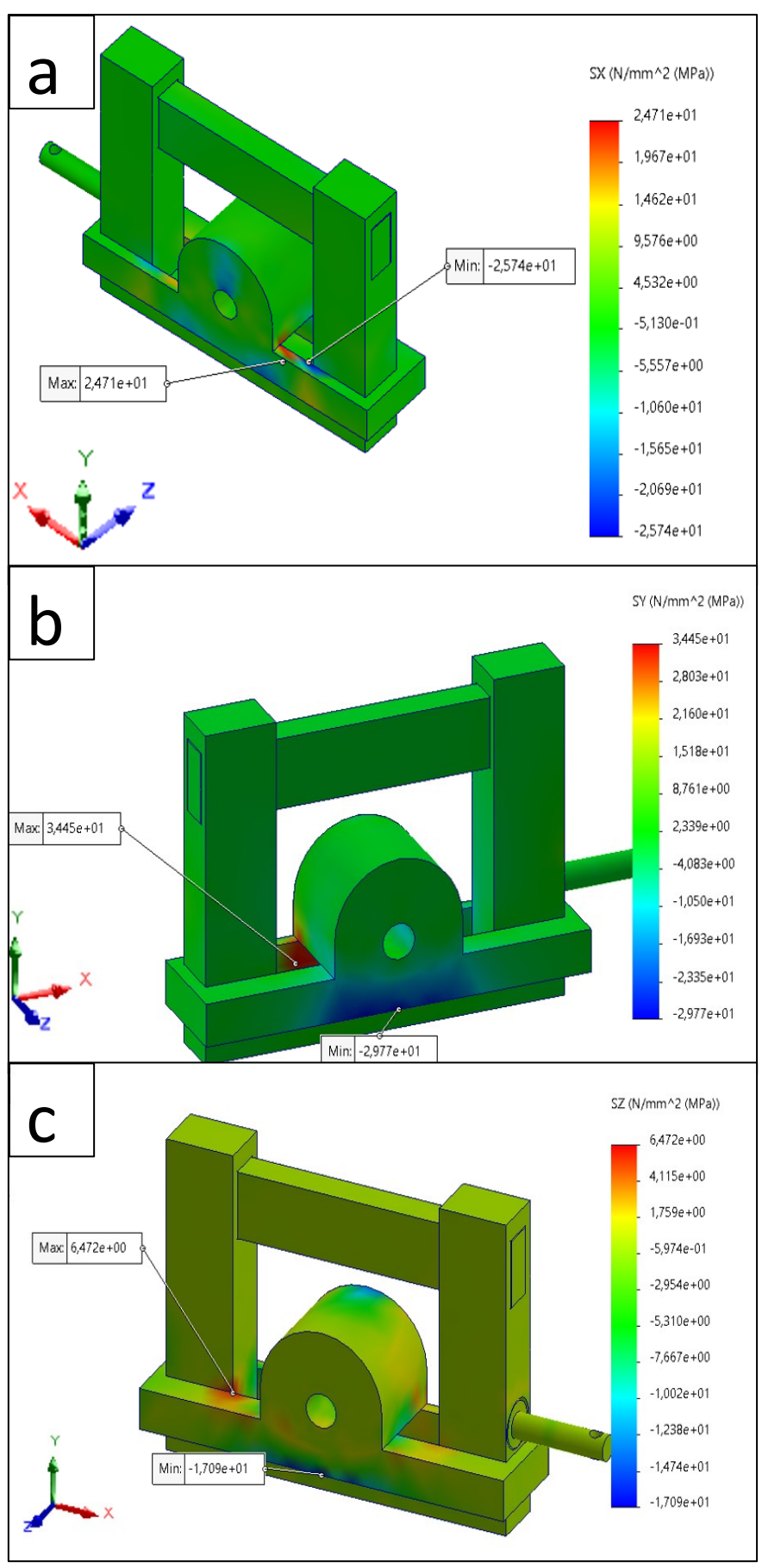


Figure 39: Normal stresses in: a) x-direction, b) y-direction, c) z-direction

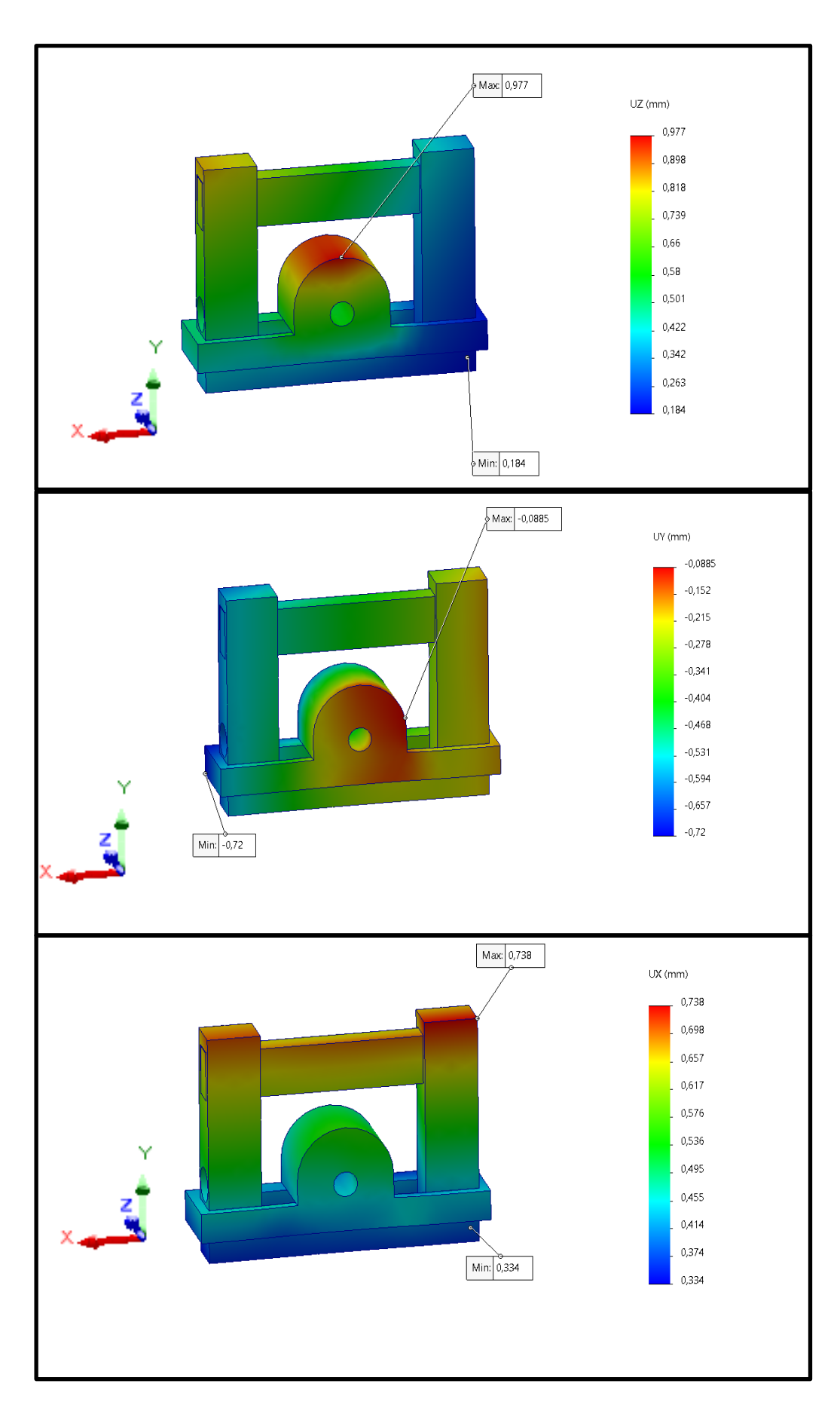
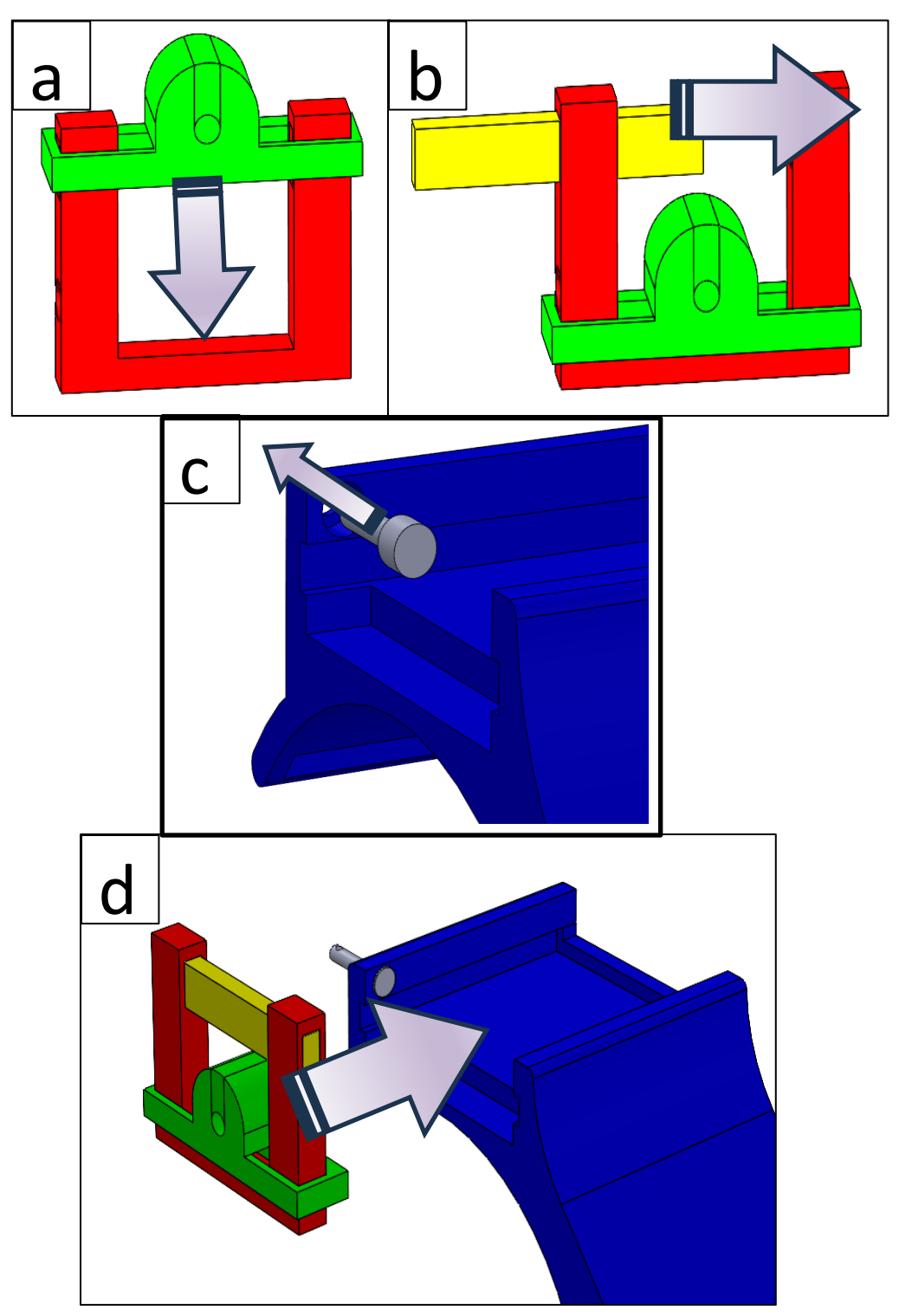


Figure 40: Displacement in a) z direction, b) y direction c) x direction

## 4.6.3. Printing and assembly

The pieces have been printed with a Bambu Lab X1 Carbon.

To assemble the bracelet the following steps have been taken, graphically shown in Figure 41.



The full Figure 41 a) the sliding part is inserted in the release part; b) The handle is inserted c) The security catch is inserted all the way through the passage in the fixed part d) the assembly of the sliding, release and handle is inserted in the fixed part. The security catch now can lock the assembly.

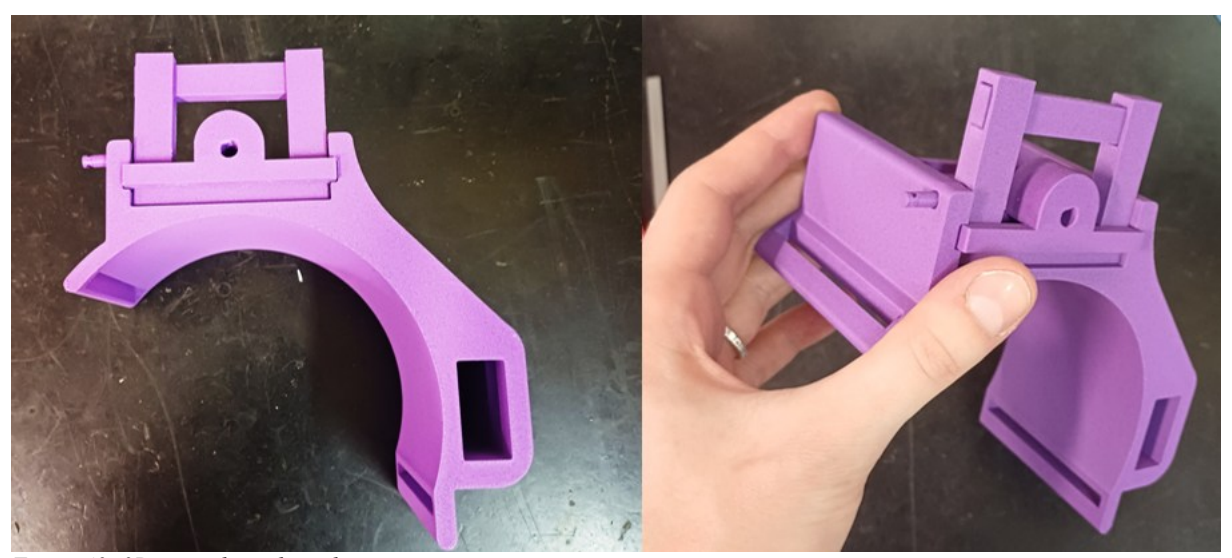


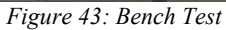
Figure 42: 3D printed new bracelet

# 4.7. Static Test

To ensure that the bracelet can withstand the tensile force applied by the actuator, a static test was carried out.

A test bench was set up, as shown in Figure 43 and schematically illustrated in Figure 44.







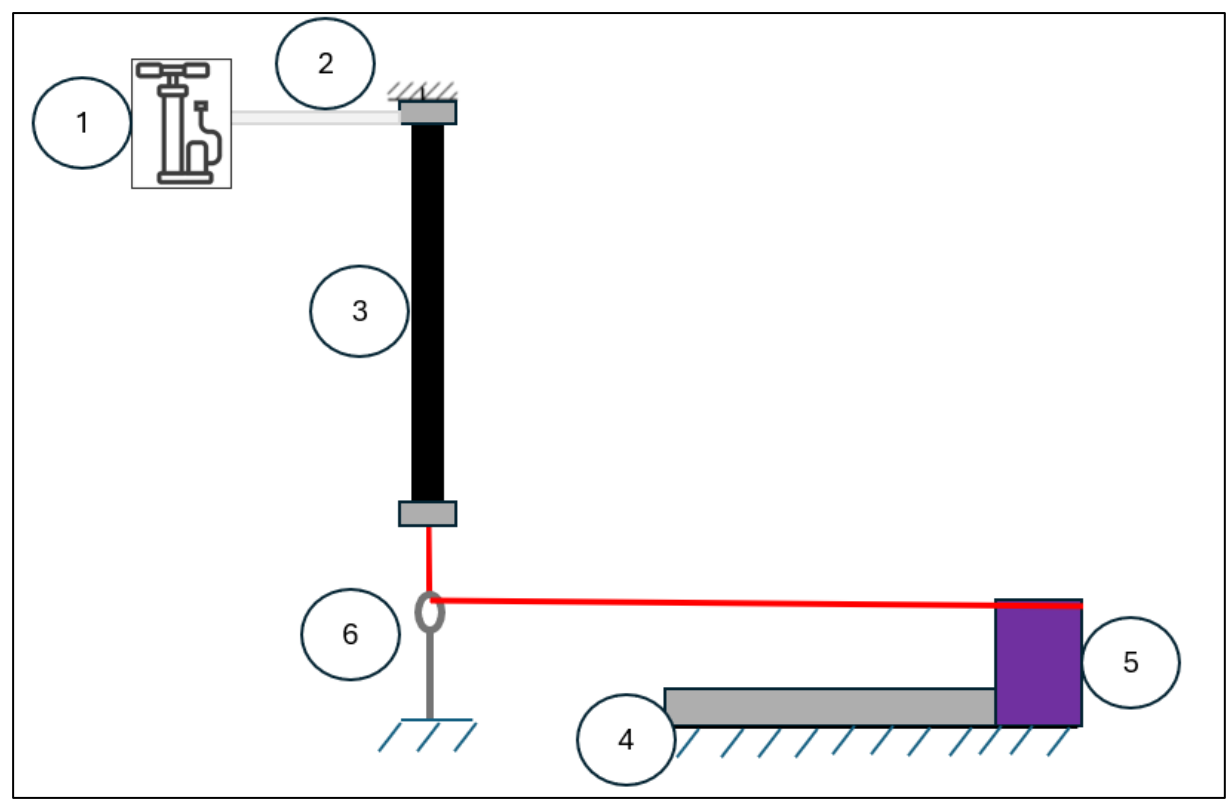


Figure 44; Schematization of the static test

The PAM (3) has its upper end fixed to a support structure, while its lower end, free to move, is connected to an inextensible cable. A redirect point (6) was introduced to guide the cable so that the resulting traction force acts roughly along the same direction as the force that would be applied to the bracelet in the actual exoskeleton configuration. The cable is then attached to the bracelet (5) through the designated passage. The bracelet was secured to the bracelet guide (4) using screws, and the guide was subsequently restrained to prevent any movement.

The PAM was pressurized using an air pumping system (1), (2).

The PAM was pressurized sequentially at 1, 2, 3, 4, 5, 6, and 7 bar, maintaining each pressure for one minute. During the test, it was observed that the bracelet did not break, but it experienced slight deformation at higher pressures. At 5, 6, and 7 bar, this deformation prevented the security catch from fully disengaging. The release mechanism was tested at each pressure level, confirming its functionality at lower pressures, while at the highest pressures its operation was partially hindered by the bracelet deformation.

## 4.8. Discussion

The innovative release system effectively extends the exoskeleton's range of motion, allowing arm flexion between 90° and 18°. Although the exoskeleton's performance worsened, an easy optimization of the cable attachment position on the bracelet system could lead to better results.

Considering the issues observed on the test bench, an optimization of the material selection could also be implemented for instance, using PLA-CF, a PLA reinforced with carbon fiber that often presents a better tensile strength. Moreover, the bench test has some limitations, the direction of the cable was qualitatively

assessed and the weight of the arm was completely neglected. Therefore, the results of the test bench should be interpreted with caution.

# **Chapter 5**

## **CAM-based transmission**

Before developing the prototype discussed in Chapter 3, Paterna[25] evaluated three different transmission systems: one based on a pulley, one based on the previously mentioned and subsequently developed shoulder pad, and one based on a cam. The cam-based mechanism extended the range of motion, allowing the flexion of the arm from 135° to 45°. Figure 45 shows the configuration with the cam-based transmission developed by Paterna[25].

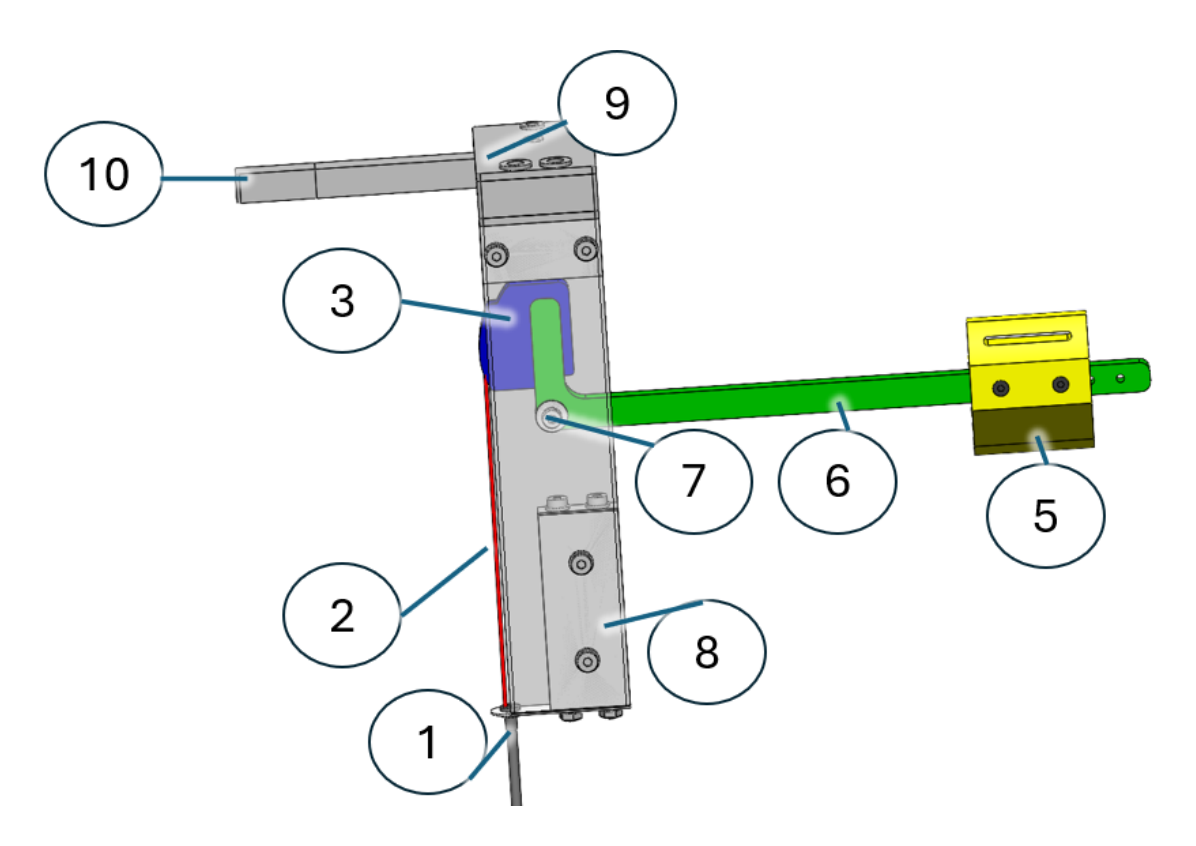


Figure 45: Cam-based transmission system.

The transmission cable (2) is connected to the PAM and guided through a sheath to the cam support structure, where it is fixed by a sheath clip (1). The cable is attached to the cam (3), which is mounted on a strut (6) integrating a supporting bracelet (5) for the arm. Upon pressurization of the PAM, the induced cable tension produces a rotational motion of the cam, resulting in the elevation of the arm.

Similar to the shoulder pad, the cam was developed using a graphical method. Its design was specifically aimed to extend the ROM of the exoskeleton. The hinges are similar to the shoulder pad configuration, there is the abduction/adduction hinge in (9) and the flexion hinge in (7). A flexion stop (8) limits the flexion to 45 degrees. Similar to the flexion stop, there is a abduction stop in (9) that limits the shoulder abduction to 30°.

Briefly, the cam profile, developed by Paterna[25], has the following characteristics. In Figure 46, O is the cam center, A is the sheath clip, and BC is the cam long axis. To achieve an MKM lever arm that increases with shoulder flexion, BC is vertical at  $\theta 1 = 90^{\circ}$ . The maximum lever arm,  $r_f = 50$  mm, defines the OB distance, while the minimum lever arm,  $r_i = 10$  mm, defines OC. The working range is  $\theta 1 \in [45^{\circ}, 135^{\circ}]$ , and r90, the PAM lever arm at 90°, is 30 mm. The first part of the cam profile ( $\theta 1 \in [90^{\circ}, 135^{\circ}]$ ) coincides with the TB arc, and the second part ( $\theta 1 \in [45^{\circ}, 90^{\circ}]$ ) is defined as the arc tangent to T'B'' (rotated 45° from TB) and the tangent to the  $r_i$  circle through A, with the total cam profile being T''B''.[25]

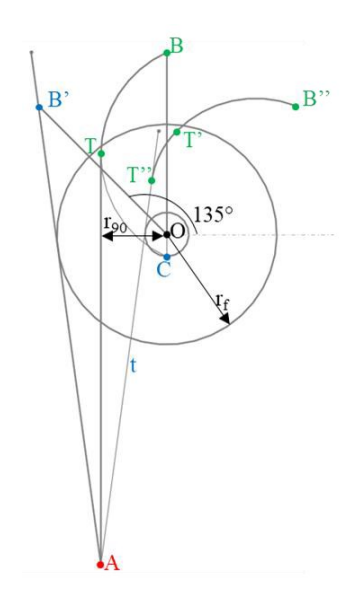


Figure 46: Cam profile design using graphical method[25]

Similarly to the shoulder pad, Paterna[25] calculated the torque of the cam and compared it to the gravitational torque, with the results shown in Figure 43.

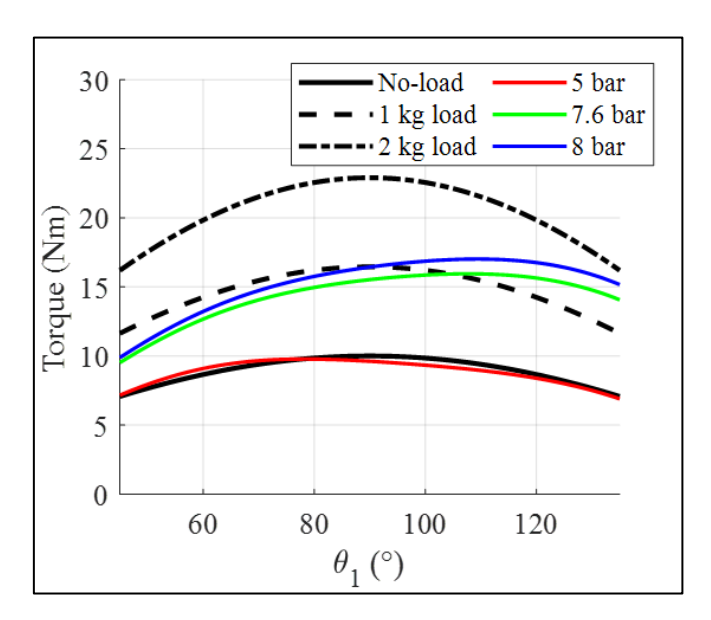


Figure 47: Gravitational torque is shown for no-load (solid black line), 1 kg load (dashed black line), and 2 kg load (dotdashed black line) conditions, alongside the torque generated by the exoskeleton at various supply pressures (colored lines), using the cam-based transmission.[25]

Although this solution offered the best range of motion, it was not prototyped due to its bulky, underdeveloped design and the insufficient torque it provided when assuming a load in the hand. Moreover, positioning the cam laterally is likely to generate unintended abduction moments due to misalignment of the SJC.

Nevertheless, the solution has been refined and redesigned to make it less bulky and evaluated in order to comprehend the magnitude of the parasitic abduction torque.

#### 5.1. Redesign of the cam support structure

One of the crucial issues with this cam-based design was its bulky and heavy structure. Moreover, since this solution was not chosen by Paterna [25] for prototyping, no structural analyses were performed on the cam.

The objective of this thesis was to redesign the cam support structure so that it would be:

- As lightweight as possible;
- Cost-effective;
- Easy to assemble.

The support structure redesign was therefore carried out with these requirements in mind, resulting in the solution shown in Figure 44.

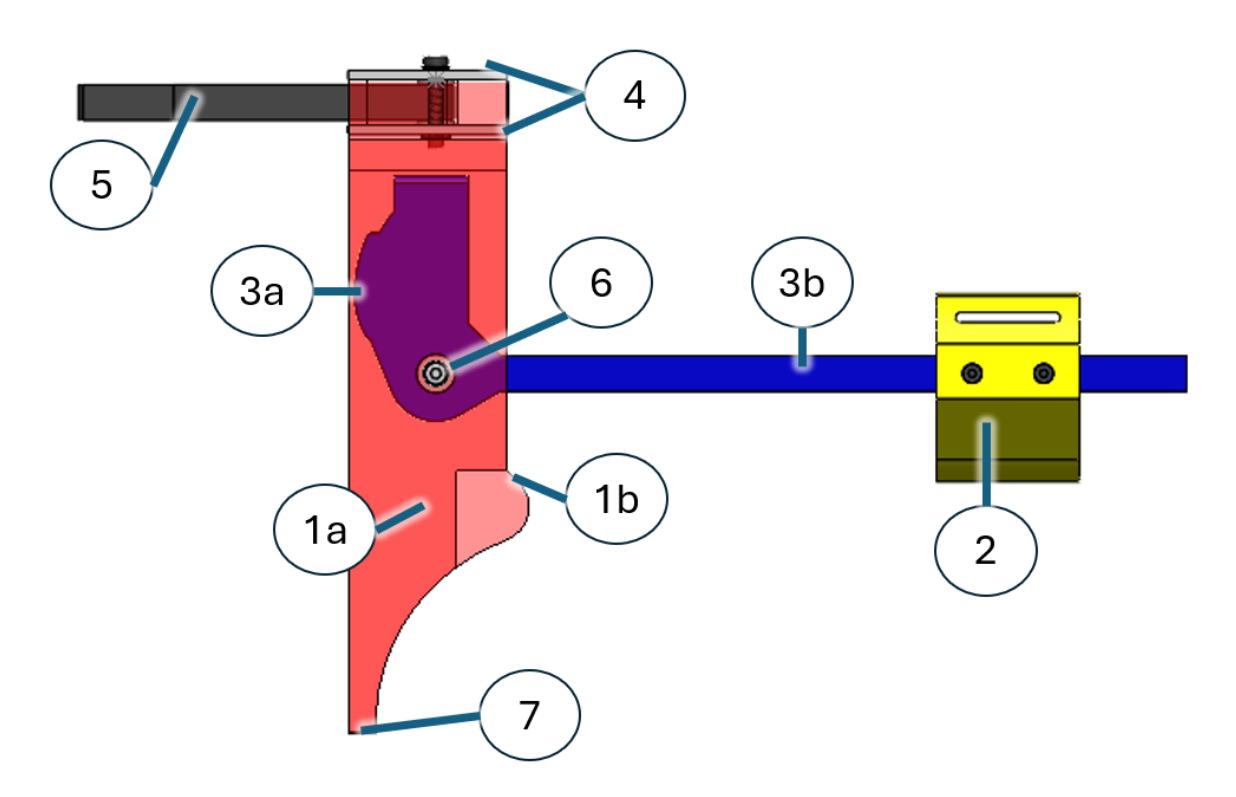


Figure 48: Lateral CAD view of the new support structure for the CAM-based design.

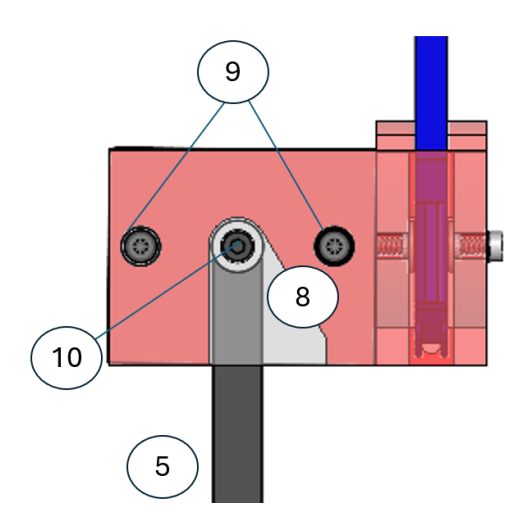


Figure 49: CAD upper view of the new support structure for the CAM-based design.

The operating principle remains unchanged. The support structure has been redesigned with the aim of 3D printing almost all the structures. The cam (3a) and strut (3b) have now been integrated into a single, unified component. Shown in Figure 45, the adduction/abduction stopper (8) is incorporated within the cam support stand (1a). The sheath clip is positioned through a passage in (7), positioned at the same height as previously, to preserve the moment arm as calculated by Paterna [25]. Additionally, the cam now features a passage allowing the cable to be inserted and securely fixed. The connection to the back frame (5) remains unchanged. Finally, the arched component (1b) functions as the flexion stopper. The upper part of the cam support structure, shown in Figure 45, was fixed to the hinge joint using two metal plates (4) and three bolts two M6 (9) and one M5 (10), as shown in Figure 45. The M5 bolt (10) is surrounded by a bushing, which enables the hinge to function, allowing abduction and adduction movements

#### 5.2. FEM Analysis

A Finite Element Analysis (FEM) was performed in SolidWorks Simulation to assess whether the system could withstand the applied forces. The first step is the definition of all the components materials. The mechanical characteristics of the materials can be found in Table 9. The materials were PLA for the entire support structure (1), the cam and the strut (3a) (3b) and the bracelet (2). Alloy Steel 8.8 was selected for all the fasteners. Stainless steel was selected for the external plates (4) connecting the support structure (3) with bar (5) that is connected to the back frame, which is also in stainless steel.

Table 9: Mechanical characteristics of the material used in the FEM analysis.

	Elastic Modulus [MPa]	v	Yield Strength [MPa]	Tensile Strength [Mpa]	Shear Modulus [MPa]
Stainless steel DIN.14313 X3CrNiMo13-4	200000	0.28	520	56	79000
PLA Printing Direction	2790	0.35	36	36	955

PLA Other Directions	2060	0.35	31	31	763
Alloy Steel 8.8	210000	0.3	640	800	80000

Then the forces and the constraint has been applied as follows, as shown in Figure 50:

- The traction force generated by the PAM was applied to the cam at a 90° arm position. With the MKM pressurized at 8 bar and a 2 kg load in the hand, the resulting force at the last attachment point of the cam results in FPAM<sub>z</sub>=-650 N. This same magnitude force was applied both at the cam profile contact point F<sub>MKMy</sub>=-650 N and at the sheath clip location F<sub>MKMy</sub>=650N.
- The arm weight has been estimated to be 7 kg.
- The bar (5) is attached to the back frame through a clamp, therefore it was modeled as a fixed constraint. The bracelet translation was constrained to simulate the user's force who keep the arm still.
- The gravitational load has been applied at the center of gravity.
- Bolts were preloaded respectively with 6Nm preload for the M6 and 1.8 Nm for the M5.

A curvature-based tetrahedral mesh with a maximum element size of 10.73 mm and a minimum element size of 0.70 mm has been applied.

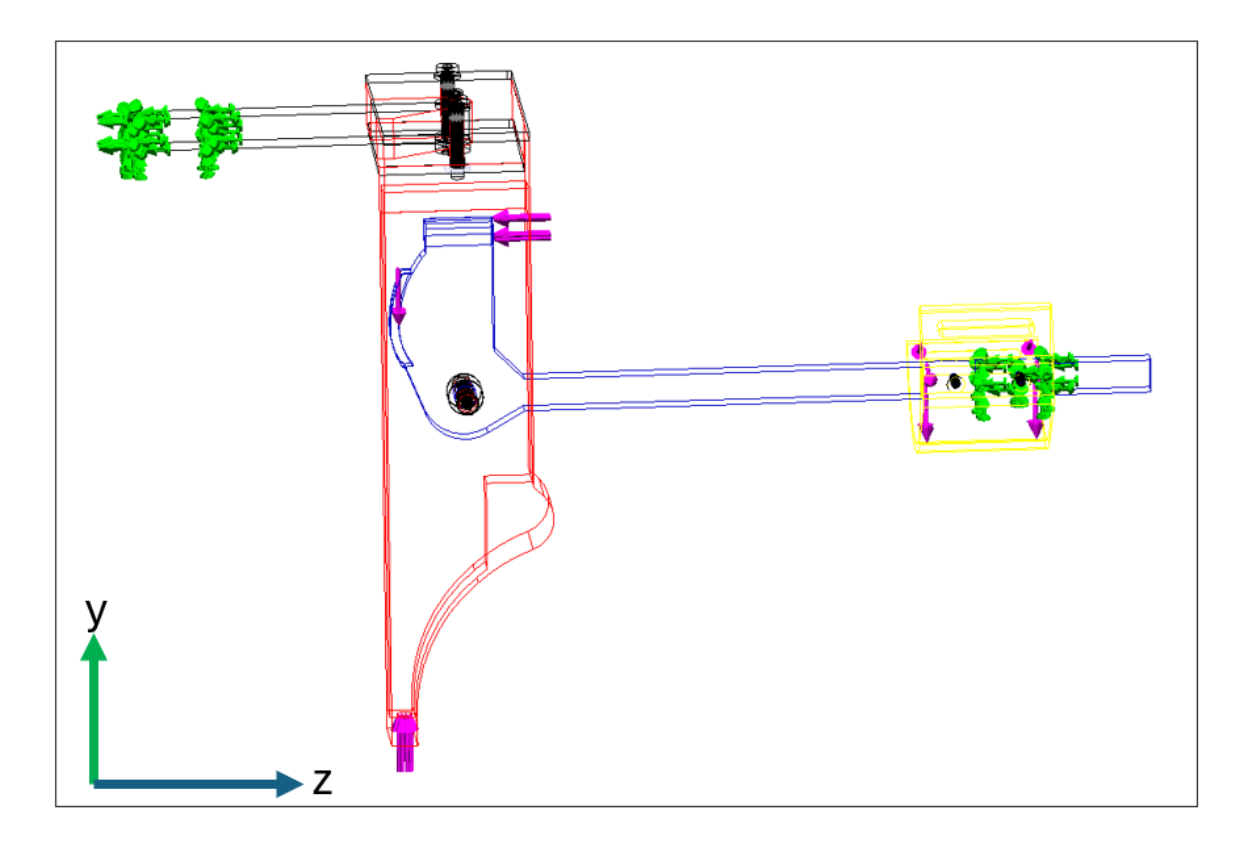


Figure 50: Force and constraints applied to the CAD model.

#### 5.2.1. FEM Results of the metal parts

For the metallic components, the Von Mises criterion was applied. Accordingly, the yield stress of each part was compared with the corresponding Von Mises

stress obtained from the simulation. The selected stainless steel DIN.14313 has a yield stress equal to 520 MPa.

Figure 51 shows the Von Mises Stress distribution of the metal parts. The most stressed metal part, as expected, are the two washers. Nonetheless the maximum stress equals 466 MPa, still below the yield strength of the chosen stainless steel. The other two elements that present the highest von mises stress are the two plates that connect the upper part of the support structure. Here the maximus stresses were respectively 229 MPa for the upper plate and 168 MPa for the lower plate, still in under the yield stress of the steel.

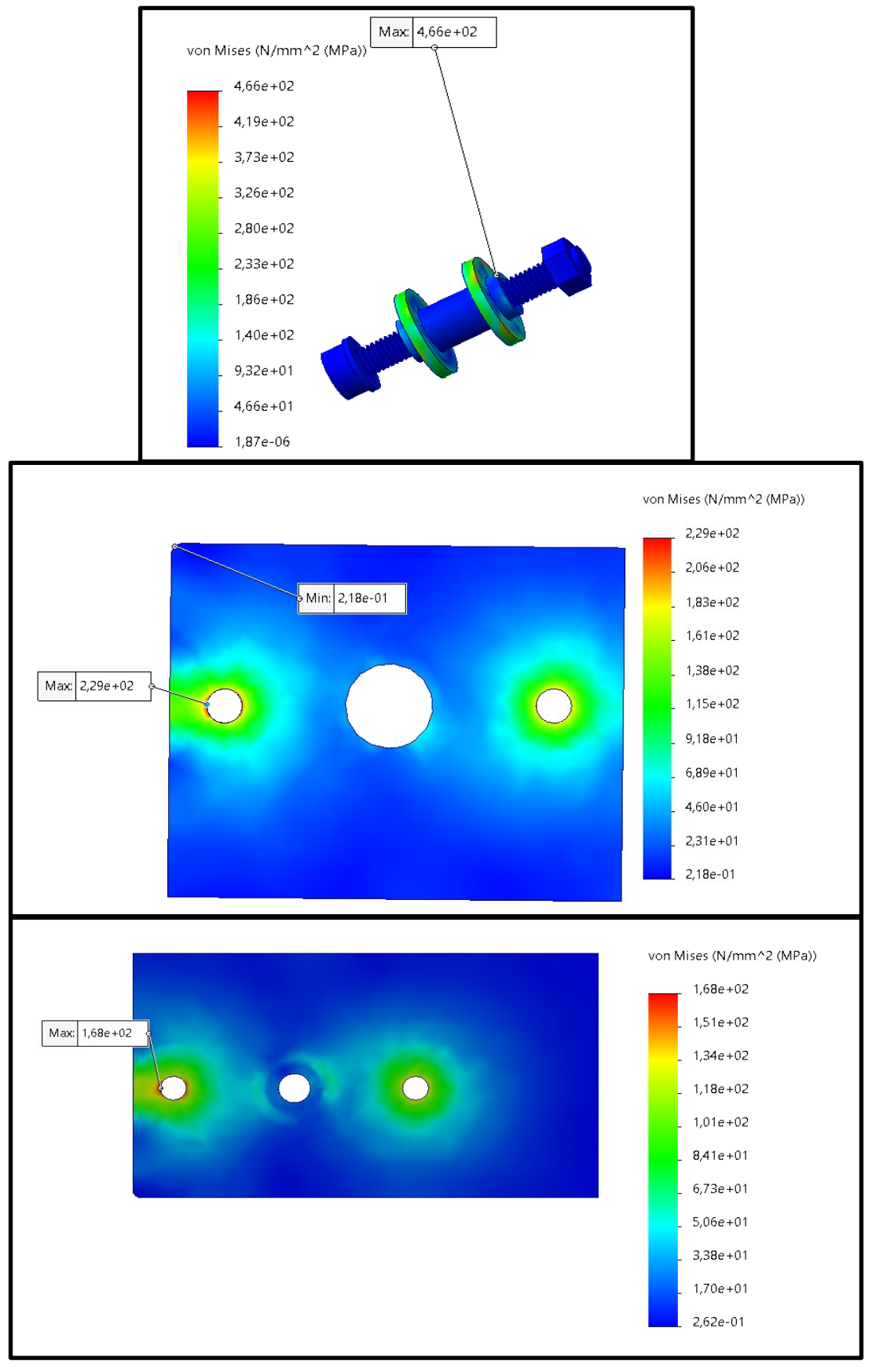


Figure 51: From top to bottom: Von Mises stresses of the bolt, the two washers and the bushing; Von Mises stresses of the lower plaque, Von Mises stresses of the upper plaque.

Figure 48 presents the von Mises stress of the last metal element of the assembly, the bar that connects with the back frame. Here the highest von Mises stress results in 77 MPa.

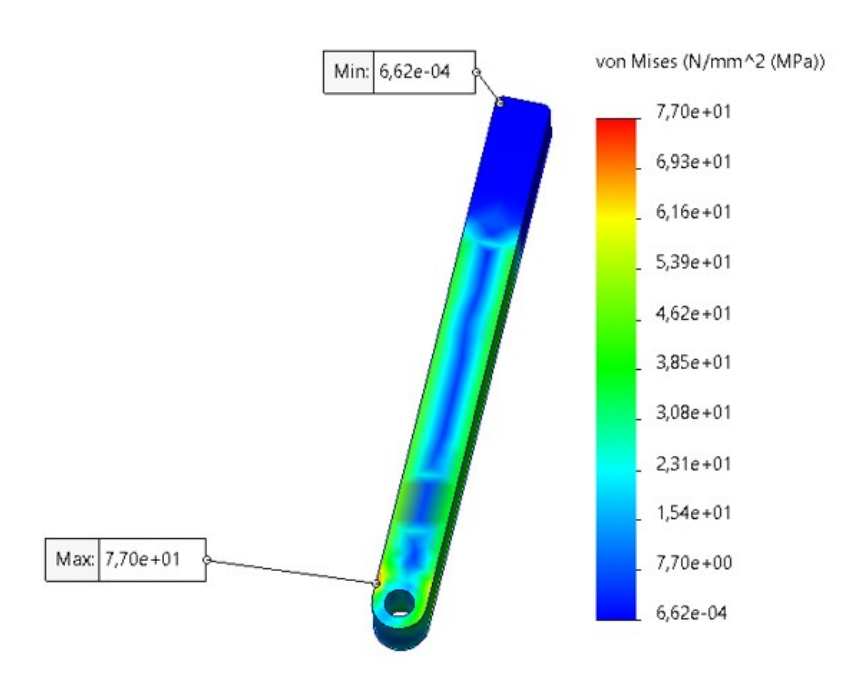


Figure 52: von Mises stress for the bar

### 5.2.2. FEM Results of the PLA parts

The parts largest of the assembly are made of PLA. Since they are designed to be 3D printed, the printing direction significantly influences the mechanical properties the components. of the printing orientation shown in Figure 53 For this reason, was selected. Following the approach described in Section 4.4.3, the maximum normal stress criterion was applied to verify that, in every direction, the normal stress did not exceed the tensile strength of the material Figure 54, Figure 55 and Figure 56 represent respectively the normal stress in the three directions for the support structure of the cam, the cam with the strut and the bracelet.

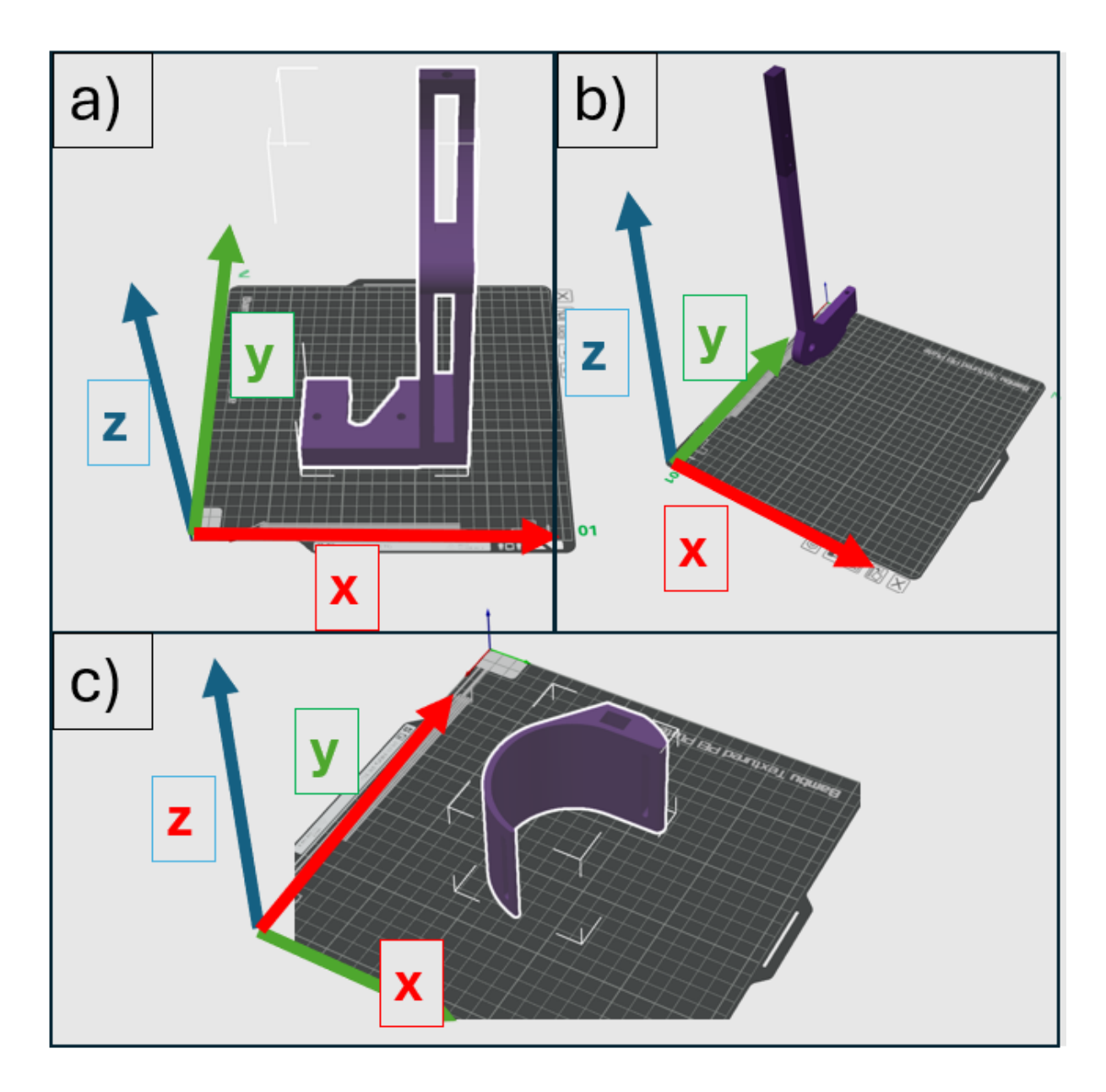


Figure 53: Printing direction for a) Cam support structure, b) Cam and strut structure, c) Bracelet

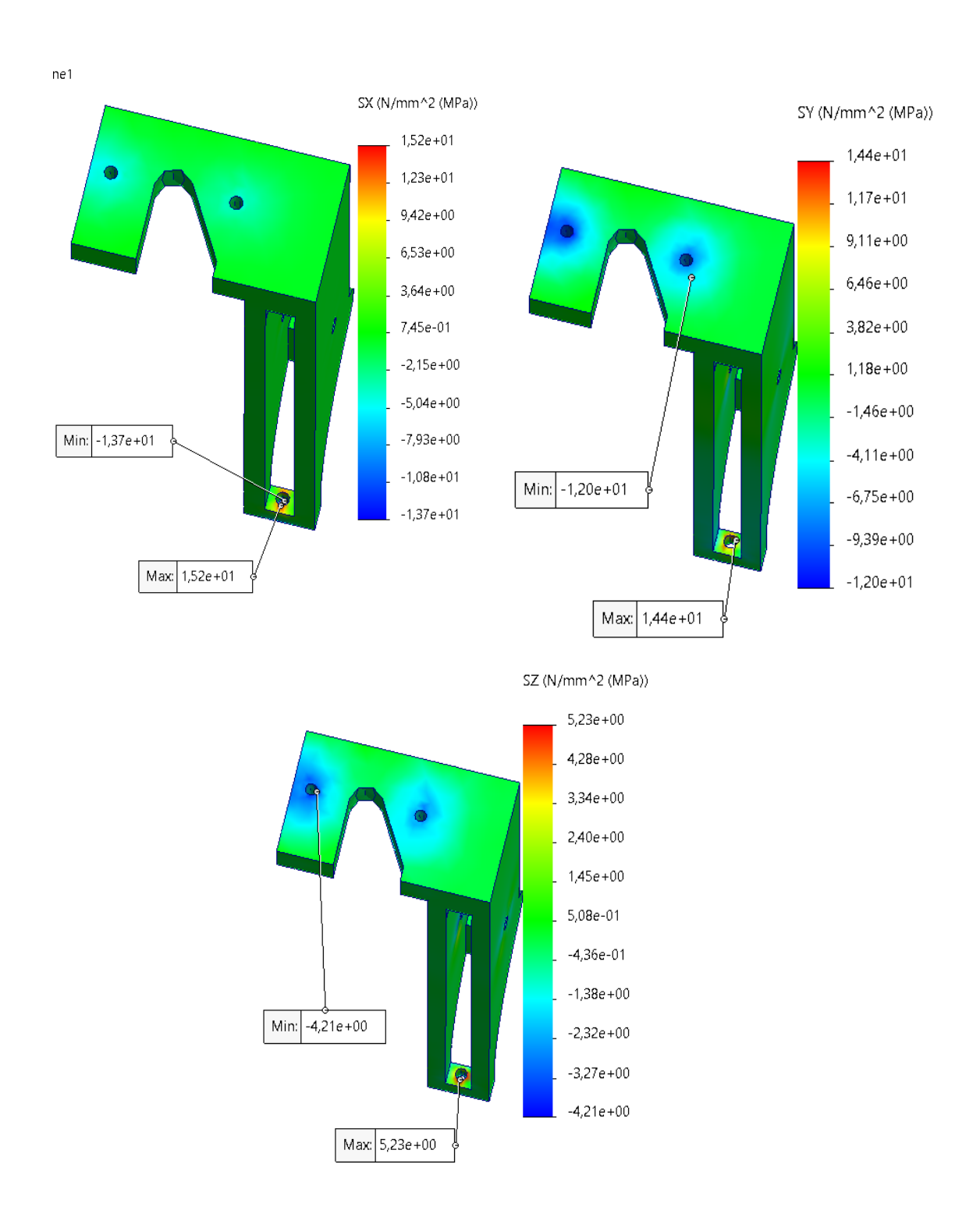


Figure 54: normal stresses in the three direction SX, SY, and SZ for the cam support structure.

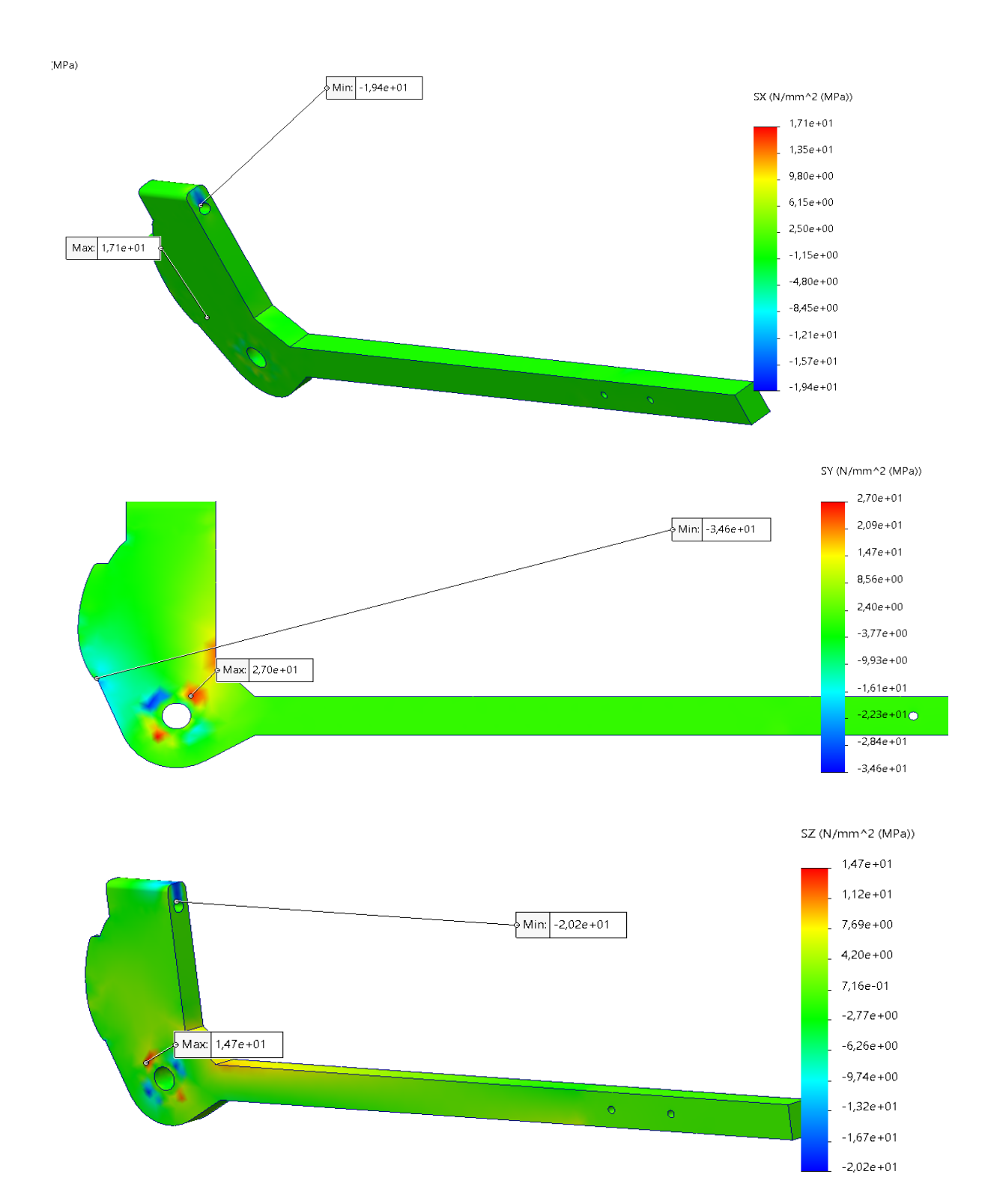


Figure 55: Normal stresses in the three directions for the cam and strut structure.

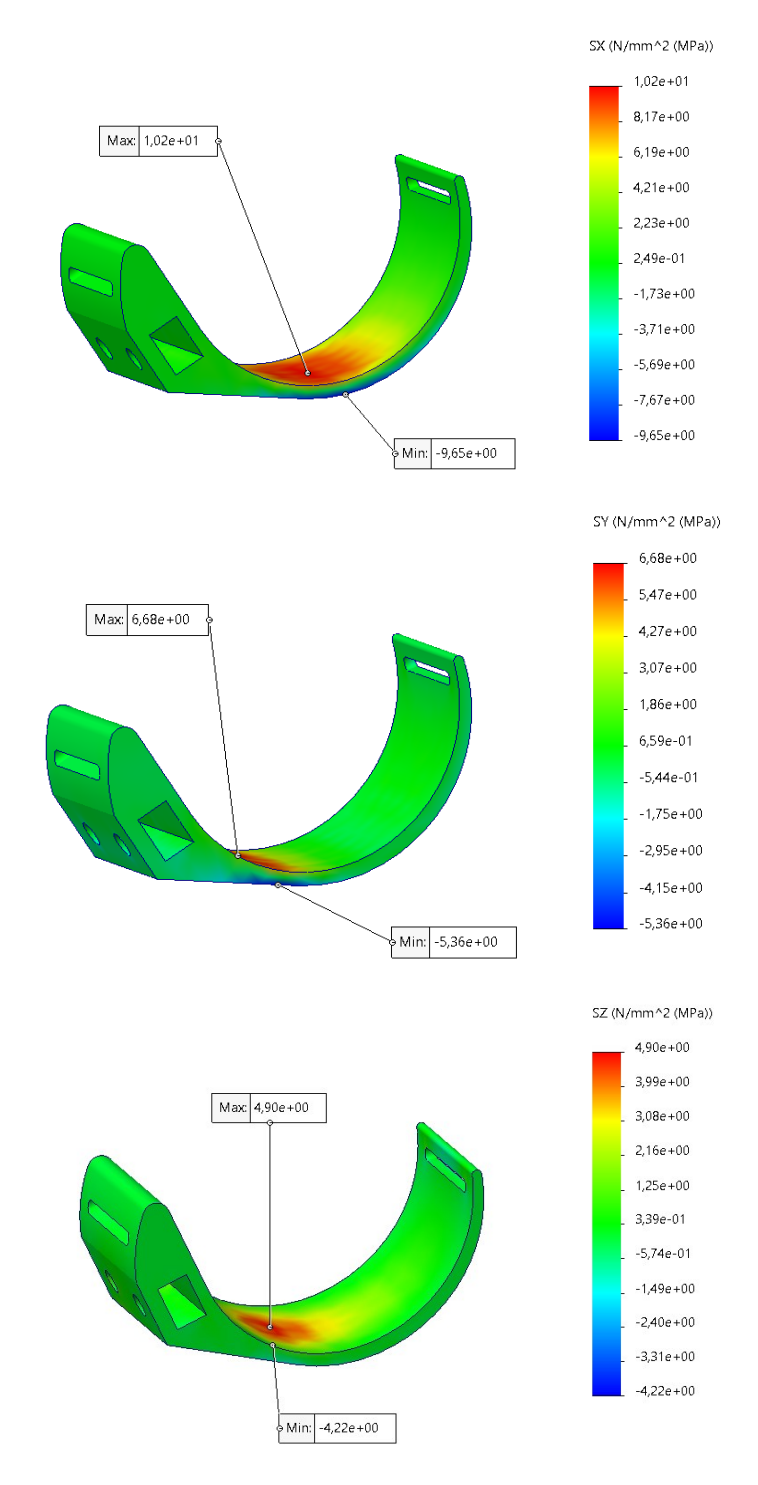


Figure 56: normal stresses in the three directions for the bracelet.

# 5.4. Displacements analysis

As expected, the most noticeable displacements occurred in the cam structure along the z direction, and in the bracelet along the and directions. In the cam structure, the cam moves backward due to the force applied by the MKM, resulting displacement of 2.95 mm, as shown in Figures Figure 59 instead shows that the bracelet bends downward significantly, reaching a deflection distal respect of mm end with to 6 its As a consequence of this deformation, an additional 3 mm displacement occurs along the X direction, shown Figure in

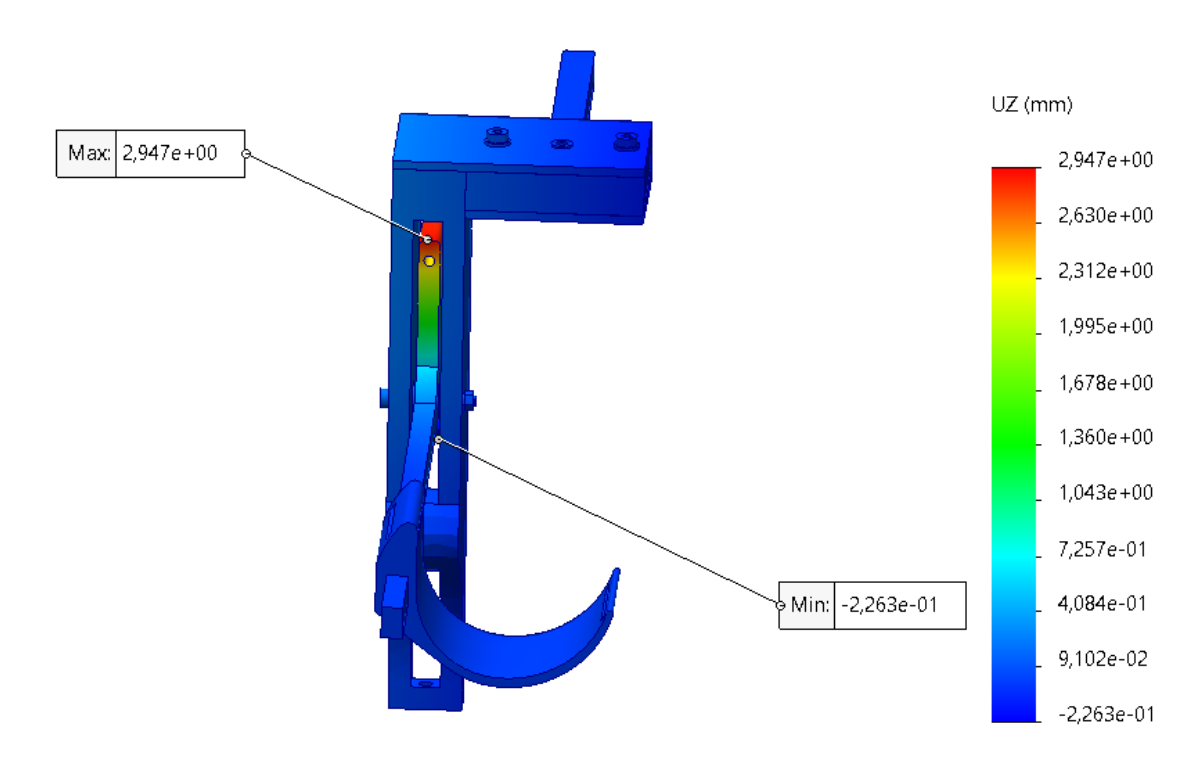


Figure 57: Deformation on the z direction of the whole structure

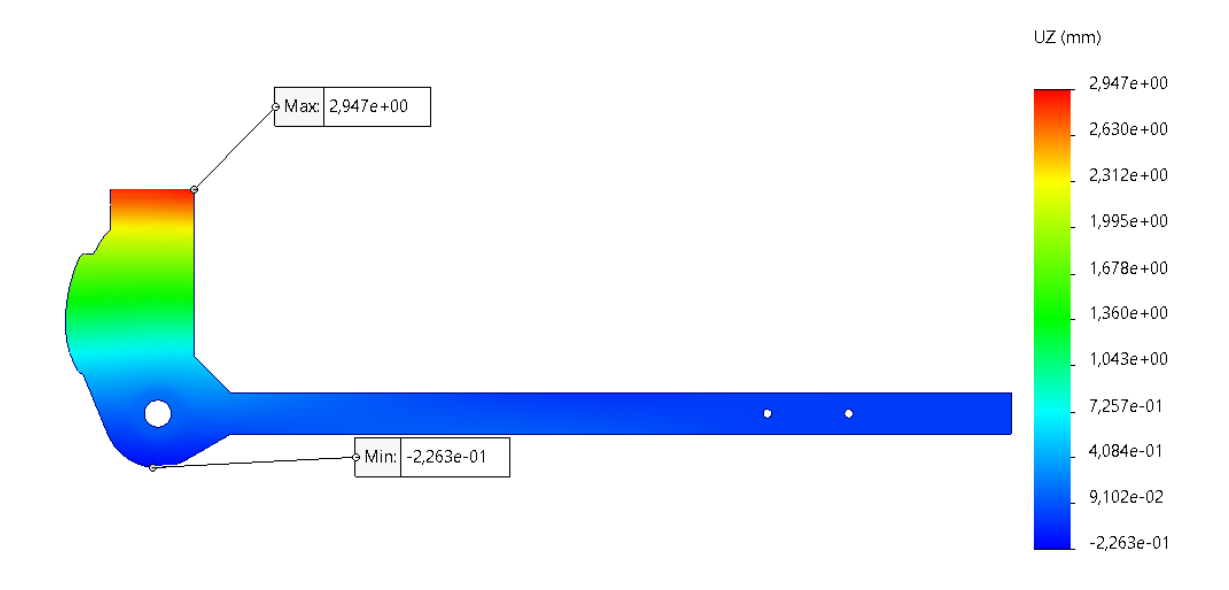


Figure 58: Deformation on the z direction of the cam structure.

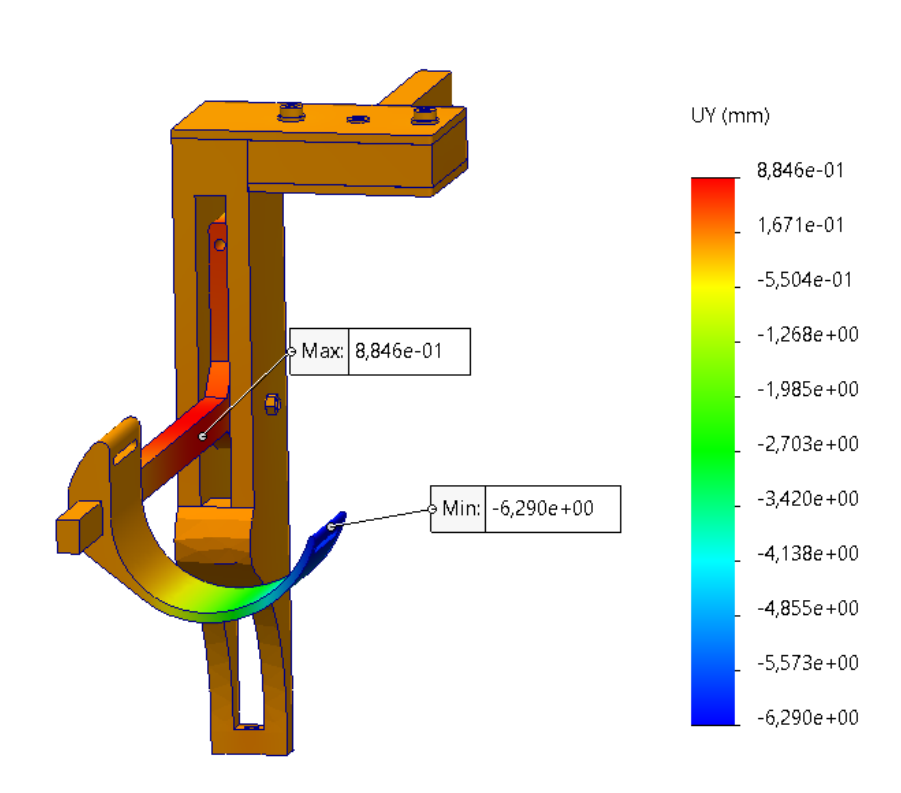


Figure 59: Deformation on the y direction for the whole structure.

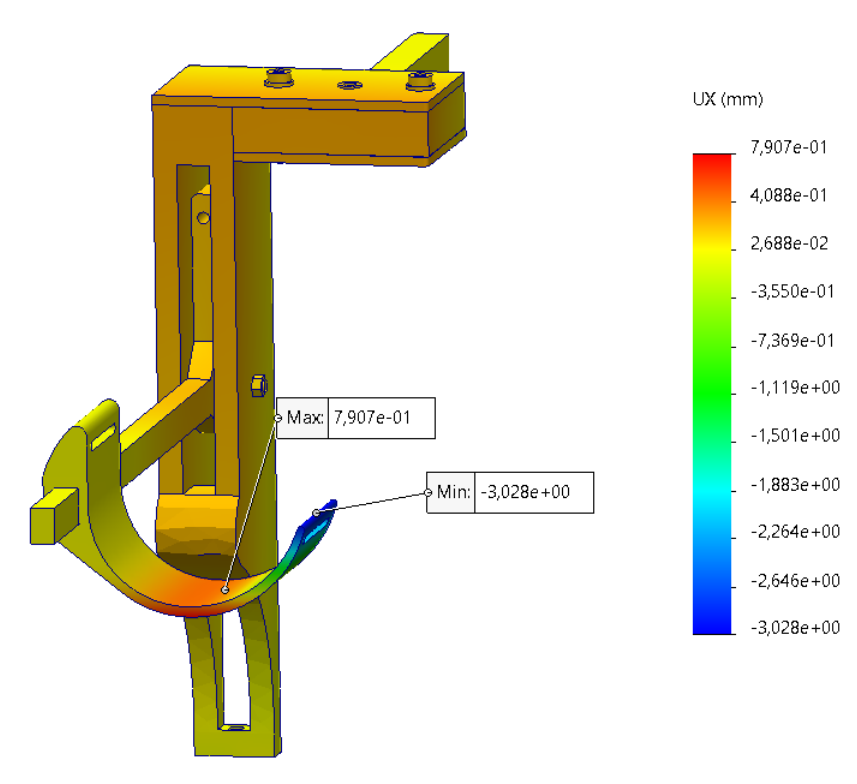


Figure 60: Deformation for the x direction for the whole structure.

#### 5.5. Parasitic Abduction Moment

Another major issue of the cam-based solution is the parasitic abduction torque, which is caused by the misalignment between the Shoulder Joint Center (SJC) and the cam rotation center  $(CAM_r)$  and by the horizontal force  $F_h$  that is the horizontal component of the force applied by the PAMs.

The angle between the direction of the applied force and its horizontal component was measured in the CAD model for seven elevation angles. The remaining values were then estimated using a polynomial fitting.

To evaluate the magnitude of this parasitic torque, it was assumed that the distance between the sternoclavicular joint (SC) and the most lateral point of the shoulder (the acromion) corresponds to the clavicular length. According to the literature, this distance is approximately 144 mm [43].

Referring to Eq. 1 by Nef and Riener [8], the distance between the SC and the SJC can be calculated.

Knowing the position of the SJC ( $x_{SJC}$ ) and the distance between the SC and the lateral acromion of the shoulder, and assuming that the cam rotation center is located at that point (as close as possible to the body), an additional 1.2 cm was added to account for the thickness of the cam support structure. This allows estimating the distance between the SJC and the cam rotation center, including its displacement in the frontal plane.

Eq. 12 express how the distance has been calculated, where CAM<sub>r</sub> is the cam rotation center,  $d_{r-SJC}$  is the distance between r and SJC,  $l_{clavicula}$  is the distance between AC and the lateral acromion,  $x_{SJC}$  is the distance between AC and the SJC and  $x_{supp}$  is lateral bulk of the cam support structure.

$$d_{CAM_r-SJC} = l_{clavicula} - x_{SJC} + x_{supp} Eq. 12$$

Knowing the distance between the cam rotation center and the Shoulder Joint Center (SJC) at different elevation angles, the parasitic abduction torque can be calculated as a function of the angle, as shown in Eq. 13.

$$M_{abd} = F_{hPAM} * d_{r-SIC} Eq. 13$$

This torque was calculated for the three load conditions in the hand: no load, 1 kg load, and 2 kg load. The results are presented in Figure 61, while  $F_{hPAM}$  is illustrated in Figure 62.

The parasitic abduction torque increases as the elevation angle decreases. It can be observed that for elevation angles above 90°, the initial adduction followed moment should not significantly affect overhead work. However, although the parasitic torque becomes higher below 90°, it should not prevent the user from lowering the arms.

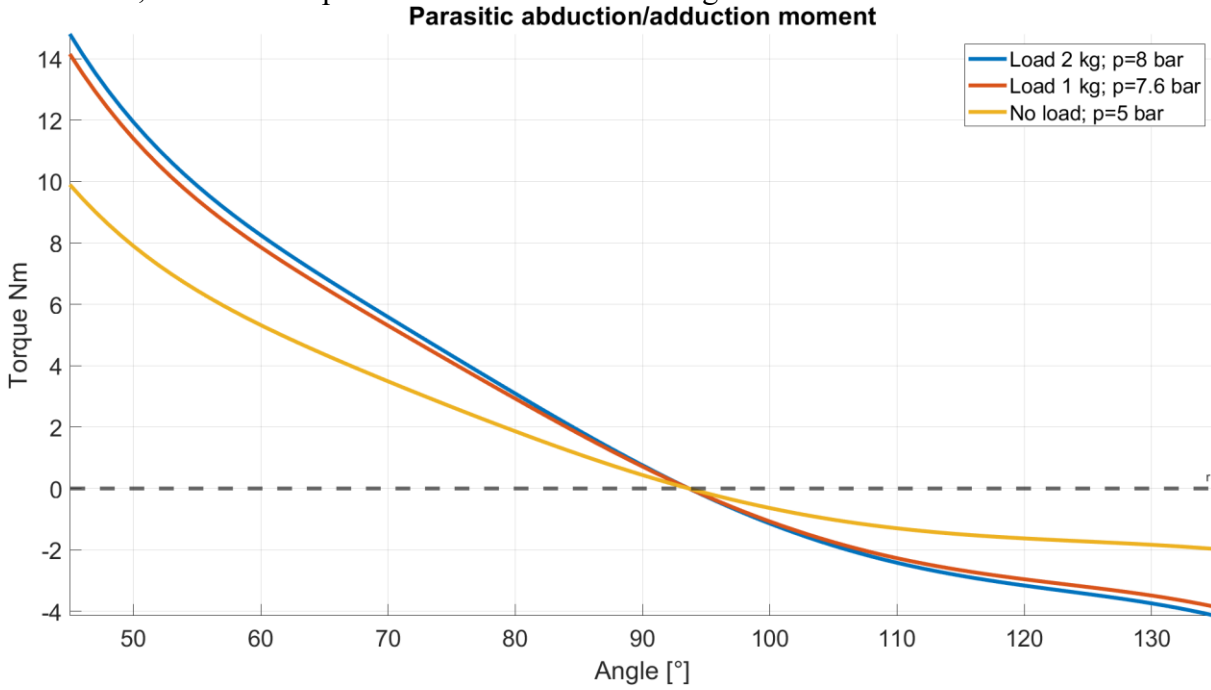


Figure 61: Parasitic abduction moment by elevation angle.

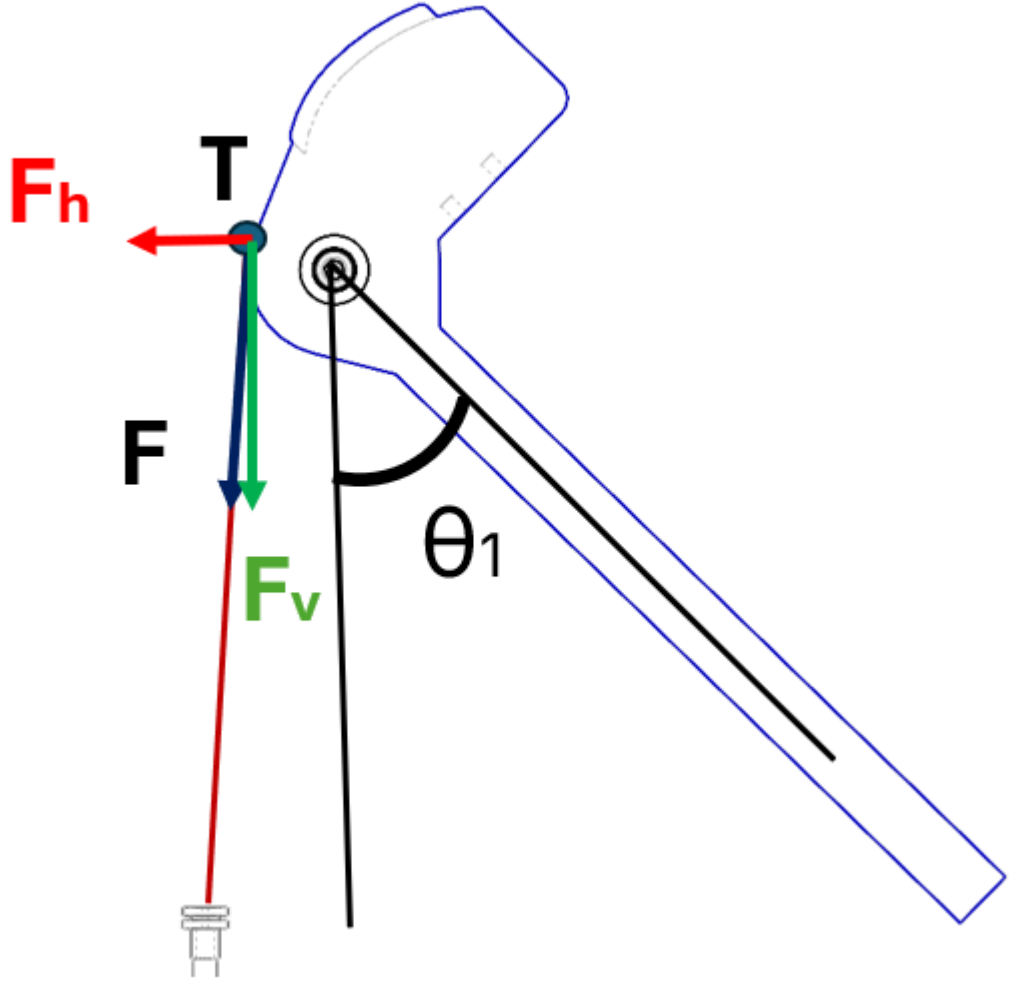


Figure 62: Horizontal Force that gave abduction moment. In the antero-posterior plane. F is the force of the Pam, Fv the vertical component and Fh the horizontal component. Thetal is the elevation angle. T is the tangent point between the cam and the cable.

#### 5.5. Discussion

Due to excessive deformation of the bracelet, its thickness was increased by 1 cm to enhance rigidity.

Following this modification, the maximum displacement along the x direction (in magnitude) was reduced by 79%, while the maximum displacement along the y direction (in magnitude) decreased by 89%. Figure 62 illustrates the displacement in x and y direction of the redesigned, thicker bracelet.

Overall, following the increase in bracelet thickness, it can be concluded that the PLA cam structure exhibits sufficient rigidity and acceptable displacements, making it feasible for fabrication, and it only weights 0.753 kg. So less then 1 kg.

This transmission solution effectively augment the flexion ROM, allowing a range from 45° to 135°. However, this system gave a big parasitic torque as seen in Figure 63.

The parasitic torque increases with the load. However, since the system cannot support the required torque when an object is in the hand, it is reasonable to focus on the curve

representing the parasitic moment with no load. The torque becomes unacceptable at angles below 90°, which makes the solution optimal for flexion, as it allows the arm to be lowered, but it introduce this parasitic torque.

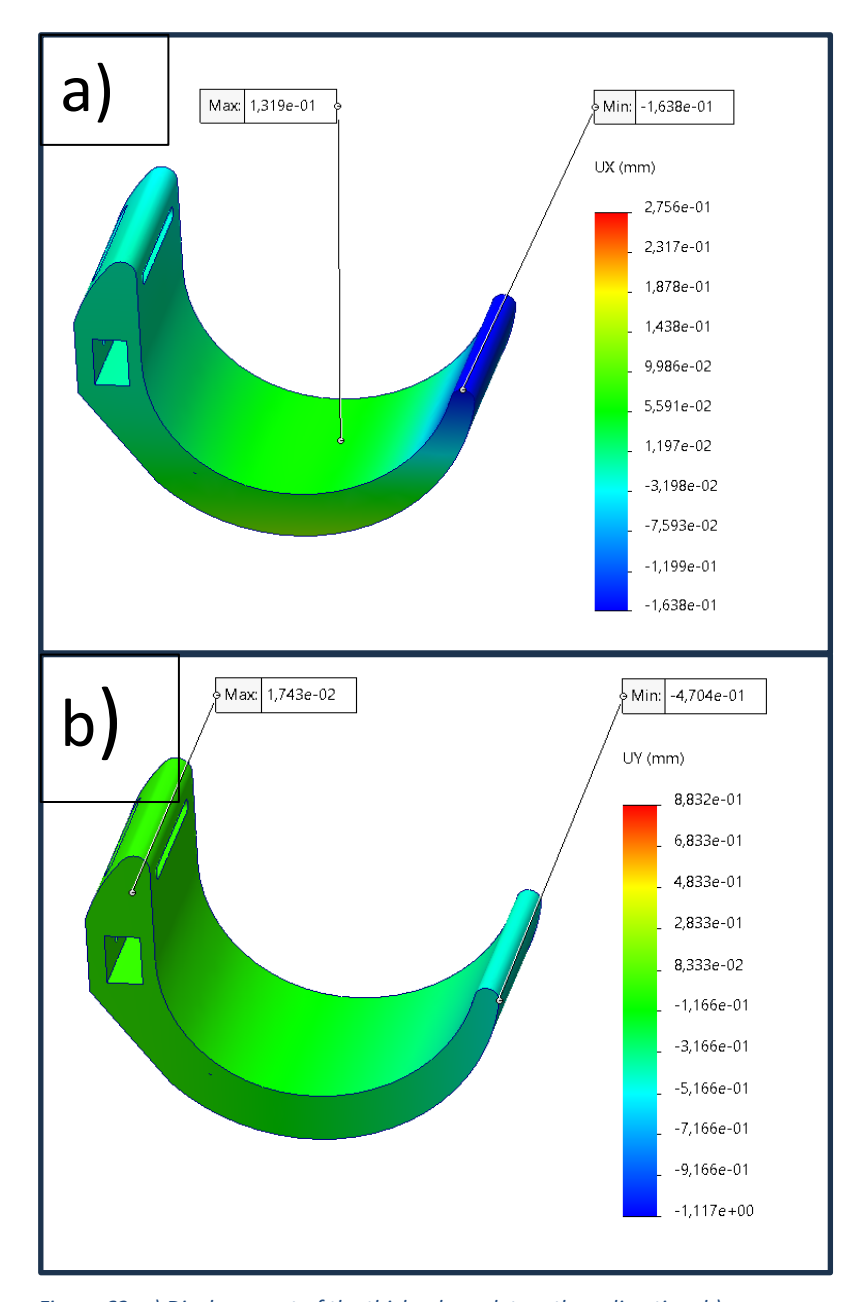


Figure 63: a) Displacement of the thicker bracelet on the x direction. b) Displacement of the ticker bracelet on the y direction.

# Chapter 6

## **Conclusions and future developments**

In this thesis, the range of motion (ROM), in particular of the flexion, of the passive industrial exoskeleton developed by Paterna[25] was investigated.

The initial prototype exhibited a limitation in flexion, which was restricted to the range 135°-90°, since the transmission system, the shoulder pad, generated torques that were significantly higher than the gravitational torques below 90°. This made it impossible for the user to lower the arms.

However, the support provided between 90° and 135°, and therefore for overhead work applications, was highly effective, compensating for approximately 75% of the required torque.

To address the ROM limitation, two improvement strategies were proposed. The first involved a modification that did not affect the transmission system itself: the release mechanism. The second concerns the feasibility evaluation of an alternative transmission concept, also proposed by Paterna[25], based on a cam mechanism that inherently extended the ROM but had not been previously developed, due to insufficient torque with loads, parasitic torque limitations and bulky structure.

Both solutions were explored computationally through FEM simulations, and the release mechanism was experimentally tested.

the both configurations, shoulder flexion ROM was clearly extended. In the first case, the flexion range was increased from 18° to 135°, although continuous torque support was maintained throughout the entire not range. The second solution provided continuous assistance within a flexion range between 45° and 135°, but this support was only able to compensate for the gravitational torque without external loads applied on the hand, which reduces its versatility.

Nevertheless, the new design demonstrated that the cam-based system can be feasibly developed and potentially tested in future prototypes.

Although neither solution represents the final configuration which should ideally provide assistance from 0° to 180°, both significantly expand the ROM of the exoskeleton. The first solution can be easily implemented on the current prototype, as it can be manufactured using 3D printing. The second solution, requiring only a few metallic components, is also relatively straightforward to produce.

Between the two, the release mechanism appears more immediately useful. With an optimization of the cable attachment point, aimed at reducing the mismatch between the support torque and the gravitational torque, this approach could effectively extend the ROM of the current transmission system maintaining the positive feature of it.

However, the cam mechanism shows greater potential for future development. The parasitic torques remain acceptable, particularly within the range where the exoskeleton is primarily intended to operate, between 90° and 135°, for overhead work. This solution allows the arms to be lowered while maintaining reasonably low abduction torques. Moreover, the support torque of this solution perfectly follows the gravitational torque during free-hand flexion within the considered range of motion. Therefore, this solution is perfectly suited for situations that require support throughout the full ROM when using light weights in the hands.

It should be noted that the FEM simulations and bench tests were performed under simplified boundary conditions. The arm weight was neglected, and the dynamic behaviour of the system during motion was not analysed. Future experimental campaigns including dynamic tests and user trials would allow a more accurate validation of the proposed solutions.

Further improvements are still required for the prototype to become suitable for commercialization.

A promising direction could be the introduction of an additional elastic element within the transmission system, capable of compensating for the extra torque. However, this would also increase the complexity of both the model and its construction. Overall, this work contributes to the ongoing development of lightweight and low-cost exoskeletons for industrial use, demonstrating that targeted mechanical improvements can significantly enhance usability without compromising simplicity or reliability.

## LIST OF FIGURES

Figure 1: Position of joints on osseus anatomy [2]

Figure 2: Shoulder ligaments. Adapted from[3]

Figure 3 a) Shoulder principal axis: on the left coronal view, on the right sagittal view.

Created in [13] b) Planes of the body.[14]

Figure 4: Shoulder movements. a) In black: Abduction; in red: Adduction b) In black:

Flexion; in red: Extension c) in black: horizontal abduction; in red: horizontal Adduction d) In red: Internal rotation; in black: external rotation. Created in [6]

Figure 5: Shoulder Muscles. [7]

Figure 6: a) Visual representation of the movement of the SJC (referenced here as Center of Glenohumeral Joint CGH) when the arm elevates in the frontal plane.[8] b) Representation of the GH AC SC joints, with the three joint angles.[8]

Figure 7: Position of SJC at different angles of elevation [8]

Figure 8: Most common types of passive elements and actuators in exoskeletons

Figure 9: Diagrams of DoF of industrial exoskeletons[16]

Figure 10: Photo of proto-MATE[20]

Figure 11: Illustration of passive exoskeleton PAEXO [22]

Figure 12: CDYS Passive exoskeleton by Crimson Dynamics[18], [23]

Figure 13: Visualization of the three shoulder ROMs tass[18]

Figure 14: Prototype CAD with mannequin. 1. Shoulder Pad 2. Bracelet 3. Guide for the

bracelet 4. Telescopic rod 5. Transmission wire 6. Harness 7. Pneumatic artificial muscle

Figure 15: PAMs positioning in the prototype with transmission elements.

Figure 16: Different PAM types[26]

Figure 17: Braided PAM functioning[31]

Figure 18: FESTO MKM[34]

Figure 19: Static characteristics of MKM FESTO DMSP-10[25]

Figure 20: Simplified geometry of MKM. Adapted from [28]

Figure 21: Phenomenological model[38]

Figure 22:CAD visualization of bracelet and shoulder pad

Figure 23: Scheme of the shoulder pad

Figure 24:In black: Gravitational torque Colored: Support torque. Comparison between support and gravitational torque in three different configuration: without external load in the user's hand (red line e and solid black line), with 1kg external load (green line and dashed black line), with 2kg external load (blue line and dotted and dashed black line)[25]

Figure 25: Prototype hinge joints

Figure 26: Cad overview of the new bracelet with the release system

Figure 27: Simplified Schematization of the new bracelet in the exoskeleton prototype

Figure 28: CAD assembly of the new bracelet in different state: a) locked state, locked safety catch. b) locked state, removed safety catch. c) Locked state, lifting of the release part. d)

Release state, release part totally lifted. e) Release state, sliding of the Sliding Part. f) Release state, Release Part stopped by the stop block.

Figure 29: CAD of the Fixed Part with highlighted parts

Figure 30: Cad of Sliding Part, Release Part and Handle in the locked state

Figure 31: Cad of Sliding Part, Release Part and Handle in the released state

Figure 32: CAD of the safety catch

Figure 33: New supportive Torque

Figure 34: Stroke length seen in the CAD of the fixed part

Figure 35: visualization of the distance between shoulder pad and attachment point of the bracelet for 90°(dashed line in red) and for 75° (dashed line in blu)

- Figure 36: Sliding distance required in order to lower the arms by a certain angle
- Figure 37: Printing orientation of the bracelet parts
- Figure 38: Bracelet with mesh and applied forces.
- Figure 39: Normal stresses in: a) x-direction, b) y-direction, c) z-direction
- Figure 40: Displacement in a) z direction, b) y direction c) x direction
- Figure 41 a) the sliding part is inserted in the release part; b) The handle is inserted c) The security catch is inserted all the way through the passage in the fixed part d) the assembly of the sliding, release and handle is inserted in the fixed part. The security catch now can lock the assembly.
- Figure 42: 3D printed new bracelet
- Figure 43: Bench Test
- Figure 44; Schematization of the static test
- Figure 45: Cam-based transmission system.
- Figure 46: Cam profile design using graphical method[25]
- Figure 47: Gravitational torque is shown for no-load (solid black line), 1 kg load (dashed black line), and 2 kg load (dot-dashed black line) conditions, alongside the torque generated by the exoskeleton at various supply pressures (colored lines), using the cam-based transmission.[25]
- Figure 48: Lateral CAD view of the new support structure for the CAM-based design.
- Figure 49: CAD upper view of the new support structure for the CAM-based design.
- Figure 50: Force and constraints applied to the CAD model.
- Figure 51: From top to bottom: Von Mises stresses of the bolt, the two washers and the
- bushing; Von Mises stresses of the lower plaque, Von Mises stresses of the upper plaque.
- Figure 52: von Mises stress for the bar
- Figure 53: Printing direction for a) Cam support structure, b) Cam and strut structure, c) Bracelet
- Figure 54: normal stresses in the three direction SX, SY, and SZ for the cam support structure.
- Figure 55: Normal stresses in the three directions for the cam and strut structure.
- Figure 56: normal stresses in the three directions for the bracelet.
- Figure 57: Deformation on the z direction of the whole structure
- Figure 58: Deformation on the z direction of the cam structure.
- Figure 59: Deformation on the y direction for the whole structure.
- Figure 60: Deformation for the x direction for the whole structure.
- Figure 61: Parasitic abduction moment by elevation angle.
- Figure 62: Horizontal Force that gave abduction moment. In the antero-posterior plane. F is the force of the Pam, Fv the vertical component and Fh the horizontal component. Theta1 is the elevation angle. T is the tangent point between the cam and the cable.
- Figure 63: a) Displacement of the thicker bracelet on the x direction. b) Displacement of the ticker bracelet on the y direction.

# REFERENCES

- [1] A. J. Felstead and D. Ricketts, "Biomechanics of the shoulder and elbow," *Orthop Trauma*, vol. 31, no. 5, pp. 300–305, Oct. 2017, doi: 10.1016/j.mporth.2017.07.004.
- [2] "Lippincott\_Professional\_Guides\_Anatomy\_&\_Physiolog...\_----\_(4\_Musculoskeletal\_system)".
- [3] Gray Henry and Lewis Warren Harmon, Anatomy of the Human Body. 1825.
- [4] W. van den Hoorn *et al.*, "The Future of Clinical Active Shoulder Range of Motion Assessment, Best Practice, and Its Challenges: Narrative Review," Feb. 01, 2025, *Multidisciplinary Digital Publishing Institute (MDPI)*. doi: 10.3390/s25030667.
- [5] I. A. Kapandji and L. Gui, Fisiologia articolare: schemi commentati di meccanica umana. Roma: DEMI, 1974.
- [6] "Created in https://BioRender.com."
- [7] K. A. Y. J. A. W. E. J. B. P. D. H. K. O. K. J. E. J. M. W. P. D. J. Gordon Betts, *Anatomy and Physiology*. Houston, Texas: OpenStax, 2013. Accessed: May 18, 2025. [Online]. Available: https://openstax.org/books/anatomy-and-physiology/pages/9-introduction
- [8] Proceedings of the 2nd Biennial IEEE/RAS-EMBS International Conference on Biomedical Robotics and Biomechatronics: Scottsdale, AZ, USA, October 19-22, 2008. IEEE Xplore, 2009.
- [9] A. Kumar, C. Jobe, and S. Saha, "Location of the instantaneous center of rotation for shoulder motion," in *Southern Biomedical Engineering Conference Proceedings*, IEEE, 1995, pp. 245–247. doi: 10.1109/sbec.1995.514490.
- [10] R. Krishnan, N. Björsell, E. M. Gutierrez-Farewik, and C. Smith, "A survey of human shoulder functional kinematic representations," Feb. 13, 2019, *Springer Verlag*. doi: 10.1007/s11517-018-1903-3.
- [11] A. Voilqué, J. Masood, J. C. Fauroux, L. Sabourin, and O. Guezet, *Industrial Exoskeleton Technology: Classification, Structural Analysis, and Structural Complexity Indicator; Industrial Exoskeleton Technology: Classification, Structural Analysis, and Structural Complexity Indicator.* 2019. doi: 10.0/Linux-x86 64.
- [12] A. Voilqué, J. Masood, J. C. Fauroux, L. Sabourin, and O. Guezet, *Industrial Exoskeleton Technology: Classification, Structural Analysis, and Structural Complexity Indicator; Industrial Exoskeleton Technology: Classification, Structural Analysis, and Structural Complexity Indicator.* 2019. doi: 10.0/Linux-x86 64.
- [13] G. Ashta, S. Finco, D. Battini, and A. Persona, "Passive Exoskeletons to Enhance Workforce Sustainability: Literature Review and Future Research Agenda," May 01, 2023, MDPI. doi: 10.3390/su15097339.
- [14] D. M. G. Preethichandra *et al.*, "Passive and Active Exoskeleton Solutions: Sensors, Actuators, Applications, and Recent Trends," Nov. 01, 2024, *Multidisciplinary Digital Publishing Institute (MDPI)*. doi: 10.3390/s24217095.
- [15] S. K. Manna and V. N. Dubey, "Comparative study of actuation systems for portable upper limb exoskeletons," Oct. 01, 2018, *Elsevier Ltd.* doi: 10.1016/j.medengphy.2018.07.017.
- [16] J. Tian et al., "A Systematic Review of Occupational Shoulder Exoskeletons for Industrial Use: Mechanism Design, Actuators, Control, and Evaluation Aspects," Dec. 01, 2024, Multidisciplinary Digital Publishing Institute (MDPI). doi: 10.3390/act13120501.
- [17] J. Kim, J. Kim, Y. Jung, D. Lee, and J. Bae, "A Passive Upper Limb Exoskeleton With Tilted and Offset Shoulder Joints for Assisting Overhead Tasks," *IEEE/ASME Transactions on Mechatronics*, vol. 27, no. 6, pp. 4963–4973, Dec. 2022, doi: 10.1109/TMECH.2022.3169617.

- [18] T. Ma, E. Jonathan, and S. Xiong, "Investigation of the Impact of a Passive Shoulder Exoskeleton on the Shoulder Range of Motion: A Preliminary Study," in *Lecture Notes in Computer Science (including subseries Lecture Notes in Artificial Intelligence and Lecture Notes in Bioinformatics)*, Springer Science and Business Media Deutschland GmbH, 2024, pp. 219–230. doi: 10.1007/978-3-031-61060-8\_16.
- [19] "https://www.comau.com/."
- [20] I. Pacifico *et al.*, "An experimental evaluation of the proto-mate: A novel ergonomic upper-limb exoskeleton to reduce workers' physical strain," *IEEE Robot Autom Mag*, vol. 27, no. 1, pp. 54–65, Mar. 2020, doi: 10.1109/MRA.2019.2954105.
- [21] "https://corporate.ottobock.com."
- [22] P. Maurice *et al.*, "Objective and Subjective Effects of a Passive Exoskeleton on Overhead Work", doi: 10.1109/TNSRE.2019.2945368ï.
- [23] "CRIMSON DYNAMICS."
- [24] T., de V. A. W., de L. M. P., & O. L. W. Kermavnar, "Effects of industrial back-support exoskeletons on body loading and user experience: an updated systematic review".
- [25] M. 'Paterna, "Passive upper-limb exoskeleton based on Pneumatic Artificial Muscles."
- [26] Z. Situm, P. Trslic, D. Trivic, V. Stahan, H. Brezak, and D. Sremi'c, "Pneumatic muscle actuators within robotic and mechatronic systems," *Proceedings of International Conference Fluid Power, Fluidna tehnika 2015, pp. 175–188, Faculty of Mechanical Engineering, 2015.*
- [27] W. Al-Mayahi and H. Al-Fahaam, "A Review of Design and Modeling of Pneumatic Artificial Muscle," Jun. 01, 2024, *College of Engineering, University of Basrah*. doi: 10.37917/ijeee.20.1.13.
- [28] B. Kalita, A. Leonessa, and S. K. Dwivedy, "A Review on the Development of Pneumatic Artificial Muscle Actuators: Force Model and Application," Oct. 01, 2022, *MDPI*. doi: 10.3390/act11100288.
- [29] M. Martens and I. Boblan, "Modeling the static force of a Festo pneumatic muscle actuator: A new approach and a comparison to existing models," *Actuators*, vol. 6, no. 4, Dec. 2017, doi: 10.3390/act6040033.
- [30] O. Sokolov, A. Hošovský, and M. Trojanová, "Design, Modelling, and Control of Continuum Arms with Pneumatic Artificial Muscles: A Review," Oct. 01, 2023, *Multidisciplinary Digital Publishing Institute (MDPI)*. doi: 10.3390/machines11100936.
- [31] T. Beullens, "Hydraulic or Pneumatic Drive Device. U.S. Patent 4,841,845, 27 June 1989."
- [32] J. E. Takosoglu, P. A. Laski, S. Blasiak, G. Bracha, and D. Pietrala, "Determining the Static Characteristics of Pneumatic Muscles," *Measurement and Control (United Kingdom)*, vol. 49, no. 2, pp. 62–71, Mar. 2016, doi: 10.1177/0020294016629176.
- [33] S. A. Mohareb, A. Alsharkawi, and M. Zgoul, "Hysteresis modeling of a pam system using anfis," *Actuators*, vol. 10, no. 11, Nov. 2021, doi: 10.3390/act10110280.
- [34] "FESTO." [Online]. Available: https://www.festo.com/it/it/c/prodotti/attuatori/attuatori-pneumatici/attuatori-a-membrana-e-soffietti/muscolo-pneumatico-id pim397/?page=0
- [35] C.-P. Chou and B. Hannaford, "rement and ding of McKibben Pneumatic Artificial Muscles," 1996.
- [36] "Modeling and Control of McKibben Artificial Muscle Ro bot Act u ato r s Tmdu (tondu @insa-!lse.frl und l a p e x nre with LESIA, Electrical and."

- [37] K. C. Wickramatunge and T. Leephakpreeda, "Empirical modeling of dynamic behaviors of pneumatic artificial muscle actuators," *ISA Trans*, vol. 52, no. 6, pp. 825–834, 2013, doi: 10.1016/j.isatra.2013.06.009.
- [38] "Serres, J. L., Reynolds, D. B., Phillips, C. A., Gerschutz, M. J., & Repperger, D. W. (2009). Characterisation of a phenomenological model for commercial pneumatic muscle actuators. Computer Methods in Biomechanics and Biomedical Engineering, 12(4), 423–430. https://doi-org.ezproxy.biblio.polito.it/10.1080/10255840802654327".
- [39] J. Pitel' and M. Tóthová, "Modelling of pneumatic muscle actuator using Hill's model with different approximations of static characteristics of artificial muscle; Modelling of pneumatic muscle actuator using Hill's model with different approximations of static characteristics of artificial muscle," 2015, doi: 10.1051/02015.
- [40] "A. Hošovský and M. Havran, 'Hill's muscle modelbased modeling of pneumatic artificial muscle', in Annals of DAAAM for 2011 & Proceedings of the 22nd International DAAAM Symposium, Vienna, 2011. pp. 1005-1006 (2011)".
- [41] Anthropometric reference data for children and adults: United States, 2007-2010. U.S. Department of Health and Human Services, Centers for Disease Control and Prevention, National Center for Health Statistics, 2012.
- [42] "Bambu Filament PLA Basic."
- [43] X. S. Qiu, X. B. Wang, Y. Zhang, Y. C. Zhu, X. Guo, and Y. X. Chen, "Anatomical study of the clavicles in a Chinese population," *Biomed Res Int*, vol. 2016, 2016, doi: 10.1155/2016/6219761.